

UNIVERSITY OF NAPLES “FEDERICO II”
Department of Chemical Engineering



XXIII cycle
PhD in Chemical Engineering

**Experimental Methods for Structural and
Morphological Study of Fine and Ultrafine
Particulate Produced from Combustion Processes**

Maria Mallardo

Prof. ANTONIO CAVALIERE
Prof. ELISEO RANZI
Prof. UMBERTO ARENA
Dr. ANNA CIAJOLO

October 2010



ABSTRACT

Experimental studies have been carried out to understand the chemical structures of the high molecular weight species produced in fuel-rich combustion systems and their role in the soot formation.

Different laminar flat premixed flames at atmospheric pressure were used as a basic combustion experiments. In particular the different flames used were:

- Methane/O₂ flames (C/O=0.60) burning at two different cold-gas flow velocities ($v=4$ and 5 cm/s).
- Benzene/O₂/N₂ flames (C/O=0.80) burning at two different cold-gas flow velocities ($v=3$ and 4 cm/s).
- Ethylene/O₂ flames (C/O=0.80) burning at $v=3$ cm/s).

Probe sampling and optical measurement were carried out inside the system.

Condensed species and soot were withdrawn along the axis of the flame by means of a stainless-steel water-cooled probe. These species, after gravimetric determination, were subjected to chemical: gas chromatography-mass spectrometry (GC-MS), high pressure liquid chromatography (HPLC), thermogravimetric analysis (TG), elemental analysis, size exclusion chromatography (SEC) and spectroscopy analysis (UV-Vis, FT-IR).

Gas, Soot and PAHs analysis and formation have been also studied in a more complex system, such as a gasification apparatus as a Bubbling fluidized Bed, obtained as part of the on-going research performed at Second University of Naples, department of Environmental Sciences, on the evaluation of the effect that different reactant gases, i.e. steam, carbon dioxide and air enriched in oxygen content, as well as different bed materials, have on the composition of syngas and on the main performance parameters of co-gasification process.

It has been possible to assess the following statements:

- ✓ The condensed material sampled in rich premixed flames is constituted of two fraction: a lighter PAHs fraction from 2 to 7 rings, and analyzable by GC-MS techniques and a heavier one constituted of species undetectable by GC-MS.
- ✓ Species not analyzable by GC-MS were separated from PAHs using a thermogravimetric procedure. The high molecular mass of these species and their mixed aromatic/aliphatic character are suggested by spectroscopic analysis.
- ✓ By using SEC analysis, an evaluation of the molecular weights of the unknown species indicated the presence of species of 1000u along with species having molecular mass comparable with the lower mass fraction of soot (10^5 - 10^6 u). SEC analysis of soot showed also a large contribution of species having a molecular weight of about 10^8 u.

INDEX

Chapter 1

1 Introduction	1
1.1 Air pollution and effects of anthropogenic activities	2
1.2 Polycyclic Aromatic Hydrocarbons	10
1.3 Soot formation in combustion processes	15
1.4 Object of Thesis	19

Chapter 2

2 Experimental section	23
2.1 Combustion system	23
2.2 Sampling procedure	24
2.3. Fluidized bed gasification system	25
2.4 Flame Temperature Measurements	31
2.5 Extinction measurements	31
2.6 Gas combustion analysis	33
2.7 Analytical characterization of particulate matter	33
2.7.1 Thermogravimetric analysis (TGA)	34
2.7.2 Gas chromatography-mass spectrometry (GC-MS)	35
2.7.3 UV–Visible absorption spectroscopy	35
2.7.4 Fluorescence emission spectroscopy	36
2.7.5 Ft-IR spectroscopy	37
2.7.6 Elemental Analysis	37

2.7.7 Size exclusion chromatography	38
Chapter 3	40
3 Results and discussion	41
3.1 Methane flames	41
3.1.1 Concentration profiles of Gas species	42
3.1.2 Concentration profiles of condensed phases	45
3.1.3 Analysis of condensed species (Gaschromatography- Mass spectrometry)	46
3.1.4 Soot characterization	47
3.1.5 UV-Visible Spectroscopy of condensed species and soot	49
3.1.6 FT-IR analysis of condensed species and soot	51
3.1.7 Size Exclusion Chromatography of condensed species and soot	54
3.2 Benzene flames	58
3.2.1 Concentration profiles of Gas species	59
3.1.2 Concentration profiles of condensed phases	62
3.2.3 Analysis of condensed species (Gaschromatography- Mass spectrometry)	62
3.2.4 Soot characterization	64
3.2.5 UV-Visible spectroscopy of condensed species and soot	66
3.2.6 Size Exclusion Chromatography of condensed species and soot	68
3.3 Ethylene flame	71
3.3.1 Concentration profiles of Gas species	72
3.3.2 Concentration profiles of condensed phases	76
3.3.3 Analysis of condensed species (Gaschromatography- Mass spectrometry)	76

3.3.4 Soot characterization	79
3.3.5 UV-Visible Spectroscopy of condensed species and soot	80
3.3.6 FT-IR analysis of condensed species and soot	81
3.3.7 Size Exclusion Chromatography of condensed species and soot	83
3.4 Bubbling Fluidized Bed BFB Gasification system	86
3.4.1 Gas and condensed-phases analysis	87
3.4.2 PAH formation in BFB reactor	89
3.4.3 Comparison between gas and condensed-phases from methane flames and bubbling fluidized bed.	92
Conclusions	96
Figures	100
References	108



CHAPTER 1

INTRODUCTION

Introduction

1.1 Air pollution and effects of anthropogenic activities

The *atmosphere* is the gas layer that surrounds the Earth. It extends up to about 2500 Km height above ground level and its density decreases as the altitude increases (about the half of the total gas mass is within 5 Km of altitude).

The major gases in the atmosphere are oxygen, nitrogen and argon. Table 1.1 reports the mean composition of clean dry air at ground level.

The atmosphere contains also large amounts of water vapour (up to 4%) and its concentration varies in dependence of the altitude, the latitude as well as the weather conditions.

This large amount of gas is retained around the Earth by the gravitational forces. At altitude where these forces become too low, the molecules of gas “run away” from terrestrial atmosphere, spreading into the cosmos.

The study of the atmospheric pollutions is an important part of the overall study of the pollution because of the diffusion phenomena of the pollutant species in the atmosphere are more efficient than that in the condensed phases (such as the surface water and the soil) due to the greater mobility of molecules in a gaseous state.

As a matter of fact, the atmosphere is a dynamic system, whose gaseous components are continually exchanged with the vegetation, the oceans and the biological organisms.

On the other side the atmosphere acts as a filter: controls the solar radiation, intercepts a large part of the solar wind, cosmic rays and the flows of ionized particles that continuously invest the Earth.

It is important to underline that the composition of the atmospheric air varies both in space and in time, so it is not correct in many cases to "handle" the atmospheric air simply as a mixture of oxygen and nitrogen.

In order to set a conventional standard for air quality is necessary to define the concept of pollution as the introduction of contaminants into a natural environment that cause instability, disorder, harm or discomfort to the ecosystem i.e. physical systems or living organisms. The air containing some substances whose concentrations exceed set limits is considered polluted. In the case of the atmosphere the main damages caused by the large increase of pollutants generated by the anthropogenic activities are the greenhouse effect and the photochemical smog.

Gas	Concentration (ppm)
Nitrogen (N₂)	780900
Oxygen (O₂)	209400
Argon (Ar)	9300
Carbon Dioxide (CO₂)	315
Neon (Ne)	18
helium (He)	5.2
Methane (CH₄)	1.0-1.2
Krypton (Kr)	1
Nitrogen oxide (NO)	0.5
Hydrogen (H₂)	0.5
Xeno (Xe)	0.08
Nitrogen dioxide (NO₂)	0.02
Ozone (O₃)	0.01-0.04

Tab 1.1 Composition of the dry air at ground level.

The most common source of air pollution coming from both natural sources and anthropogenic activities are listed below:

- natural events such as the volcanic eruptions, fires, and decomposition processes
- industrial activities

- transportation
- power plants for the production of heat and energy
- waste incineration
- nuclear activities (radioactive dust and gases)
- use of pesticides and fertilizers
- uncontrolled combustion of solid waste

These sources are cause of serious emission of pollutants in the atmosphere with dramatic consequences on the ecosystem also at a global level. As a matter of fact, the emissions not always remain within territorial limits close to emission source, but, for example, in some cases industrial pollutants have been observed also in very remote areas of the planet. One of the greater risks derives from chemical and metallurgical industries which, for many treatments, discharge polluted air by gas or dust.

It's important to stress that the study of pollutants has to be done putting in close relationship the pollutants with the causes which lead to their emissions in the atmosphere and any chemical-physical processes that, on the contrary, carry on the removal of the pollutants. To this end it is important to note that, if the removal is chemical, the products originate from this process can be more harmful than the original pollutants, so it is possible to define two major classes of pollutants:

- Primary pollutants that are the pollutants released directly into the atmosphere owing to the process that created them.
- Secondary pollutants which rise up from the primary pollutants in the air owing to secondary chemical transformations also involving the atmospheric oxygen and the solar radiation.

Most of the primary pollutants come out from the combustion of fossil fuels. Different classes of compounds are formed in dependence of the operating conditions of the combustion process and of the chemical and physical characteristics of the fuel used.

Gaseous primary pollutants are:

- sulphur compounds (SO_2 , H_2S)
- nitrogen compounds (NO , NH_3)
- halogenated compounds (HCl , HF , HBr , CFC)
- light hydrocarbons, volatile organic compounds (VOC)

The major secondary gaseous pollutants are:

- NO₂ formed from NO oxidation
- O₃ formed as a result of photochemical reactions

These gases are involved in the complex mechanisms that underly the so-called “photochemical smog” phenomenon.

Combustion systems devoted to transportation, energy production, etc. are also the main sources of solid particulate (organic and inorganic) named primary particulate that is emitted along with gaseous and semivolatile pollutants.

Finally, a secondary particulate is often recognized resulting from reactions involving gaseous pollutants both primary and secondary. Some well-known processes are:

- the transformation of SO₂ in sulphates SO₄⁼
- the transformation of NO₂ in nitrates NO₃⁻
- the coagulation of unburned hydrocarbons on elementary carbon.

The pollutants emitted into the atmosphere owing to processes of combustion are due to an imperfect and/or partial combustion except for few, but important species that, although products of complete combustion, are considered pollutants such as the sulphur dioxide (SO₂), the carbon dioxide (CO₂), the nitrogen oxides (NO_x) and the inorganic particulate.

As the sources of pollution are very numerous, so in the same way the substances considered pollutants are countless (several tens of thousands), for some of them the environmental effects are known since a few years.

Gas and particulate matter into the atmosphere

In the urbanized and industrial regions many pollutant species as sulphur oxides, carbon dioxide (CO₂), carbon monoxide (CO), nitrogen oxides (NO_x), volatile hydrocarbons (C_xH_y), particulate matter, etc. are present in variable amounts.

Carbon dioxide (CO₂) is a gas that is produced from all combustion processes. Its concentration in Earth's atmosphere is very low (about a molecule of CO₂ every 2800 molecules of other gases in the air), but, in the last years it's increased about 28% compared to pre-industrial levels. The increase of its concentration in Earth's atmosphere causes great concern for its role in the increase of the greenhouse effect phenomenon also known as *radiative forcing*. The *radiative forcing* can alter the balance energy of the planet, due to the capacity that some compounds present in the atmosphere of increasing the amount of trapped energy retaining the incident light radiation of sun.

Carbon monoxide (CO), is known to be toxic, it, in fact, enter into the bloodstream and it combines with haemoglobin, forming the carboxyhemoglobin, which inhibits the transport of oxygen to the tissues. The first effects of a high concentration of CO in the organism can be recognised by a weakening of mental functions, to which can also follow the death.

Sulphur oxides (SO_x) and **nitrogen oxides** are extremely harmful because they induce, in contact with the water vapour in the air, the formation of acid rains. **Nitrogen oxides (NO_x)** also participate actively in the formation of smog and are among the main causes of the destruction of the atmospheric ozone.

Particulate matter is generally originated both from anthropogenic sources and from natural sources (such as the wind erosion, the forest fires, the volcanic emissions, the pollen dispersion and the marine aerosol).

Three approaches are typically used to classify particle size (US-EPA,1996):

- **modes**, based on formation mechanisms and modal structure observed in the atmosphere (e.g., nuclei and accumulation modes which comprise the fine particle mode);
- **cut point**, based on the 50% cut-point of the specific sampling device (e.g., PM_{2.5} and PM₁₀);
- **dosimetry**, based on the ability of particles to enter certain regions of the respiratory tract.

Particulate matter is constituted of organic and inorganic fractions. The **carbonaceous particulate matter**, including solid and tarry particles with diameter up to 100 μm is a significant fraction of the atmospheric particulate. The largest particles usually reach the ground in a short time and cause pollution on restricted areas.

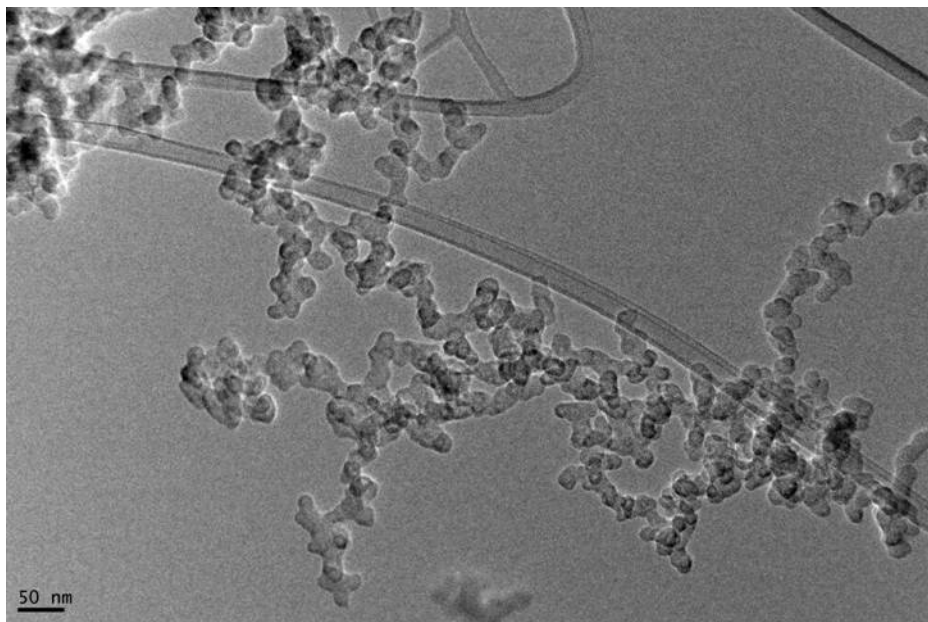


Fig. 1.1 Microscope image of the carbonaceous particulate produced in a flame

Smaller particles have a residence time in the atmosphere very long, so their deposition velocity is low. In this case the removal from the atmosphere is mainly due to the rain.

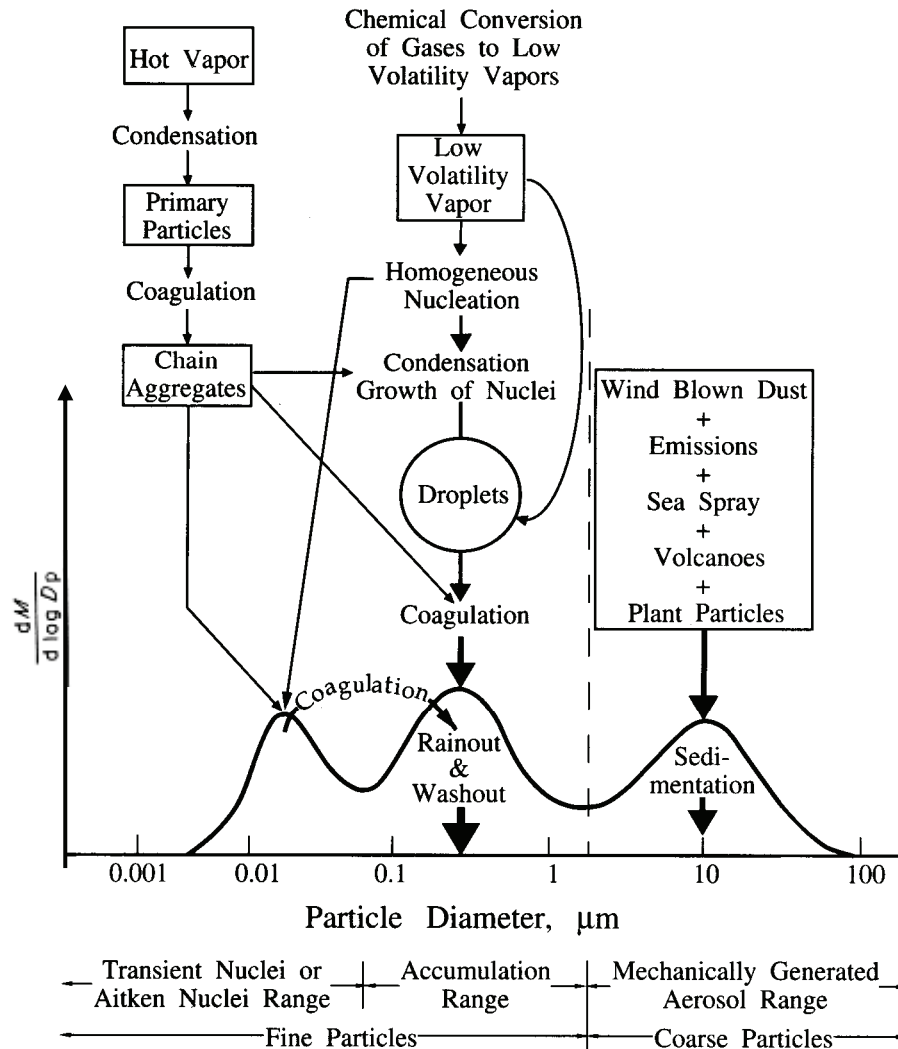


Fig.1.2 Size distribution and formation mechanisms for atmospheric aerosols (from Whitby and Cantrell, 1976)

Fig. 1.2 reports the size distribution of particulate (Whitby and Cantrell, 1976) in atmospheric aerosols showing the wide size range from fine to coarse particles. Particles with a diameter greater than 1,5 μm , are deposited in the upper respiratory tract, while fine particles can reach the pulmonary alveoli.

Recently the “ultrafine particles” having diameters less than $\sim 0.08 \mu\text{m}$ that are emitted directly from combustion sources or that condense from cooled gases are considered having the highest health effects (Oberdörster et al., 1995; Fitzgerald et al., 1997; Kotzick et al., 1997). Ultrafine particulate can interact directly with the central nervous system. In fact, some of

them have been found in correspondence with olfactory nervous terminals from which can spread, through the blood-brain barriers, to neurons.

Since these particles can be accumulated by years in the central nervous system, they can cause very serious neurotoxic effects (Oberdorster G. et al., 2003). Other studies, conducted on samples of the USA populations, have shown that the number of people died of lung cancer increases by 8% per 10 $\mu\text{g}/\text{m}^3$ of particulate matter concentration increase (Pope C. III. et al., 2002).

The emission of carbonaceous particulate is associated with the emissions of other species, also dangerous to human health, like polycyclic aromatic hydrocarbons (PAHs) which can be absorbed on carbonaceous particles and easily penetrate, mainly by inhalation, in the human body according to the mechanism above described.

Most of the PAHs have a high toxicologic potential because of its carcinogenic co-carcinogenic and mutagenic nature (Freudenthal e Jones, 1976; Gelboin e Pope, 1994).

In the processes of combustion operated in oxygen-rich or stoichiometric conditions the reaction products are CO_2 and H_2O .

The combustion operated in excess of fuel creates the conditions favourable for the formation of PAHs and carbonaceous particulate often defined as soot. It should be stressed that, even in stoichiometric or in fuel-lean conditions, the formation of these pollutants can not be excluded. In fact, in conditions of not perfect mixing of the reagents an excess of fuel in some areas of the reacting system can bring to undesired pollutant products.

The quality and quantity of PAHs and carbonaceous particulate produced depend on the combustion system, from operating conditions and from chemical and physical characteristics of the fuel. Thus, the study of combustion processes carried out in conditions that reduce the emissions of PAHs and carbonaceous particulate matter in order to limit the air pollution is very important for avoiding their emission.

In spite of many studies focused on the formation of PAHs and carbon particulate matter, their formation mechanisms are still not completely understood. This objective has not been obtained also because of limits of diagnostic techniques in the range of MW/size intermediate between low mass gaseous species and solid species where intermediates of the process leading to the first soot particles are included.

The aim of this thesis has been to set up and apply an array of analytical techniques for the study of PAH and soot formation in premixed flames burning diverse fuels in different temperature conditions. Indeed, just these two parameters: temperature and fuel structure, have shown to strongly affect soot structure and size (Alfè, 2009 and references therein). Thus,

the parametric study can also furnish interesting information on particulate formation mechanism that is the other aim of this work.

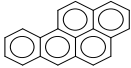
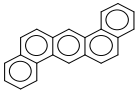
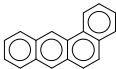
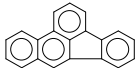
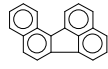
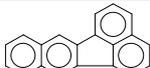
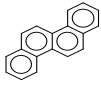
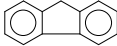
1.2 Polycyclic Aromatic Hydrocarbons

Polycyclic Aromatic Hydrocarbons are fused-ring aromatic hydrocarbons often present in fossil fuels, as coal and oil, and produced by incomplete combustion processes. Many PAHs have been identified, starting from naphthalene up to compounds with seven or more aromatic rings in the environment, in gas phase and also absorbed on the particulate matter. They are considered among the main responsible for the human health damages.

About the toxicity of PAHs, several studies have shown that the exposure to high concentrations causes an increase of the lung and skin cancer incidences and the different carcinogenic behaviour is correlated to the different molecules also in relation to the different number of condensed rings.

The Agency for the Cancer Research (IARC, Vol. 32) has classified different PAHs on the basis of their carcinogenicity. Table 1.2 shows the structure and the carcinogenicity classification for major PAHs. Their properties are similar to the benzene ones: high stability and flat geometric structure, but their chemical and physical characteristics vary with molecular weight.

Their importance is also correlated to their presence in combustion systems, in fact, they have been considered for a long time to have a role in soot formation, due both to their transient presence in the soot nucleation zone of flame and to the similarity between the PAHs structure and the graphite-like structure of soot.

Name	Carcinogenicity (IARC, 2008)	
Dibenzo(a)pyrene	1	
Benzo(a)pyrene	2A	
Benzo(a,h)anthracene	2A	
Benzo(a)anthracene	2A	
Benzo(b)fluoranthene	2B	
Benzo(j)fluoranthene	2B	
Benzo(k)fluoranthene	2B	
Chrysene	2B	
Naphthalene	3	
Pyrene	3	
Fluorene	3	
Anthracene	3	

Tab. 1.2 Typical structure and carcinogenicity classification for principal PAHs - 1: human carcinogen, 2A: probably human carcinogen, 2B: possible human carcinogen, 3: non-carcinogen.

The study of the formation of soot and PAHs is one of the most important topics of research activities in the interrelated area of combustion and environmental pollution. The interest in the subject originates mostly from environmental concerns on pollutant emission from combustion devices and on the possible role of PAHs in soot formation.

PAHs are formed in the incomplete combustion in particular in fuel rich combustion systems. In order to describe their formation in a rich combustion system many authors have suggested different model mechanisms. In particular Frenklach et al. (1986) developed a network of 600 elementary reactions and 180 species to model molecular weight growth for benzene in shock tube experiments assigning to all the reactions in a particular reaction class the same kinetic constants. This modelling approach was shown to be successful in predicting the characteristic bell-shaped curve for soot yield as a function of temperature. The modelling efforts of Frenklach et al. represent the first attempt to model soot formation as chemical reactions network starting from the initial fuel molecules, but this modelling work also showed that PAH formation chemistry is not well understood and uncertainties in rate parameter estimations were a source of difficulty in order to validate the elementary reaction mechanisms.

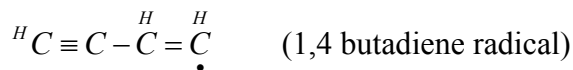
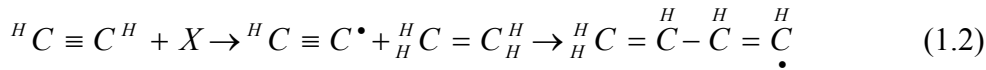
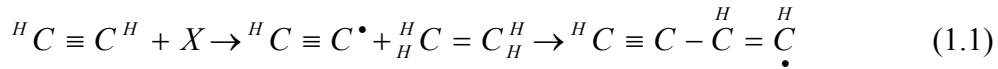
Despite many uncertainties concerning the reaction path-ways and the thermochemical data of PAH are still present, many modeling studies predicted the formation of benzene and PAH in the fuel-rich combustion of aliphatic hydrocarbon with a reasonable level of accuracy (Wang H. and Frenklach M., 1997; Freanklak et al. 2002; Miller J. A., and Melius C. F., 1992).

The primary focus is on the formation of the first aromatic ring from small aliphatic molecules, because this step is perceived by many to be the rate-limiting step in the reaction sequence to large aromatics.

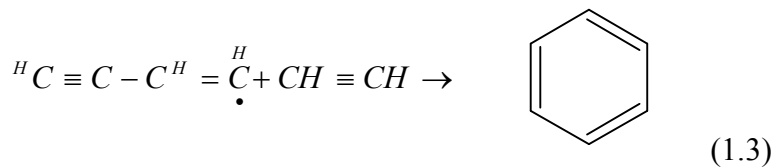
The principal role is attributed to acetylene (C_2H_2) one of the main hydrocarbons that is produced. Its importance is due to the role that it has in benzene (C_6H_6) and PAHs formation. Benzene is the first aromatic compound formed in rich hydrocarbon combustion processes and the main precursor in PAHs formation, as a matter of fact PAHs concentration is about one order of magnitude lower than benzene.

The benzene mechanisms formation is described by two main reactions set that take in to the account the addition of acetylene to $n-C_4H_3$ and $n-C_4H_5$ (Freanklach et al. 2002; Miller and Melius,1992; Pope and Miller, 2000; D'Anna and Violi,1998; Violi et al.,1999; Goldaniga et al.,1998):

- Low temperature systems ($T < 1500\text{K}$): in pyrolytic conditions, acetylene give rise to the C_4 radical (1,4 butadiene radical) (1.1-1.2):



Second reaction involves acetylene to form benzene, as reported in the mechanism (1.3)



- High temperature systems ($T > 1500\text{K}$): The reaction can occur between two C_3 radicals (propargyl $\bullet\text{C}_3\text{H}_3$), or from cyclopentadiene ($\bullet\text{C}_5\text{H}_5$) and methyl ($\bullet\text{CH}_3$), as reported in the reactions (1.4) and (1.5):



It has to be noted that propargyl and cyclopentadiene are both present in high concentration in a fuel-rich combustion systems.

Frenklach et al (2002) improved his previous model assuming that the addition of acetylene to C_4 -hydrocarbon is followed by cyclisation to form the first aromatic ring and then large polycyclic aromatics are formed from smaller ones by a sequence of steps involving Hydrogen Abstraction, acetylene Addition and cyclisation (HACA mechanism). However, the HACA-based reaction model is too slow, it can predict the PAH formation, but it contributes negligibly to the formation of total aromatics (including the aromatic species heavier than PAH) in the whole flame (Frenklach and Warnatz, 1987). As a consequence

other authors (Miller J. A. and Melius C. F., 1992; Castaldi M. J. et al. D'Anna A. and Violi A., 1998) modified this mechanism indicating that key sequences of reactions in the formation of aromatics are the re-combination of resonantly stabilised radicals.

In this case the main route involved in the formation of the first aromatic ring are the propargyl self-combination (1.4) and its addition to CH_3 radicals (1.5).

Cyclopentadienyl radical ($\cdot\text{C}_5\text{H}_5$) combination, propargyl addition to benzyl radicals ($\cdot\text{C}_6\text{H}_5$) and the subsequent addition of propargyl radicals to aromatic rings are controlling step for the formation of large aromatic species.

The experimental basis for modelling studies mainly derives from sampling and chemical analysis of PAHs present in combustion gases carried out preferentially in flat premixed flames where it is possible to measure the time-dependent formation and destruction of these species.

The PAHs concentration profiles in premixed flames generally exhibit a maximum at the end or within the primary oxidation zone. After a minimum a reincrease in the post-flame zone, has been sometimes observed.

It is important to note that the mass of PAHs evaluated by gas chromatographic-mass spectrometric technique accounts for about 20-50% of the total mass of particulate matter sampled in flame and separated from soot by solvent extraction (Ciajolo A. et al. 1994; 1996). This percentage can vary with temperature, C/O ratio and fuel composition and it was found larger at lower temperature (Ciajolo A., et al, 1996). For determining the nature of the unidentified species in the DCM-soluble fraction of particulate matter spectroscopic and mass spectrometric analysis has shown the high molecular mass and aromaticity of these unidentified species that can have an important role in soot formation as well as possible health effects (Ciajolo A., et al, 1996, 1998).

1.3 Soot formation in combustion processes

Soot particles emitted from combustion systems constitute an important part of the total mass balance of the pollutant emissions. They influence the operation and design of technical combustion devices and have implication for both effective operation and pollutant emission. Many experiments have been carried out in order to determine the effect of different operating parameters. In particular significant effects on soot formation are imputed to fuel structure, temperature, pressure and flow conditions in combustion systems.

The nature of soot varies with aging. Soot size increases, mainly by agglomeration, from a few nanometers particle diameter up to 200nm. During this process the free radical character of the soot decreases. The concentration of soot particles in post-flame gases remains typically in the range 10^6 - 10^9 cm^{-3} . The soot hydrogen content is relatively high, about 1% by weight and the soot density is about 1.8-2 g/cm^3 .

The carbon atoms network as showed by X-ray analysis appears to be in planar graphitic structures. However, in contrast to graphite, the planes are randomly oriented forming a so-called turbostratic structure (Palmer H. B. and Cullis C. F., 1965).

The stages of soot formation process have been summarized by Haynes and Wagner (Haynes and Wagner 1981) as follows:

1. Particle inception, in which the first soot particle is formed from pyrolysis products. Such products typically include different unsaturated hydrocarbon, particularly acetylene and its analogues and polycyclic aromatic hydrocarbons. These species have been often considered as the most likely precursor of soot in flames.
2. Surface growth, by which the bulk of the solid-phase material is generated. Surface growth involves the bonding of gas-phase species to the surface of the particles and their incorporation into the particulate phase.

Soot formation occurs through a nucleation process, in this step the gas-to-particle transition occurs. Several studies assume that the PAHs have an important role in the soot inception processes and they can be considered soot precursors (Homann et al., 1968).

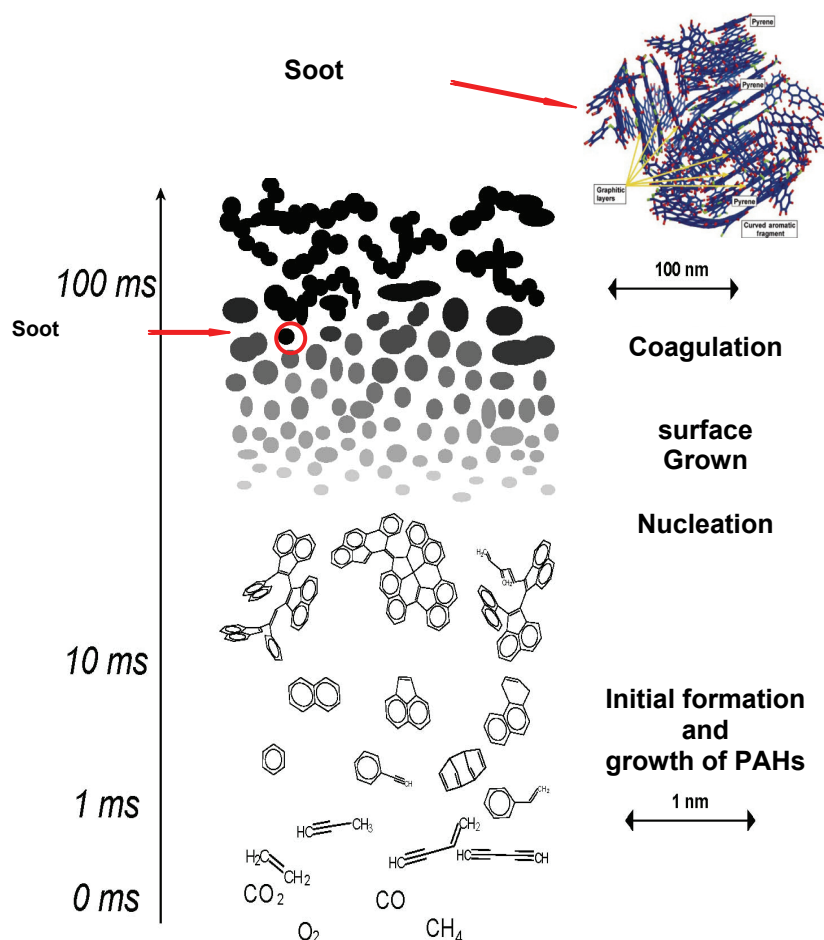


Fig.1.3 Scheme of soot formation process (from H. Bockhorn 'Soot Formation in Combustion' Springer-Verlag Berlin Heidelberg 1994)

Fig. 1.3 schematizes the process of soot formation in four steps:

- Initial formation and growth of PAHs
- Nucleation
- Surface growth
- Coagulation

The study of the nucleation step is still in progress, as a matter of fact, the reaction mechanisms that are involved in the formation of the first soot particles of nanometric size are not completely known.

The surface growth produces an increase of the particulate mass, remaining constant the number of particles (N), while in the coagulation phase, when the particles collide and

coalesce, there is a reduction of the particles number, while the volume fraction remains constant (Wagner, 1981).

Soot concentration in rich laminar flames, assuming the spherical symmetry for soot particles, is described by the relation:

$$f_{v\infty} = \frac{\pi}{6} \cdot N \cdot d^3$$

where $f_{v\infty}$ is the soot volume fraction ($\text{cm}^3 \text{ soot} / \text{cm}^3$), N is soot particle numbers (cm^{-3}) and d the particle diameter.

It has been demonstrated that the soot concentration in a fuel rich combustion system depends on the C/O ratio. At a fixed temperature for each hydrocarbon exists a specific value of C/O ratio, that is named the critical C/O ratio $(C/O)_{cr}$. The formation of soot can be observed in flames that have a C/O ratio value above the critical value.

The $f_{v\infty}$ value depends by several factors as the fuel nature, the flame temperature, and the system pressure. The results reported by Bohm et al.(1988) for C_2H_4 -air flames showed that in the high temperature region the final soot volume fraction $f_{v\infty}$ decreases strongly as the temperature increases (Fig. 1.4) and $f_{v\infty}$ -T curve reaches a maximum at intermediate temperatures. The absolute $f_{v\infty}$ values depend strongly on the C/O ratio.

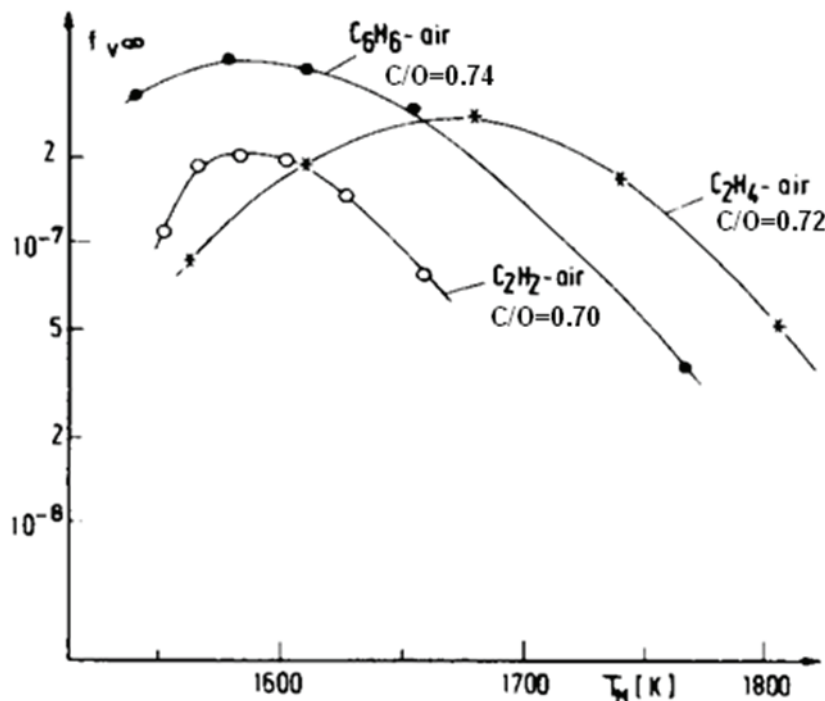


Fig. 1.4 Temperature dependence of $f_{v\infty}$ for C_2H_4 -air flames at $C/O=0.72$ (*), C_2H_2 -air at $C/O=0.70$ (o) and C_6H_6 -air flames at $C/O=0.74$ (●) (from Bohm et al, 1988)

It has also been shown that the composition of the combustion products (including gaseous and condensed phases) is strongly dependent on the flame temperature at a fixed C/O ratio (Ciajolo et.al., 1996). It has been presumed that the flame temperature affects also the soot characteristics.

Overall, it is clear that many parameters affect soot formation, the study of the effect of fuel structure and temperature should be carried out separately improving the analytical detail of high molecular mass species involved in soot formation in order to give further insights on the soot formation mechanism.

1.5 Object of Thesis

In this thesis the effects of different fuels and different operating temperatures on the formation and the chemical and structural characteristics of soot and condensed species, constituting the fine and ultrafine particulate matter, were studied in laminar fuel-rich premixed flames.

Different fuels: methane (as aliphatic fuel) and benzene (as aromatic fuel) were utilized. Methane is the major component in natural gas used in many practical applications including heating systems and gas turbines for power generation plants and it is generally regarded to be the cleanest hydrocarbon fuel. As a matter of fact, it produces less CO₂ and more H₂O than other fossil fuels, because of its high H/C ratio. Also regarding the emission of pollutants as soot and PAH, methane has been found a relatively clean fuel, however previous work was not focused on the emission of ultrafine particulates that are at now considered of particular concern. On the other hand an aromatic fuel like benzene is known to be particularly prone to generate soot and condensed species.

The effect of temperature was studied at fixed C/O ratio varying the cold gas velocity. According to this PHD thesis subject, an experimental study on the chemical composition and spectroscopic properties of soot and condensed species formed in fuel-rich combustion condition was carried out. The structures of methane and benzene flames were preliminarily obtained by measuring temperature and species concentrations profiles.

Chemical and spectroscopic methods have been developed for a careful qualitative and quantitative characterization of soot and condensed species collected inside a premixed laminar flame, chosen as basic experiment, because of it is a stationary one-dimensional system in which the results obtained have a good reproducibility and can be easily correlated to experimental parameters.

The chemical composition of soot and condensed species has been inferred by using analytical techniques typical of the analytical chemistry of combustion products (gas chromatography, mass spectrometry, high-pressure liquid chromatography, thermogravimetric analysis, elemental analysis, etc.).

Spectroscopic analysis of soot and condensed species has been developed and used in particular for the characterization of the heavy part of these materials not analyzable with conventional techniques. The characterization of the heavy part of condensed species is particularly important for two main reasons: i) these species can be the precursor in soot

inception processes ii) they, usually neglected in the mass balance of the combustion process, can have a strong impact on the human health and environment in relation to their size (small droplets and or ultrafine solids) and to their chemical composition (i.e. their aromatic nature or oxygen content).

The aliphatic content of soot and condensed species has been measured by using an infrared absorption method developed for the quantitative analysis. The aromaticity has been evaluated mainly by means of UV-visible absorption spectroscopy and fluorescence emission spectroscopy. In order to obtain information about the molecular weight of the condensed species and soot, Size Exclusion Chromatography (SEC) was used.

The advancement of diagnostic techniques for the analysis of fine and ultrafine particulate matter produced in combustion was the main objective of the thesis work. Also, the parametrical study of the effect of fuel on the chemical and structural properties of particulate matter has been carried out for giving further insights on the formation mechanism of the particulate matter.

In the course of this thesis, part of the experimental work was devoted to apply the sampling and analytical techniques, developed on the basic combustion system, on a pre-pilot fluidized-bed gasification reactor to verify the applicability of these techniques to complex practical systems. These experimental activities were carried out in the context of the research project lead by AMRA s.c.a.r.l. and co-financed by CONAI on a pre-pilot Bubbling Fluidized Bed (BFB) reactor.

CHAPTER 2

EXPERIMENTAL SECTION

Experimental section

2.1 Scale-laboratory combustion system

The combustion device used for the laboratory scale experiment was a water-cooled sintered bronze burner (d=60 mm) produced by Holthuis & Associates USA (McKenna design) surrounded by a shroud of nitrogen.

The flame was stabilized by a horizontal steel plate positioned about 30 mm height above the burner.

The atmospheric-pressure laminar premixed flat flames operated on this burner can be considered one-dimensional reacting systems, so it may be assumed that the flame is completely described when the temperature and concentration profiles along the flame axis are known. The burner moves vertically in order to allow sampling at different heights above burner (i.e. at different residence times).

The burner can be used for the study of combustion processes both gaseous and liquid fuels. In the case of liquid fuels they are pre-vaporized and the cooling temperature of the burner is kept above the dew point of the fed mixture.

Table 2.1 -2.2 report the operating conditions for the methane, benzene and ethylene flames respectively.

Experimental conditions Methane Flames

Fuel	Methane	Methane
Oxidant	Oxygen	Oxygen
C/O ratio	0.6	0.6
Methane %	54.55	54.55
Oxygen %	45.45	45.45
Cold gas velocity (cm/s)	4	5
Temperature (K)	1650	1778

*Tab. 2.1 Methane/O₂ operating conditions.***Experimental conditions Benzene Flames**

Fuel	Benzene	Benzene
Oxidant	Oxygen	Oxygen
Diluent	Nitrogen	Nitrogen
C/O ratio	0.8	0.8
Benzene %	5.78	5.78
Oxygen %	21.67	21.67
Nitrogen %	72.55	72.55
Cold gas velocity (cm/s)	3	4
Temperature (K)	1717.	1808

Tab. 2.2 Benzene/O₂/N₂ operating conditions.

Experimental conditions Ethylene Flame

Fuel	Ethylene
Oxidant	Oxygen
C/O ratio	0.8
Ethylene %	44.44
Oxygen %	55.56
Cold gas velocity (cm/s)	3
Temperature (K)	1620

Tab. 2.3 Ethylene/O₂ operating conditions.

2.2 Sampling procedures

Probe sampling followed by chemical analysis is the approach used to measure the concentration of combustion product along the flame. Several other techniques were used in order to completely characterize the sampled material.

Soot and condensed species were isokinetically sampled by means of a stainless-steel water-cooled probe (i.d.=2 mm). The combustion products have to be rapidly cooled in order to quench the reactions along the sampling line. Gas phase species were analyzed by on line gaschromatography of sampled combustion gases. Soot and condensed species (CS) were collected on a teflon filter and in a cold trap placed before the filter and extracted by dichloromethane in order to separate the condensed species, that are soluble in DCM, from the insoluble carbonaceous material, denoted soot. CS and soot were dried and weighed. Long sampling times were necessary to collect suitable quantities of condensed species and soot for the analysis.

Condensed phases collected on the probe wall, in the teflon filter (0.5 μm) and in an ice-cooled trap, were extracted by dichloromethane (DCM) to separate the condensed species, that are soluble in DCM, from soot. The handling procedure of the sample will be described in detail in the following paragraphs. Figure 2.1 reports a scheme of the experimental apparatus.

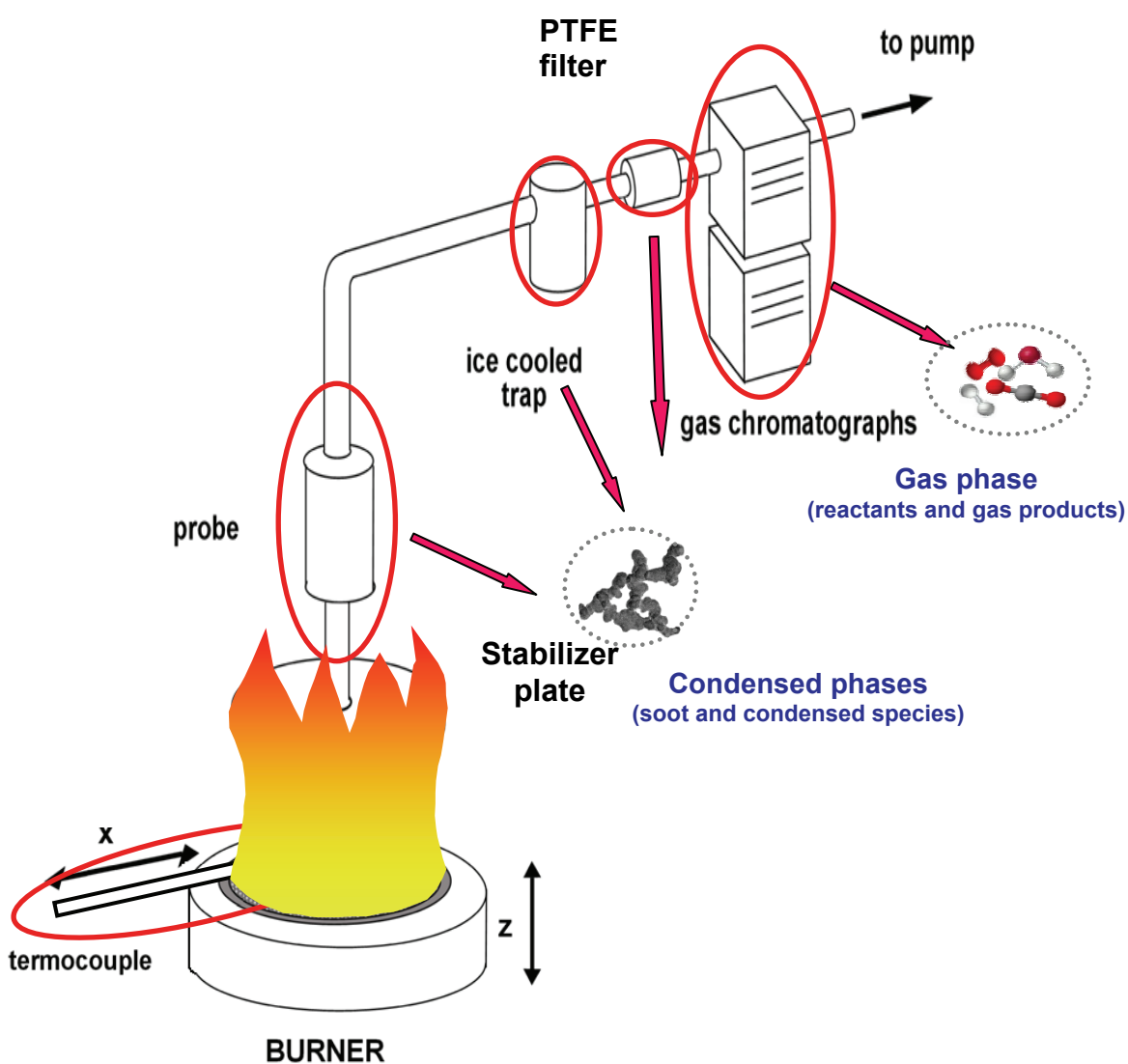


Fig. 2.1 Scale-laboratory combustion system

2.3. Fluidized bed gasification system

The results reported in this section have been obtained as part of the on-going research performed at Second University of Naples, department of Environmental Sciences, on the evaluation of the effect that different reactant gases, i.e. steam, carbon dioxide and air enriched in oxygen content, as well as different bed materials, have on the composition of syngas and on the main performance parameters of co-gasification process.

The term “co-gasification” indicates the co-feeding of different fuels into the gasifier with the aim to improve the flexibility of the process (e.g. by feeding low-quality and high-quality fuels/waste) and the performance of the process of syngas production.

Some peculiar aspects of the process as the large production of tar or carbon fines can create concerns about the operation of the plant and the economic sustainability of the process.

By consequence the analysis of tar and particulates produced during the gasification process and object of this study is important.

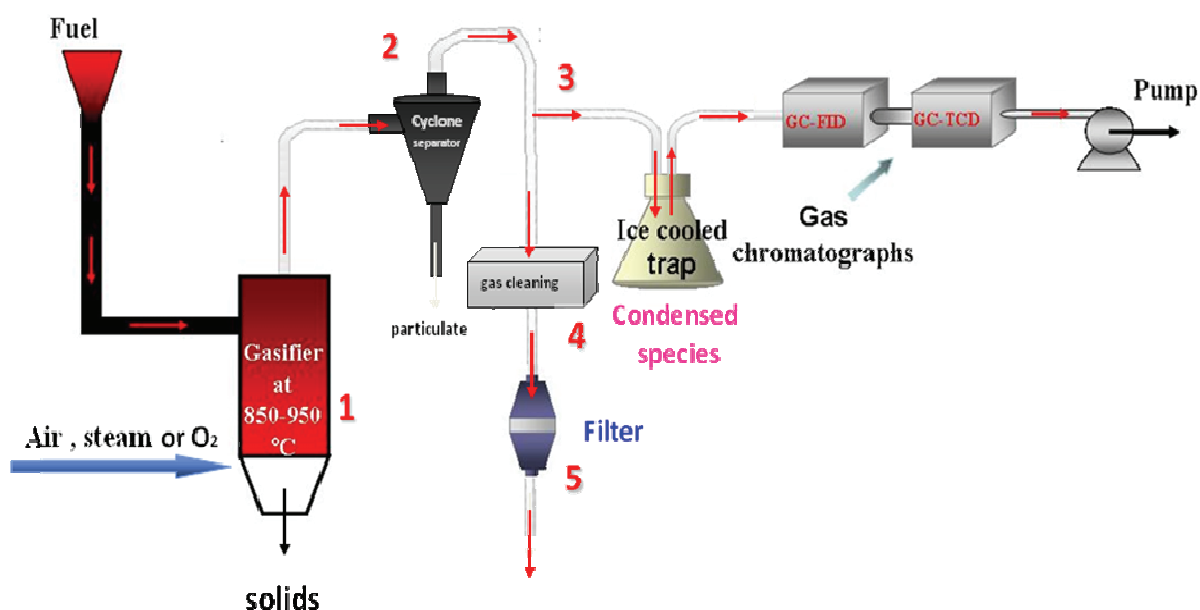


Fig. 2.2 Sampling line for gas analysis on the pre-pilot Bubbling Fluidized Bed (BFB) plant

The gasification apparatus is a bubbling fluidized bed made of AISI 316L, 102mmID and 2.5m high (Figure 2.3 The BFB reactor). It is equipped with a series of electrical shells

able to bring the reactor temperature up to 850°C in four sections of the reactor column. The temperature is controlled by a thermocouple located at the reactor internal wall for each reactor section. The gas distributor is formed by 3 nozzles, having a truncate pyramidal shape able to guarantee a uniform distribution of the fluidizing gas.

In fact, the fluidized bed gasification process provides good mixing, high energy and matter transfer, high uniformity of temperature.

In figure 2.2 is reported the sampling line of gas analysis on the pre-pilot Bubbling Fluidized Bed (BFB).

The BFB can be fed with different fuels by means of a mechanical feeder that can be located at two levels:

- ✓ just above the fluidized bed;
- ✓ about 1m above the fluidized bed.

The possibility to vary the level of fuel injection is crucial for some fuels that need different time to be heated, dried and partly molten before entering the fluidized bed. Plastic is an example of a fuel for which the location of injection respect to the bed is important in order to avoid agglomeration between bed particles and the fuel itself.

It is equipped with a piping that allows to feed into the reactor different reactants: air, enriched air, steam, carbon dioxide and their mixtures can be alternatively used to study its effect on syngas composition and on the performance of the gasification process.

The reactor exit is connected to a cyclone for fines separation and collection and just after the cyclone top, syngas steam is divided in two parts:

- the first part of the syngas stream is sent in a gas gleaning systems and a filter system for the removal of particle matters and after sent to storage systems and/or potential uses.
- The second part of syngas steam is sent in a ice-cooled trap for the removal of the condensed phases (particle matters, soot, condensed species, PAHs). The clean syngas, after, is sent an on-line gas-cromatographs. Stable C1-C6 hydrocarbons were analyzed by gaschromatography on gas chromatograph equipped with flame ionization detector (FID). CO₂, CO, H₂, N₂ were analyzed on gas chromatograph with a thermoconductibility detector (TCD)

A series of diagnostic apparatus are available for off-line analyses in particular:

- ✓ the GC-MS, a TGA and a C-H-N-S analyser for the condensed species in particular for the PAHs identification.
- ✓ TGA and a C-H-N-S for soot analysis.
- ✓ to identify and quantify the content of NH₃, HCl, and H₂S.



Fig. 2.3 Bubbling Fluidized Bed (BFB)

A fuel mixture having 50% of german brown coal, 30% of plastic waste (PE, PP and PET) and 20% of wood was chosen as reference fuel named P8.

The gasification tests reported in this thesis work have been carried out in a bubbling fluidized bed, 102mmID and 2.5m high, at a fixed equivalence ratio ($ER=0.25$), a gas velocity in the range 0.4-0.5m/s and a reactor temperature of 850 °C. The gasification apparatus is a BFB made of AISI 316L, 102 mm ID and 2.5 m high.

Experimental conditions

Fuel	P8 plastics (30%), coal (50%) and wood (20%)	P8 plastics (30%), coal (50%) and wood (20%)	P8 plastics (30%), coal (50%) and wood (20%)
Oxidant	Air	Air	Air
Material bed	Quartz sand	Olivine	70% Olivine- 30% Dolomite
E.R. ratio (oxygen/stechyometric oxygen)	0.25	0.25	0.25
Fuel flow rate (g/min)	20	20	20
Oxidant flow rate (Nl/h)	3000	3000	3000
Cold gas velocity (m/s)	0.4-0.5m/s	0.4-0.5m/s	0.4-0.5m/s
BED Temperature (°C)	850	850	850

Tab.2.4 Experimental condition of the bubbling fluidized bed gasification system

In this section the gas and condensed phases analyses are reported for different bed materials. as Quartz sand, Olivine, and a mixture of bed materials (70% Olivine -30% Dolomite).

- quartz sand is the typical bed material utilized for both circulating and bubbling fluidized bed gasification and combustion;
- olivine is a ferrous-magnesium silicate that has been recently utilized in bubbling fluidized bed gasification of biomasses with good results. The tested olivine comes from Austria and has the following composition: MgO=48-50%; SiO₂=39-42%; Fe₂O₃=8-10.5%; Al₂O₃+Cr₂O₃+Mg₃O₄=0.8%; CaO<0.4%.
- dolomite is a calcium-magnesium carbonate, called, whose catalytic properties are well known and used in reactors where the thermochemical conversion of solid fuels is required.

The composition of syngas has been obtained by analysis downstream the cleaning syngas line constituted by a water bubbler and two filters.

It must be highlighted that the effect of cleaning can be crucial if the syngas is rich of condensable and/or soluble compounds that remain trapped in the water and in the filters.

The syngas, where the principal components are H₂, CO, CO₂ and CH₄, is sampled downstream the main sampling line for the identification and quantification of PAHs and the evaluation of NH₃, HCl, and H₂S.

Condensed species were analyzed by means of gas chromatography/mass spectrometry (GC-MS) for the quantification of PAH up to 300 u. GC-MS was performed on an Clarus 500-GC gas chromatograph equipped with an DB-35Ms crosslinked 5% PhMe siloxane 30 m x 0.25 mm x 0.25 μm film thickness column coupled with an Clarus 500-Ms mass spectrometer with an electron impact/chemical ionization ion source.

The analysis was performed on the condensed phases trapped in an ice-cooled trap and on condensed species extracted by DCM on the filter.

2.4 Flame Temperature Measurements

Flame temperature was measured using a fast-response thermocouple by means of a fast-insertion procedure. The thermocouple was made using thin wires of Pt / Pt - 13% Rh having a diameter of 25 μm .

Thermocouple was inserted into the flame for a time of a few hundred milliseconds to prevent the soot covering, in order to avoid the change of both the surface emissivity and the thermal conductivity coefficient of the thermocouple.

The data obtained were corrected taking into account the radiative losses. The correction may be estimated by equating the heat transferred to the probe from the gas to that lost by radiation:

$$2 * \frac{\lambda}{d} * (T_g - T_w) = \varepsilon * \sigma * (T_c^4 - T_w^4)$$

λ = gas thermal conductivity

d = thermocouple bed diameter

T_g = gas temperature

T_c = temperature measured by thermocouple

ε = thermocouple emissivity

σ = Stefan Boltzmann constant ($=1.355*10^{-12}$ cal sec⁻¹ cm⁻² K⁻⁴)

T_w = room temperature

The measuring procedure above described gives out the temperature of the gas (T_g) with error of about 100 K.

2.5 Extinction measurements

Extinction at fixed wavelength was used in order to obtain in “situ” measurements of the soot volume fraction axial profile. This technique, widely used in the combustion experiments for his easiness, provides instantaneous and not intrusive measurements. The extinction measurements were obtained using a solid-state laser operating at 632 nm and a power meter

equipped with an interferential filter to measure the laser light intensity at different heights above the burner on the flame axis.

Different experiments have shown that soot and PAHs, present in a gas mixture, absorb at different wavelengths. It was also observed that PAH absorption decreases gradually, moving downstream from ultraviolet to the visible region (McKinnon, 1989; Weiner e Harris, 1989), so, using a 632 nm wavelength is possible to neglect the rate of radiation absorbed by PAHs and condensed species present in the flame and to consider the signal reduction due only to soot absorption.

For extinction measures it is important to evaluate the initial intensity of laser radiation, I_0 , this value is obtained when the flame is off. In the extinction profiles are reported the coefficient extinction profiles, K , in function of the distance above the burner (z).

K is a function of the radiation intensity according to the law:

$$K(z) = \frac{1}{L(z)} * \ln \frac{I_0}{I(z)}$$

$L(z)$ = optical path measured at different heights above burner

I_0 = unperturbed radiation intensity

$I(z)$ = radiation intensity measured at different flame heights

In the hypothesis that the radiation scattered and/or reflected from the flame is negligible the reduction of radiation intensity for high flame height is due only to soot particle absorption and K is proportional to the soot volume fraction f_v :

$$K(z) \propto f_v(z)$$

where:

$$f_v = \frac{\pi}{6} * N * d^3$$

The soot profile measured by extinction measures can be compared to the gravimetric concentration profile obtained from sampling in order to obtain information about the optical characteristics of the soot.

2.6 Analysis of Gas-phase

The reactant and combustion gases, devoid of condensable species and soot, were sampled along the flame axis and driven to two gas chromatograph valves. On-line gas analysis of C1–C6 hydrocarbon species was carried out using an HP5890A gas chromatograph equipped with a 7515 Chrompack Al₂O₃=KCl 50m \times 0.92-mm (i.d.) capillary column and a flame ionization detector (GC-FID). Another HP5890A gas chromatograph equipped with an 8700 Alltech coaxial column and a thermal conductivity detector (GC-TCD) was used to perform the the analysis of CO₂, CO, H₂, and N₂.

2.7 Analytical characterization of particulate matter

The complete analytical characterization scheme of particulate matter is shown in figure 2.4 The condensed species collected on the probe walls, on the teflon filter and in ice-cooled trap were extracted by dichloromethane (DCM) and separated from soot.

The extracted organic species were named DCM-extract. The soot was washed with dichloromethane until there was no significant fluorescence signal in the washing solvent, in order to extract the organic species adsorbed on it.

Both the DCM-extract dried under vacuum and the soot were weighed in order to obtain the soot and condensed species concentration in flame (mg/Nl).

Polycyclic aromatic hydrocarbons (PAHs) in the condensed species up to 300u (coronene), were analyzed and quantified by gaschromatography-mass spectrometry (GC– MS) on a HP5890 gas chromatograph, equipped by a HP-5970 mass spectrometer.

This technique, commonly adopted in the field of combustion chemistry, allows only the qualitative and quantitative analysis of the species having molecular weight up to 300-400.

After the DCM-extraction, soot was re-extracted with a little volume of 1-methyl-2-pyrrolidinone (NMP) in order to detach strongly adsorbed species.

The extract obtained is named NMP-extract. Both DCM-extract and NMP-extract were separated by SEC (Size Exclusion Ghromatography) for further analysis by spectroscopic and mass spectrometric techniques.

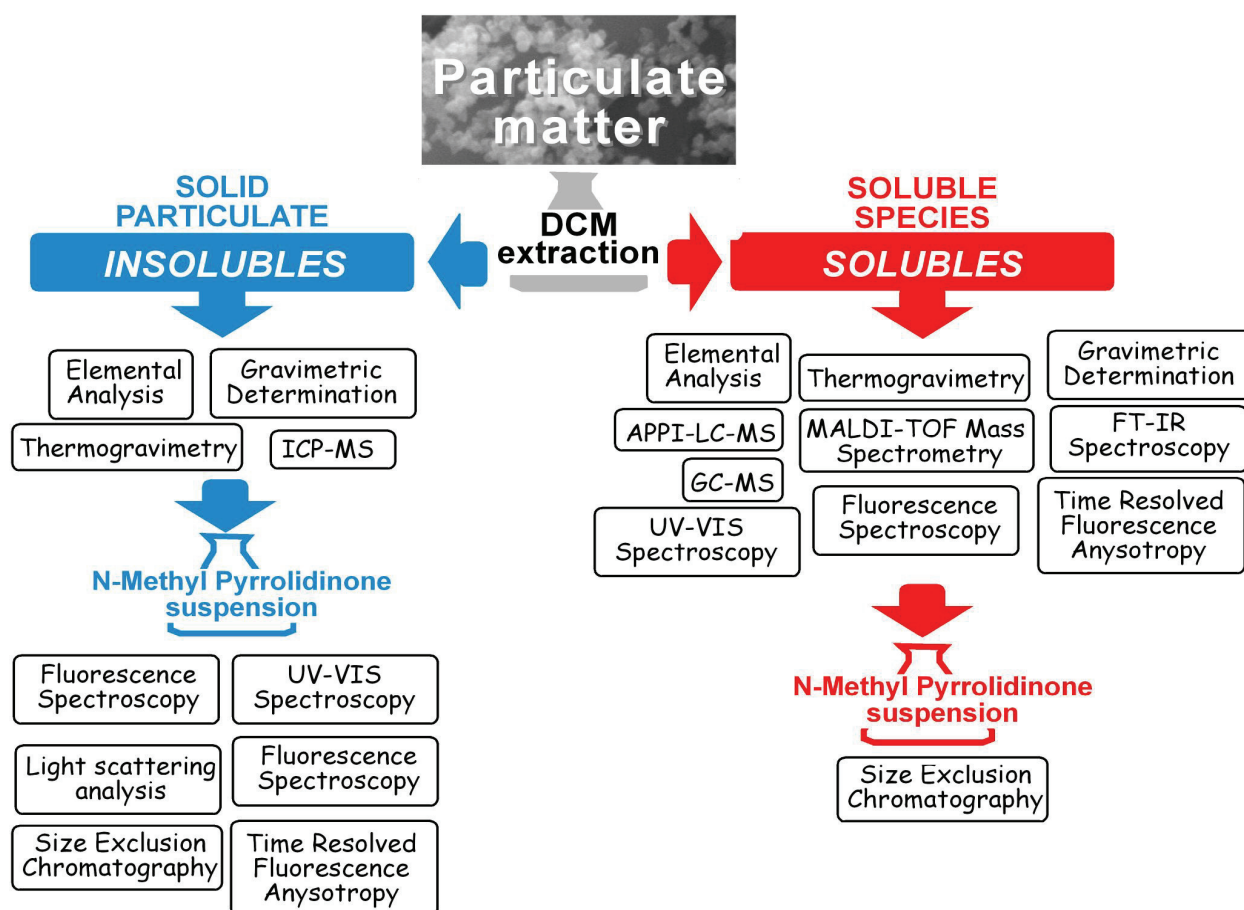


Fig 2.4 Analytical characterization scheme of particulate matter.

2.7.1 Thermogravimetric analysis (TGA)

Thermogravimetric analysis or thermal gravimetric analysis (TGA) is commonly used to determine the degradation temperatures, the level of inorganic and organic components in materials, the decomposition points and weight changes in a material in a controlled atmosphere system in function of time and temperature.

In this work, TGA was used to determine the weight changes in condensed species and soot samples in function of temperature change.

Analysis is carried out increasing the temperature gradually and plotting the weight loss percentage against temperature. The temperature in many testing methods routinely reaches 1000°C or more. In this work, the thermogravimetric analyses (TGA) were performed on a Perkin-Elmer Pyris 1 TGA thermogravimetric analyzer by heating the soot at atmospheric pressure in oxidative environment (air, 30 ml/min) from 30°C up to 850°C at a rate of 10°C/min.

2.7.2 Gas chromatography-mass spectrometry (GC-MS)

Gas chromatography interfaced with mass spectrometry identify and quantify species in condensed phase with molecular weight from 128 u (naphthalene) and 300 u (coronene.).

This technique uses a gas chromatograph HP 5890 equipped with a column HP-5MS Crosslinked 5% PhMe Siloxane 30m * 0.25mm* 0.25 µm film thickness column, coupled with an HP 5970 and mass spectrometer with electronic impact ions / chemical ionization source (EI / CI).

The mass spectrometry detector allows to quantify PAHs using the factors response of known composition mixtures. The species identification is made by comparison with mass spectrum in Wiley computer library with 138,000 spectra. Using a detector equipped with "particle beam" mass spectrometry it is possible the PAHs identification up to a molecular weight of 400 u.

2.7.3 UV–Visible absorption spectroscopy

The absorption of ultraviolet or visible radiation by a molecule is due to electronic transitions, i.e. the promotion of an electron from an orbital of lower energy to one of higher energy. This mainly occurs for unsaturated compounds i.e. compounds with at least a double bound like ethylene up to benzene and polycyclic aromatic compounds. As the number of double bounds and/or the conjugation degree of these bounds increase the absorption wavelength increase. Moreover the increase of conjugation and/or aromatization degree cause also a steep increase of the absorption coefficients that can vary by as much as a factor of two, tree order of magnitudes going from benzene to PAH (Clar, e., 1974).

On this basis, it can be affirmed that aromatic species like benzene and PAHs should be the main responsible for uv-visible absorption in spite of their relatively low abundance with respect to light unsaturated hydrocarbon ethylene, acetylene, etc. usually present in relevant amounts in fuel-rich combustion process. In this sense graphitic materials like soot and tar, having a high aromatization degree, are highly absorbing species in the uv-visible range. As a consequence, the uv-visible absorption technique is particularly useful to follow the formation of aromatic and carbonaceous species that are typical products of fuel-rich combustion processes (Friedel, 1970).

UV–visible spectra (200–800 nm) of the soot and condensed species sampled were measured on an HP 84523 diode array spectrophotometer connected to a computer. Soot is dissolved in 1-methyl-2-pyrrolidinone (NMP) while the condensed species are dissolved in DCM, using 1 cm quartz cuvette, with a concentration about (10–20 mg/l) in order to avoid the signal saturation. NMP has the ability, not only, to well dissolve condensed PAHs and other species with greater molecular mass, but also to disperse very fine soot particles, making it possible to extend the application of UV-visible in the solid phase too. The interference of the NMP on the UV absorption limits the evaluation of the spectra to 260– 800 nm wavelength range. (240–800 nm, for DCM).

2.7.4 Fluorescence emission spectroscopy

Fluorescence spectroscopy is an useful diagnostic tool to evaluate polycyclic aromatic hydrocarbon (PAH) in complex PAH mixture (Lee M.L. et al. 1981).

Fluorescence is a spectroscopic method of analysis where the molecules of the sample are excited by irradiation at a certain wavelength and emit radiation of a different wavelength. The emission spectrum provides information for both qualitative and quantitative analysis. When light of a suitable wavelength is absorbed by a molecule, the electronic state of the molecule changes from the ground state to the one of the several vibrational levels of the excited electronic state.

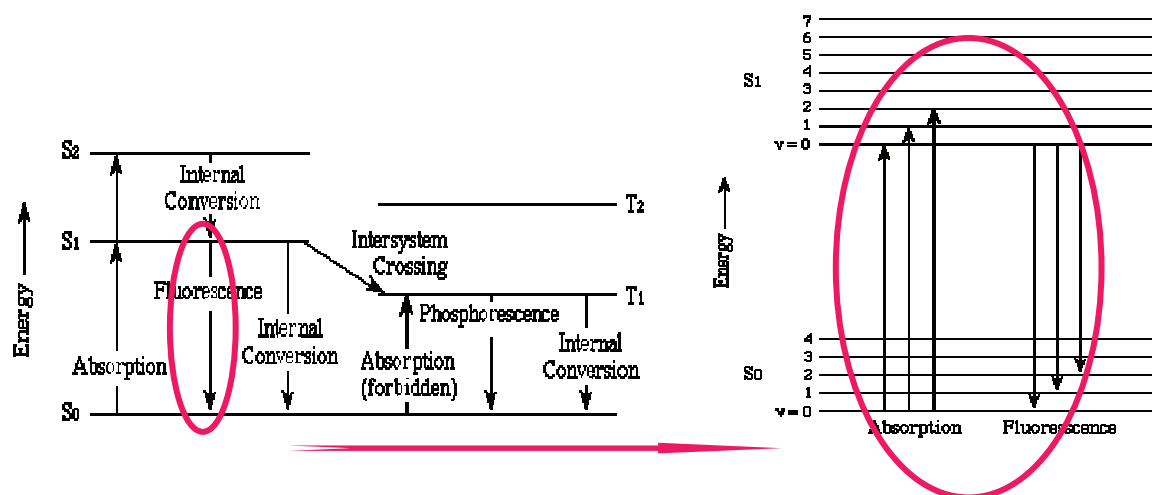


Fig 2.5 Scheme of fluorescence emission energy.

The excited electronic state is usually the first excited singlet state, S_1 (Figure 2.5).

In consequence of the absorption, a number of vibrational levels of the excited state are populated.

Molecules in these higher vibrational levels when relax to the lowest vibrational level of the excited state (vibrational relaxation) emit its energy as “fluorescence”. In particular, the fluorescence corresponds to the relaxation of the molecule from the singlet excited state to the singlet ground state with emission of radiation. The fluorescence lifetime is about $\sim 10^{-8}$ sec.

Fluorescence emission spectra of the samples were measured at $\lambda_{exc} = 350$ nm on a Perkin-Elmer LS-50 spectrofluorimeter connected to a computer. A xenon discharge lamp equivalent to 20 kW for 8 μ s duration was used as excitation light source.

The detection device was a gated photomultiplier with modified S5 response for operation to about 650 nm. Monk-Gillieson type of monochromator was used which covers the following ranges: excitation 200–800 nm, emission 200–900 nm. The wavelength accuracy was ± 1.0 nm and the wavelength reproducibility was ± 0.5 nm.

Instrumental parameters were controlled by the Fluorescence Data Manager Perkin-Elmer software.

2.7.5 Ft-IR spectroscopy

FT-IR (Fourier Transform Infrared) Spectroscopy, or simply FT-IR Analysis provides information about the chemical bonding or molecular structure of materials, both organic and inorganic.

FT-IR analyses in the $3400\text{--}2700$ cm^{-1} wavenumber region of standard mixtures, condensed species and soot with carbon tetrachloride as solvent was performed on a Perkin-Elmer 1600 FT-IR spectrophotometer.

2.7.6 Elemental Analysis

Elemental analysis was used for carbon, hydrogen, and nitrogen (CHN) analysis of particulate matter. In particular, the H/C ratios of soot and condensed species samples were measured by a Perkin-Elmer 2400 CHNSO elemental analyzer.

2.7.7 Size Exclusion Chromatography (SEC)

SEC analysis for the evaluation of molecular weight distribution of particulate matter and its fraction was carried out on a liquid chromatograph equipped with UV-visible diode array detector.

The SEC chromatography is a chromatographic method that separates molecules in solution according to their size (more correctly, their hydrodynamic volume). The principle underlying the SEC is that particles of different size elute through a stationary phase at different velocities.

A requirement for the SEC is that the sample does not interact with the surface of stationary phases. The different elution times are based solely on the molecular size, a small molecule can penetrate every corner of the pores system of the stationary phase "sees" both the pore volume and interparticle volume and elute later ("see" ~ 80 % of the volume of the column). On the other hand, a very large molecule cannot penetrate the pore system and "sees" only the interparticle volume (~ 35% of the volume of the column) so it elutes faster.

Typically, the SEC elution order is in inverse relation with MW, i.e., the lower the MW the longer the elution time. The SEC analysis of soot extracts and condensed species was carried out by elution with 1-methyl-2-pyrrolidinone (NMP) on a PL-gel styrene-divinylbenzene individual pore column (Polymer Laboratories, Ltd, UK) with a stationary phase particle diameter of 5 μm and a pore dimension of 50 nm. This column is able to separate polystyrene standards in to the molecular mass range from 100 up to 10^5 u (corresponding to particles up to 5 nm of diameter). The plot of polystyrenes and PAH molecular mass versus retention time reported in fig 2.4, is used as reference for the evaluation of the MW of soot extracts. The injection volume was 100 μl and the analyses were performed at a temperature of 80 °C with a flow rate of 0.5 ml/min. The on-line detection of species eluted from the SEC column was an HP1050 UV-visible diode array detector that measured the absorbance signal (265 nm for polystyrene standards and 265, 280, 350, 450 and 500 nm for the samples).

The detector also allows the acquisition of the complete UV-visible spectra (200-600 nm) in correspondence of the chromatographic peaks of the eluting species. Polystyrene (PS) standards (Polymer laboratories) in the molecular mass range 580-13,200,000u were used in order to obtain the calibration curve.

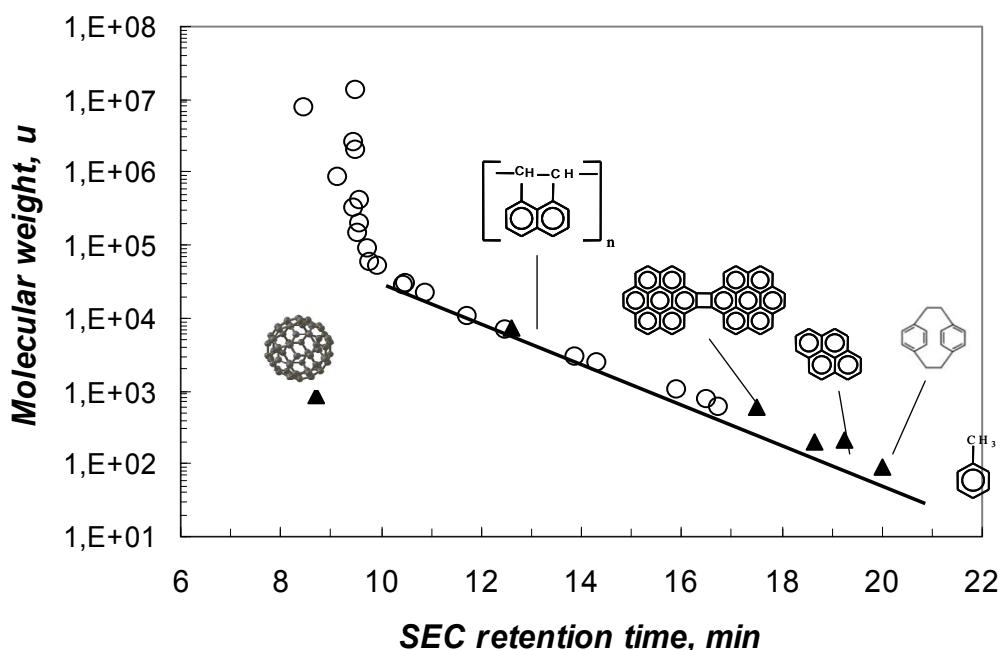


Fig 2.6 SEC polystyrene calibration curve (o). Other standard compounds are reported on the curve as follows: (▲) polyacenaphthylene, dicoronylene, paracyclophane, fullerite, pyrene, and toluene.

The exclusion limit of the column is detected at 9.8 min (MW 59,500u) and the calibration curve is linear in the 580-59,500u MW range, thus allowing the reliable evaluation of MW (figure 2.6). The separation beyond 59,500 u up to 13,200,000u is very poor although a rough MW separation can be still observed. In order to test the reliability of the PS calibration curve for molecules with a large number of condensed aromatic rings, the following standards from Aldrich were tested: polyacenaphthylene (7500u), fullerite (C60, 720u, and C70, 840u), dicoronylene (596u), paracyclophane (208u), and pyrene (202u). The permeation limit is defined by toluene (92u) which eluted at 20 min.

CHAPTER 3

RESULTS AND DISCUSSION

Results and discussion

3.1 Methane flames

The sooting structure of fuel-rich methane/O₂ flames (C/O=0.60) burning at two different cold-gas flow velocities ($v=4$ and 5 cm/s), i.e at two different flame temperatures, is given by the profiles of temperature and extinction coefficient measured with a laser at 632 nm and reported in Fig. 3.1. The maximum temperature, located at the same height above the burner (2.2 mm) in both flames is lower, 1650 K, at lower cold-gas velocity ($v=4$ cm/s) and higher (1770 K) in the higher cold gas velocity ($v=5$ cm/s) flame. In this temperature range the decrease of the extinction signal, mainly due to absorption of soot particles, testifies the lower sooting tendency of methane in higher temperature conditions in agreement with the bell-shaped profile of soot yield as a function of temperature (Bohm H., et al. 1988).

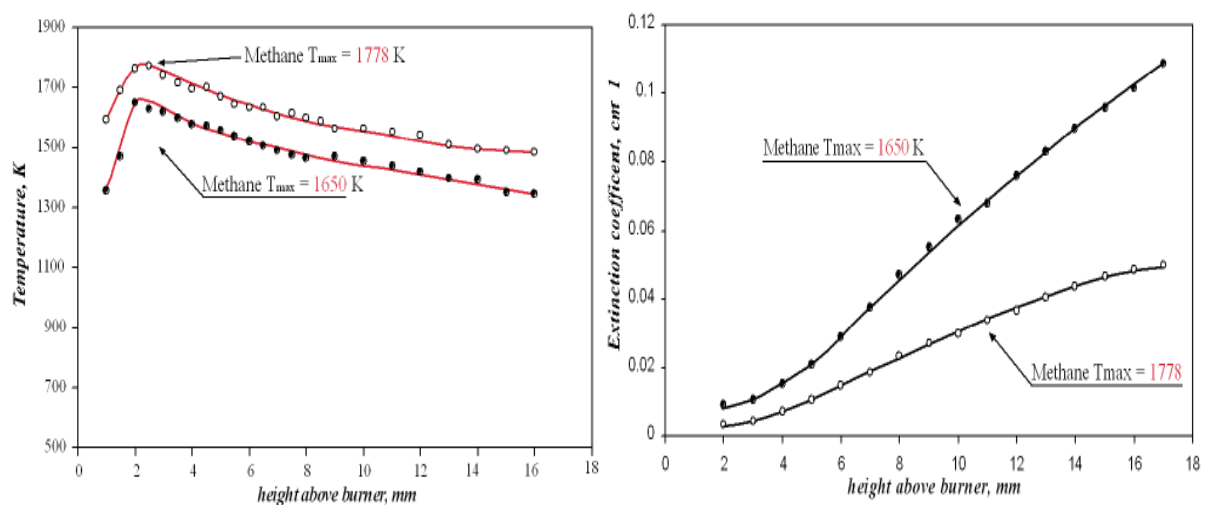


Fig. 3.1 Temperature and extinction coefficient profiles measured along the axis of methane flames burning at $v=4$ cm/s (T_{max} 1650K) and at $v=5$ cm/s (T_{max} 1780K).

3.1.1 Concentration profiles of Gas species

The axial concentration profiles of reactants and main combustion products measured in the higher and lower temperature conditions are reported in Fig. 3.2. To account for thermal probe effects the mole fraction profiles were shifted 3.4 mm and 1.5 mm upstream for the $v=4$ cm/s and $v=5$ cm/s flames, respectively by considering that the maximum of CO formation rate has to correspond to the maximum temperature.

In both flames the main oxidation zone extends up to 3 mm where the complete oxygen consumption and the maximum formation of combustion products (CO, CO₂ H₂) occurs.

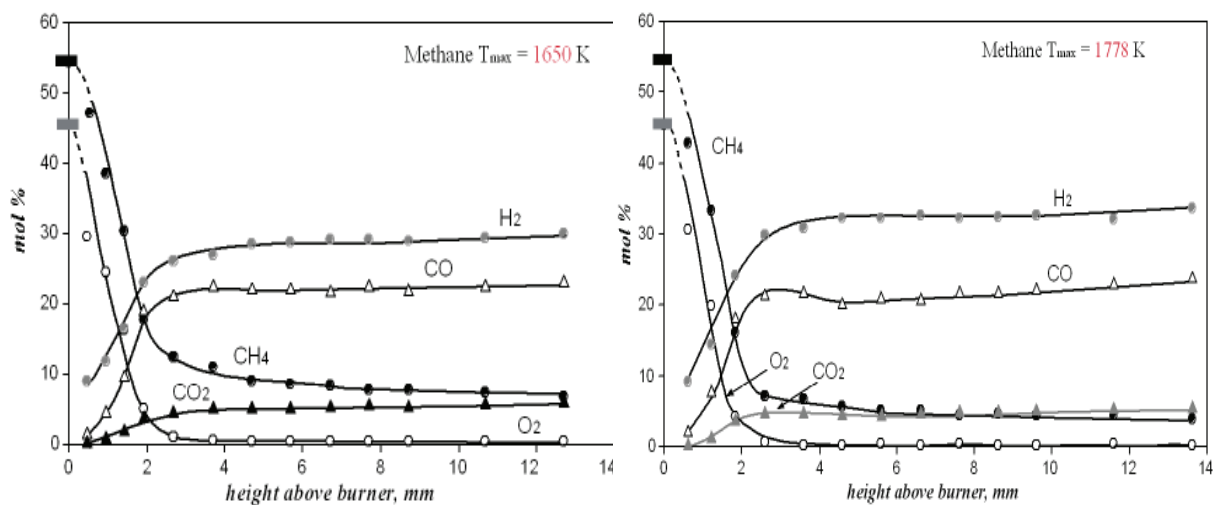


Fig. 3.2 Concentration profiles of reactants and main combustion products in the high temperature ($v=4$ cm/s (left) and low temperature ($v=5$ cm/s) (right) methane flames.

A larger oxidation/decomposition of CH₄ with a higher formation of H₂ can be noted in the flame at higher temperature ($v=5$ cm/s). This is consistent with the higher formation of a dehydrogenated product as C₂H₂ whose concentration profile, contrasted with the H₂ profile, is reported in Fig. 3.3.

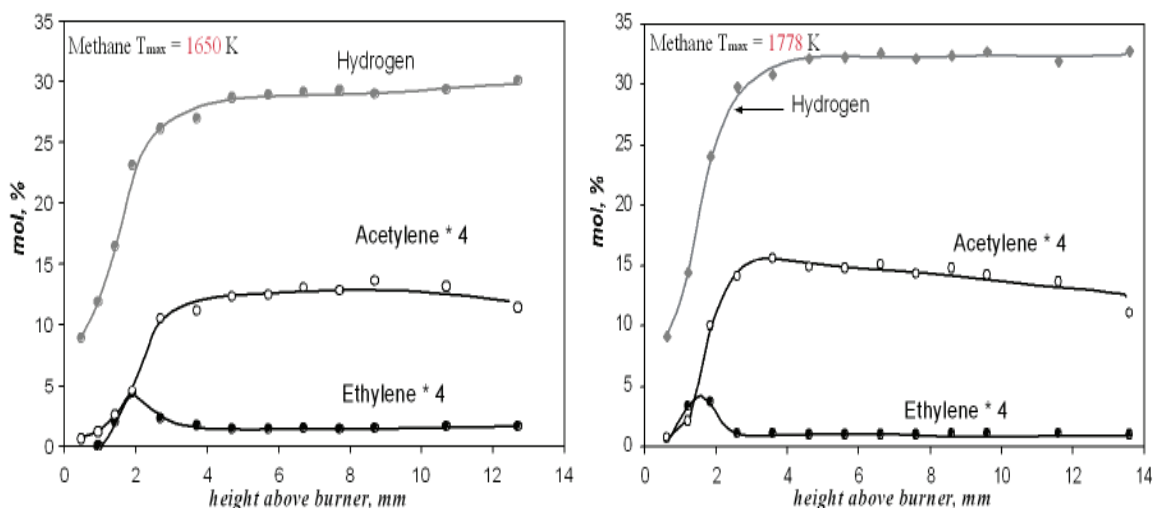


Fig. 3.3 Concentration profiles of hydrogen, ethylene and acetylene in the low temperature ($v=4$ cm/s) (left) and high temperature ($v=5$ cm/s) (right) methane flames.

In the main oxidation zone of both flames the ethylene concentration profile, also reported in Fig. 3.3, presents the rise-decay profile typical of reaction intermediates being readily dehydrogenated to acetylene that reaches the maximum concentration later on.

The concentration profiles of minor C_3 and C_4 hydrocarbons are reported in Fig. 3.4 for both flames. They are mainly composed of unsaturated hydrocarbons as propene, propyne, butadiene, diacetylene, butyne and 1-butene-3-yne.

Propene, 1,2-propadiene, butyne and butadiene are reaction intermediates being formed in the oxidation zone and readily destroyed at the end of the oxidation region.

Propyne and diacetylene are formed downstream the oxidation region and slightly decrease in the pyrolysis region of the flames.

The concentration profiles of C_3 - C_4 products do not show significant differences in the two temperature conditions with the exception of diacetylene that, similarly to the acetylene (Fig. 3.3), is produced in larger amounts in the higher-temperature flame.

Figure 3.5 reports the concentration profiles of benzene and cyclopentadiene. Similar trends are observed in both flames: benzene concentration rises in the main oxidation zone reaching a constant value at the beginning of the postoxidation region; cyclopentadiene shows a rise-decay profile peaked in the main oxidation region before the maximum formation rate of benzene, consistently with its role both in benzene oxidation

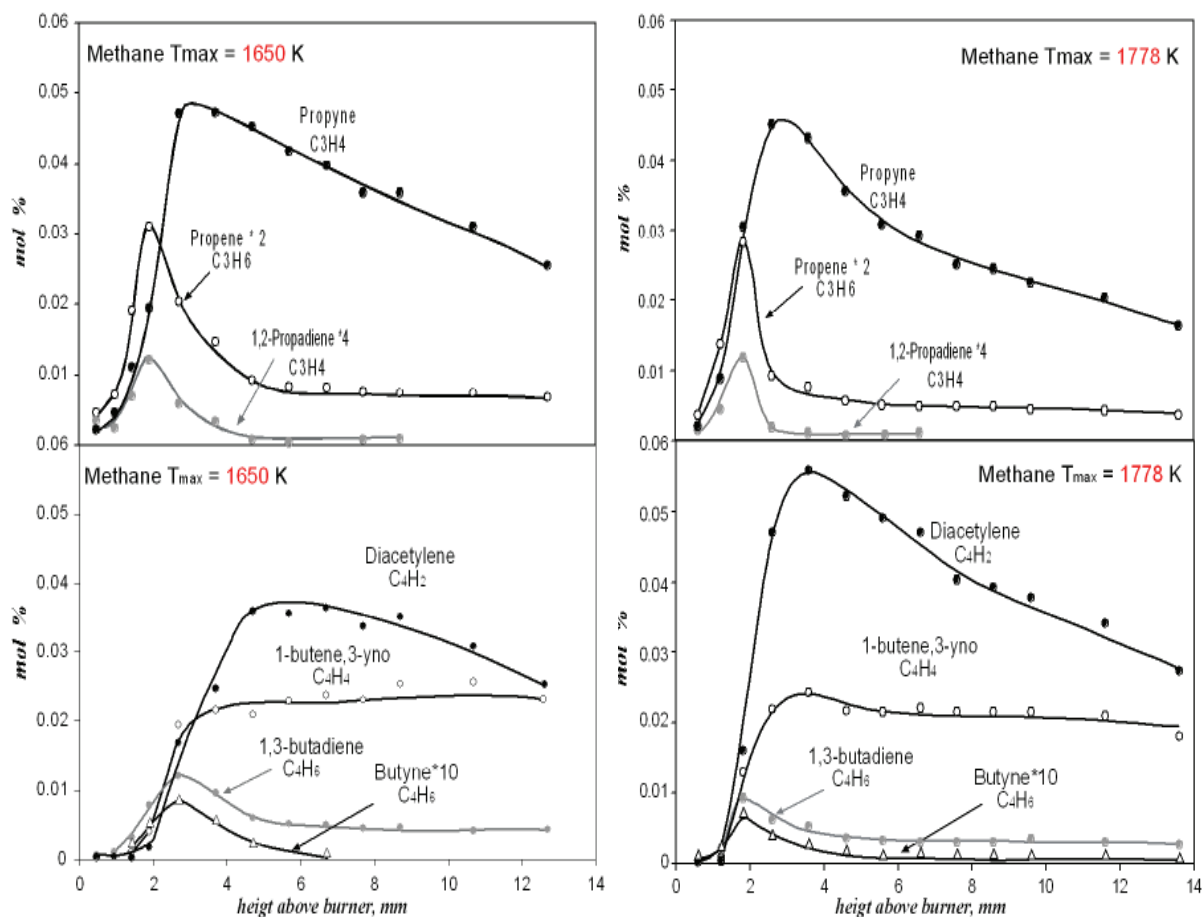


Fig. 3.4 Concentration profiles of the most abundant C_3 (upper) and C_4 hydrocarbons (lower) in the low temperature ($v=4$ cm/s) (left) and high temperature ($v=5$ cm/s) (right) methane flames.

and in naphthalene formation process through the self-combination of resonantly stabilized cyclopentadienyl radicals (Ciajolo et al., 1994; Galvez, M. Herlin-Boime, et al. 2002). It is noteworthy that the yields of benzene and cyclopentadiene are higher in the lower temperature flame ($v=4$ cm/s).

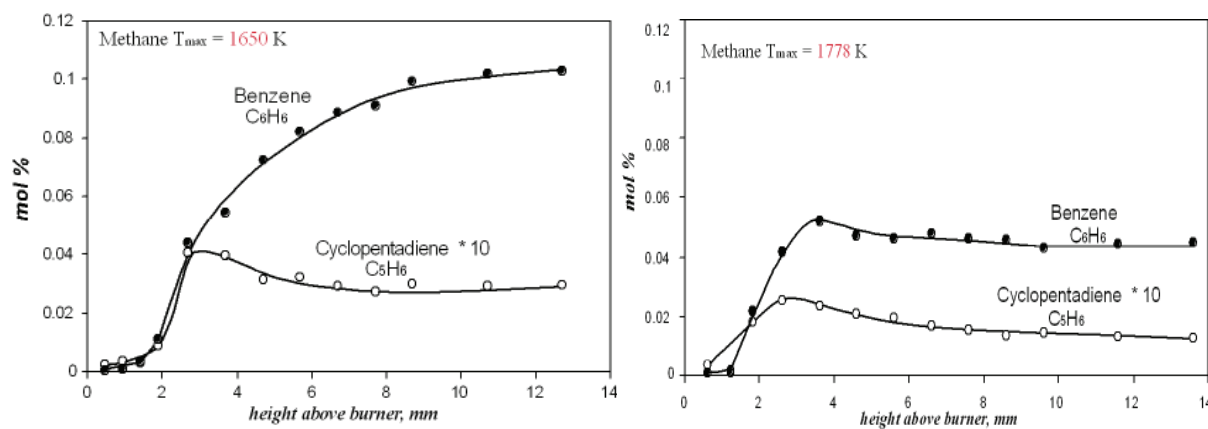


Fig. 3.5 Concentration profiles of cyclopentadiene and benzene in methane flames in the low temperature at $v=4$ cm/s (left) and high temperature ($v=5$ cm/s) methane flames at (right).

3.1.2 Concentration profiles of condensed phases

Figure 3.6 reports the concentration profiles of soot and condensed species, constituting the condensed phases and separated by their extraction with dichloromethane. The analysis of condensed species soluble in dichloromethane has been carried out by means of gas chromatography/mass spectrometry (GC-MS) for the identification and quantification of PAH up to 300 u. The profiles of total PAH concentration is also reported in Fig. 3.6.

In the lower temperature flame, condensed species and soot concentration rise along the flame with the soot inception occurring after condensed species appearance and just downstream the oxidation zone. Moreover, soot concentration is lower than condensed species concentration along the whole flame. Soot and condensed species are formed in lower amounts in the higher-temperature flame and the condensed species exhibit a maximum in correspondence of the maximum soot formation rate, suggesting their role in soot formation process. It is noteworthy that the larger soot yield is higher in the flame where benzene concentration is higher (Fig.3.6) and acetylene is lower (Fig. 3.3). This is in agreement with previous study showing that PAH and soot formation processes in the methane flame are not influenced by the levels of acetylene present in the flame (Melton, et al., 1998).

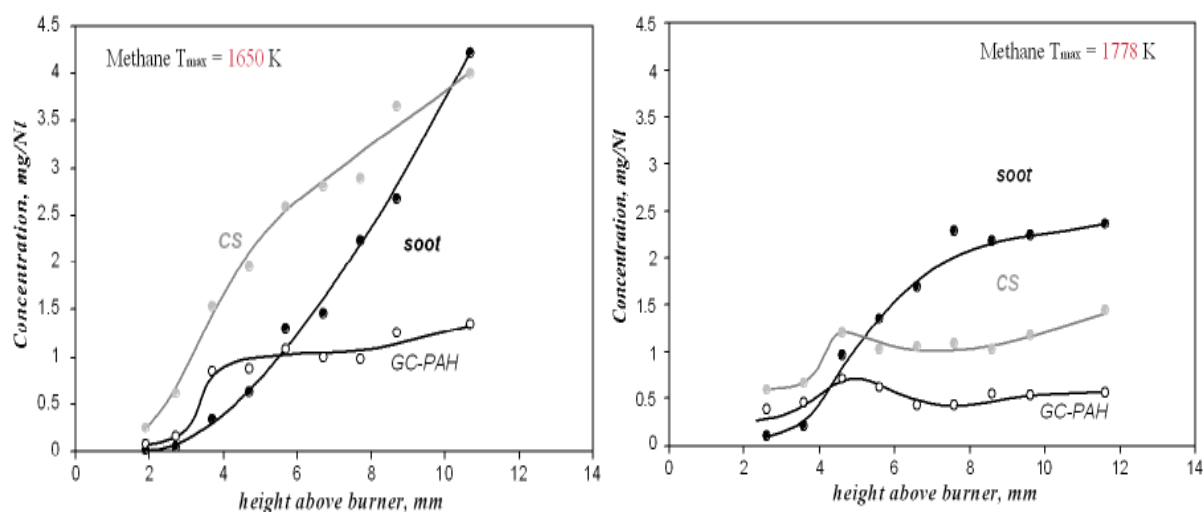


Fig. 3.6 Concentration profiles of GC-PAH, DCM soot extract and soot in methane flames at $v=4$ cm/s (left) and at $v=5$ cm/s (right)

3.1.3 Analysis of condensed species (Gaschromatography-Mass spectrometry)

The single PAH, whose profiles are reported in Figs. 3.7-3.10, exhibit the typical distribution with a larger abundance of small PAH (naphthalene and acenaphthylene) and a lower presence of larger PAH up to coronene.

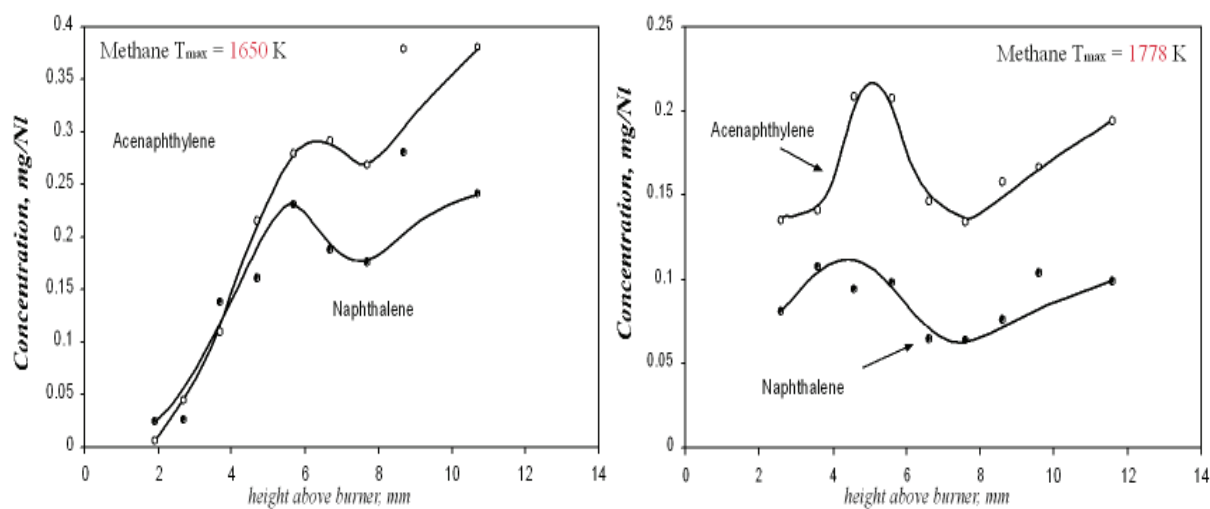


Fig.3.7 Concentration profiles of acenaphthylene and naphthalene in the low temperature at $v=4$ cm/s (left) and high temperature ($v=5$ cm/s) (right) methane flames.

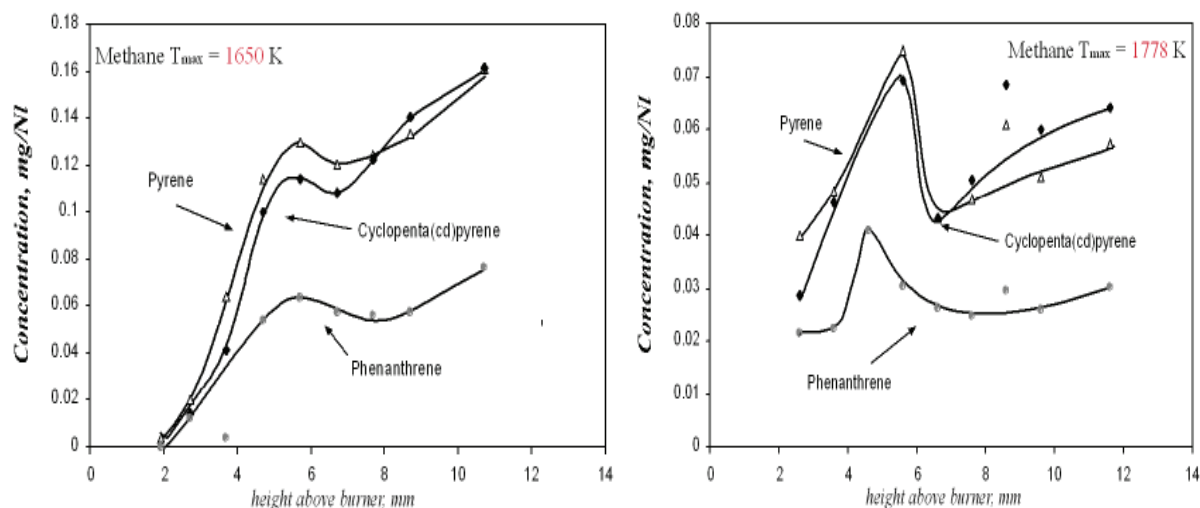


Fig.3.8 Concentration profiles of cyclopenta(cd)pyrene, pyrene and phenanthrene in the low temperature ($v=4$ cm/s) (left) and high temperature ($v=5$ cm/s) (right) methane flames.

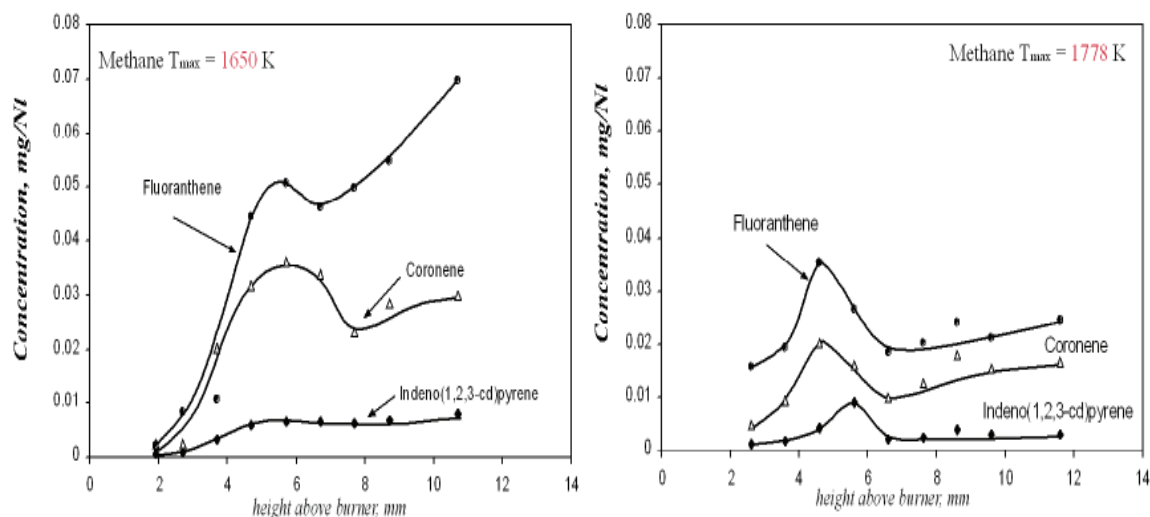


Fig.3.9 Concentration profiles of fluoranthene, coronene and indeno(1,2,3-cde) in the low temperature ($v=4$ cm/s) (left) and high temperature ($v=5$ cm/s) (right) methane flames.

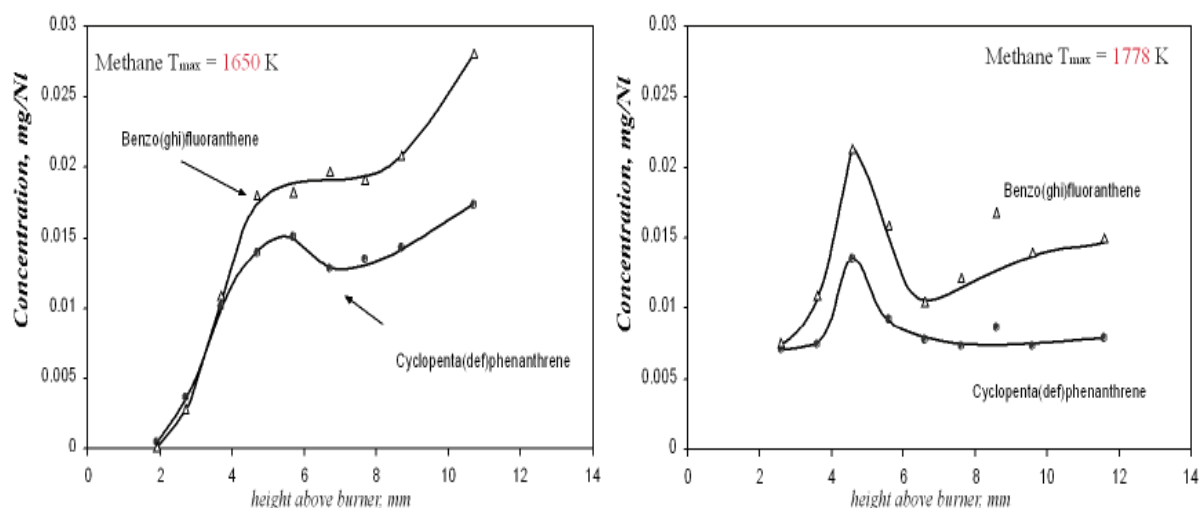


Fig.3.10 Concentration profiles of benzo(ghi)fluorantene and cyclopenta(def)phenantrene in methane flames at $v=4$ cm/s (left) and at $v=5$ cm/s (right).

3.1.4 Soot characterization

Thermogravimetric (TG) analysis of soot was performed by heating it from 50 to 800 °C in air flow in order to obtain insights about soot oxidation reactivity that is related to its morphology and composition.

The temperature of the maximum combustion rate of soot (i.e. the temperature to which the maximum weight loss occurs) along the flame axis is reported in Fig. 3.11. As higher is the maximum combustion temperature lower is the oxidation reactivity.

Overall, soot exhibits an increase of the maximum combustion temperature, from 620 to 660°C, along the flame testifying the decrease of soot oxidation reactivity during the soot formation/maturation process. It is noteworthy that the oxidation reactivity of high-temperature flame soot is lower respect to the low-temperature flame soot.

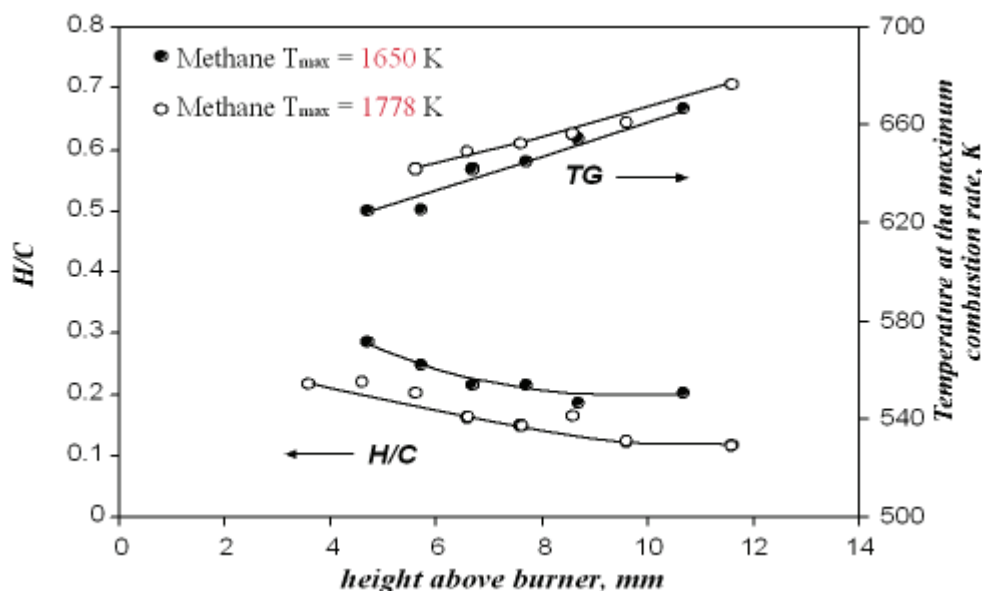


Fig. 3.11 Temperatures of the maximum combustion rate under air (30 ml min^{-1}) and H/C atomic ratio of low-temperature methane soot at $v=4 \text{ cm/s}$ (●) and high-temperature methane soot at $v=5 \text{ cm/s}$ (○) as a function of height above burner.

The H/C atomic ratios, also reported in Fig. 3.11, slightly decrease as soot ages along the flame axis testifying the progressive soot evolution toward a more graphitic organization (Emdee J.L. et al. 1992).

The H/C of the high-temperature flame soot is lower with respect to the low-temperature flame soot indicating a higher degree of dehydrogenation consistently with the higher formation of hydrogen and acetylene products in the high-temperature flame (Figs. 3.2-3.3). To this lower H/C ratio can be attributed the lower oxidation reactivity of soot before described.

The decrease of H/C should imply a change of the internal electronic structure in terms of the increase of sp^2/sp^3 hybridization ratio corresponding to the increase of graphitic planar structures (<http://www.combustioninstitute.org/Connections/4F02.pdf> 5). The UV-Visible spectroscopy reported in the following is a suitable diagnostic tool for investigating the electronic structure of carbonaceous materials because of its sensitivity to the sp^2 and sp^3 hybridization states.

3.1.5 UV-Visible Spectroscopy of condensed species and soot

Fig. 3.12 shows the normalized absorbance spectra of condensed species in the two flame temperature conditions. In the low-temperature flame it can be noted that along the flame the absorbance increases in the visible with respect to the UV region indicating the increase of aromatic size. This does not occur in the high-temperature flame where the spectra appear to be similar at different heights above burner.

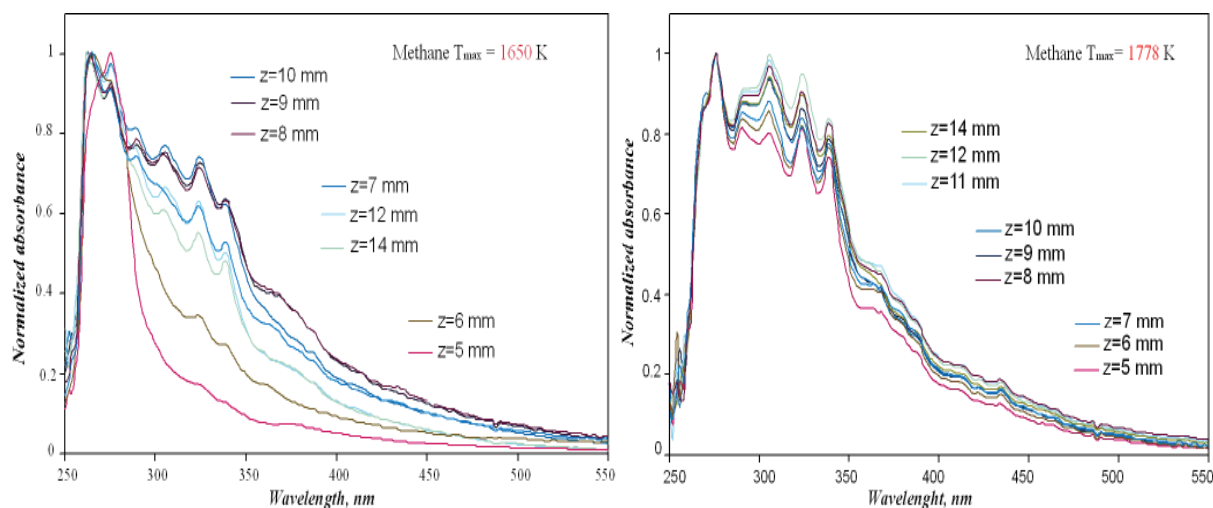


Fig. 3.12 Normalized UV-visible spectra of condensed species in methane flames at $v=4$ cm/s (left) and at $v=5$ cm/s (right).

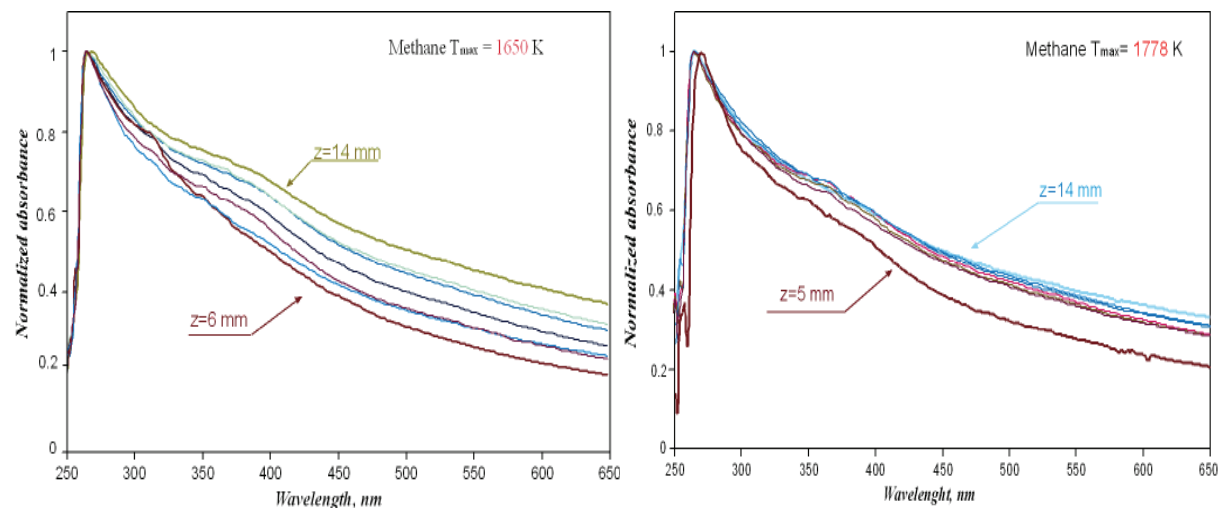


Fig. 3.13 Normalized absorbance of soot in methane flames at $v=4$ cm/s (left) and at $v=5$ cm/s (right).

UV-visible spectra of soot, reported in Fig. 3.13, exhibit a broad shape with the maximum absorbance peaked in the UV and decreasing toward the visible. It is noteworthy that, similarly to condensed species, in the low-temperature flame the absorbance in the visible

gradually increase with respect to UV along the flame whereas this feature is much less evident in the high-temperature flame where the increase in the visible occurs suddenly only at the beginning of soot formation region.

The absorption coefficients of soot in the UV (300 nm) and in the visible (500 nm), reported in Fig. 3.14, are expressed on mass basis (m^2/g) since soot suspensions are complex mixtures of unknown molecular weight.

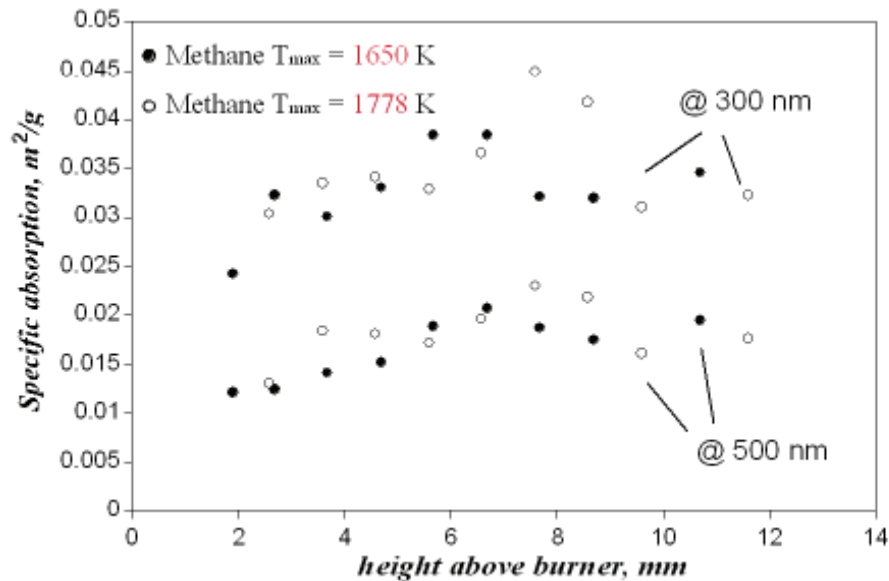


Fig. 3.14 Specific absorption (m^2/g) of methane soot at $v=4 \text{ cm/s}$ measured at 300 nm (●) and 500 nm (●) and at $v=5 \text{ cm/s}$ measured at 300 nm (○) and 500 nm (○).

It is noteworthy that the soot absorptivity slightly increases along the flames reaching a final value that is much lower than that shown by soot produced in flame of other hydrocarbons (Tregrossi A. and Ciajolo A., 2007; Tregrossi A. and Alfè M., 2007).

This suggests that the aromaticity of methane soot is quite independent on the flame temperature and generally lower than that of soot formed from other less hydrogenated hydrocarbons as heptane, ethylene, etc. (Tregrossi A. and Ciajolo, 2007).

3.1.6 FT-IR analysis of condensed species and soot

More studies suggest that soot formed in premixed flat flames can contain a substantial amount of aliphatic compounds. Presence of these compounds may affect the kinetics of soot mass growth and oxidation in a way that is currently not understood.

Using a FT-IR (Fourier Transform Infrared) Spectroscopy is possible to obtain information about the chemical bonding or molecular structure of materials.

In this section the FT-IR was used for to analyze the composition of condensed species and soot sampled by methane flames at two different height above burner in particular 8mm and 14mm.

FT-IR analyses in the $3800\text{--}650\text{ cm}^{-1}$ wavenumber region of standard mixtures, soot and condensed species with carbon tetrachloride as solvent was performed on a Perkin-Elmer 1600 FT-IR spectrophotometer.

The FT-IR spectra revealed the presence of aliphatic C–H, aromatic C–H and various oxygenated functional groups, including carbonyl (C=O), C–O–C and C–OH groups. Spectral analyses were made to examine variations of these functional groups with flame temperature, sampling position and particle size.

In figure 3.00A are reported the FT-IR analysis of condensed species at different coal gas velocities ($v=4\text{ cm/s}$ and at $v=5\text{ cm/s}$) for $z=8\text{ mm}$.

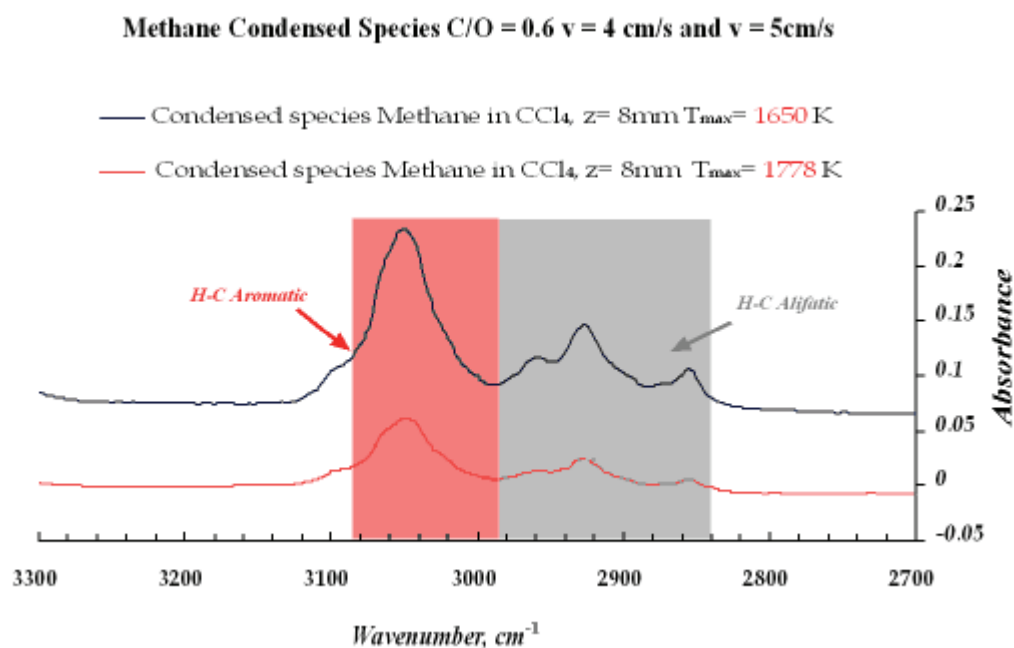


Fig. 3.15 FTIR analysis of condensed species in methane flames for $z=8\text{ mm}$ at $v=4\text{ cm/s}$ and at $v=5\text{ cm/s}$.

FT-IR spectra of the condensed species sampled are dissolved in CCl_4 using 1 cm quartz cuvette, with a concentration about (100-200 ppm) in order to avoid the signal saturation. Results indicate that in the coal flame are present higher contents of aromatic C-H (stretch at $\lambda=3050 \text{ cm}^{-1}$) and aliphatic H-C (Alkane CH_3 with asymmetric stretch at $\lambda=2960 \text{ cm}^{-1}$; Alkane CH_2 with asymmetric stretch at $\lambda=2920 \text{ cm}^{-1}$; Alkane CH_3 with symmetric stretch at $\lambda=2860 \text{ cm}^{-1}$) respect the hot flame.

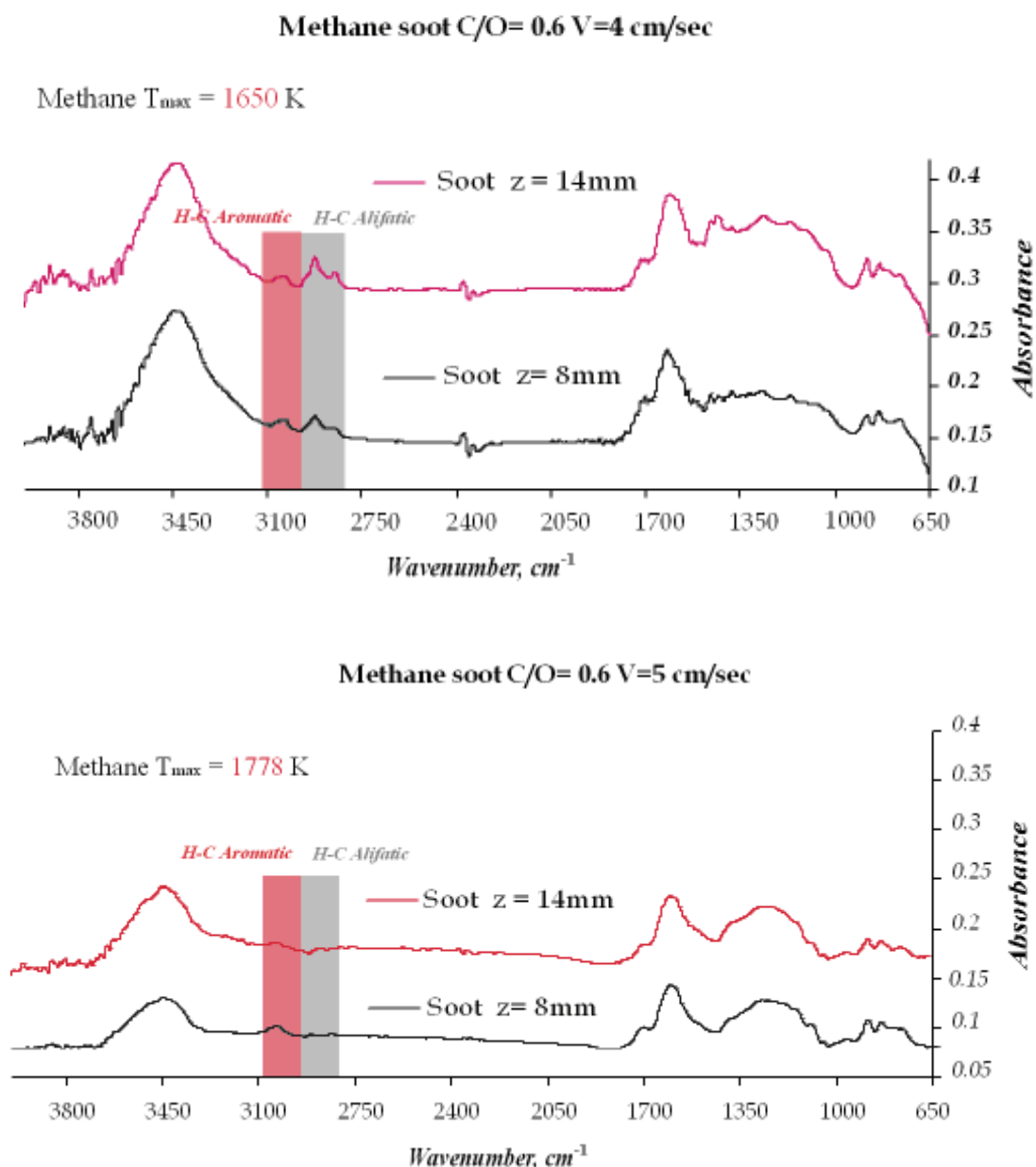


Fig. 3.16 FTIR analysis of soot in methane flames for $z=8 \text{ mm}$ at $v=4 \text{ cm/s}$ and at $v=5 \text{ cm/s}$

The solid samples, as the soot, were analyzed in the instrument in the form of potassium bromide (KBr) tablet (soot/KBr mass ratio is approximately 5/200).

Potassium bromide (a ionic solids) do not has covalent bonds and for this reason is transparent to infrared. It produces excellent spectra, transmits most of the IR region and necessary a small amount of sample in use.

In figure 3.00B are reported the FTIR analysis of soot at different coal gas velocities ($v=4$ cm/s and at $v=5$ cm/s) for $z=8$ mm and $z=14$ mm.

It can be noted that in the coal flame are present higher contents of aromatic H-C and aliphatic H-C respect the hot flame, in according to the H/C ratio.

Several oxygen-related functionalities were also observed in the soot spectra. The presence of a carbonyl group is detected not only by its peak ($\lambda=1720$ cm⁻¹), but also from an aromatic C=C vibration that is enhanced by the carbonyl (C=O) group bonded ($\lambda=1600$ cm⁻¹) to the PAH structures (D. M. Smith et al., 1995).

Oxygen-carbon stretches imputed to the ether (1260 cm⁻¹), esters (1100 cm⁻¹) and hydroxyl (1050 cm⁻¹) groups are not observed very well.

Three peaks in the range of $\lambda= 900-700$ cm⁻¹ have been observed very well in soot samples, i.e. $\lambda= 880, 840$ and 760 cm⁻¹. The origin of these peaks has been attributed to C-H out-of-plane bending of highly substituted aromatic compounds (A. Santamaria et al., 2006, J. A. Jassim et al., 1986).

3.1.7 Size Exclusion Chromatography of condensed species and soot

The separation mechanism of a mixture by SEC (Size Exclusion Chromatography) is based on a different penetration degree of a molecule, transported by a liquid mobile phase, into the pores of a stationary phase consisting of a porous organic polymer.

From the SEC chromatogram to a MW distribution

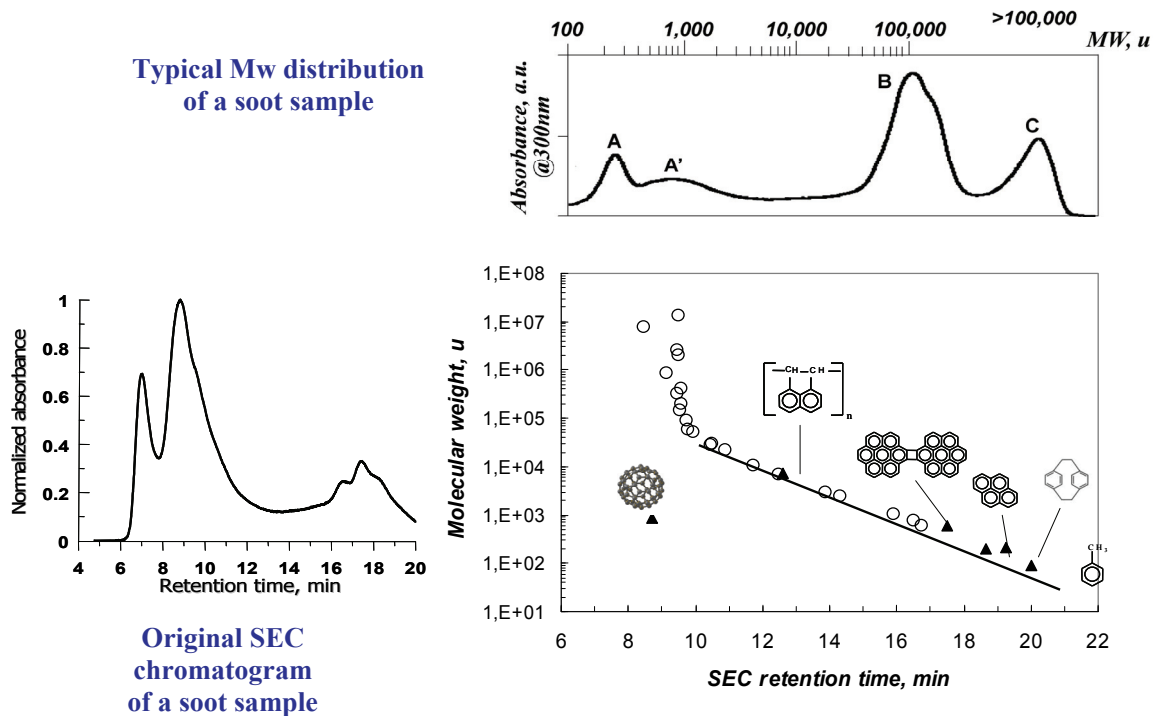


Fig3.17 ...From the SEC chromatogram to a MW distribution.

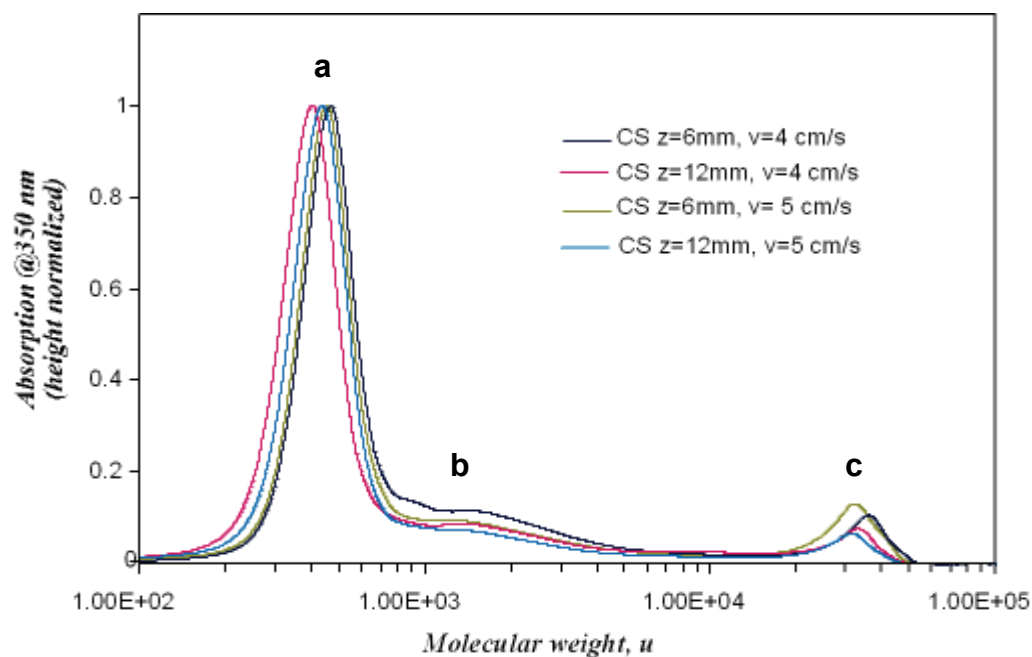


Fig. 3.18 Molecular weight distributions (MW) inferred by SEC of condensed species in methane flames for $z=6\text{mm}$ and $z=12\text{mm}$ at $v=4\text{ cm/s}$ and at $v=5\text{ cm/s}$.

The different elution volumes correspond to a different retention times of the molecules in the column. Larger molecule have a lower retention time because it had to pass through a smaller volume. The attribution of a molecular weight to a specific retention time has been made on the basic of calibration curves using polystyrene standards. The logarithm of molecular weight versus elution volume is linear over a large molecular weight range. In Fig. 3.17 the scheme that describes the transformation from a SEC Chromatogram to a MW distribution is reported.

The molecular weight distributions of condensed species inferred by SEC in methane flames, are reported in Fig 3.18.

The SEC profiles of condensed species (DCM-extract) exhibit no significant differences moving from the soot inception to the zone of mature soot. The PAH peak (**a**: 200-400u) is predominant in both flames with respect to the higher MW peaks (**b**: 600-2000u; **c**: 1.00E4-1.00E5u).

In Fig. 3.19 the molecular weight distributions inferred by SEC of soot samples are reported. It can be noted that the contribution of PAH peak (**a**: 200-400u) is comparable to that of larger MW species (peaks **b** and **c**).

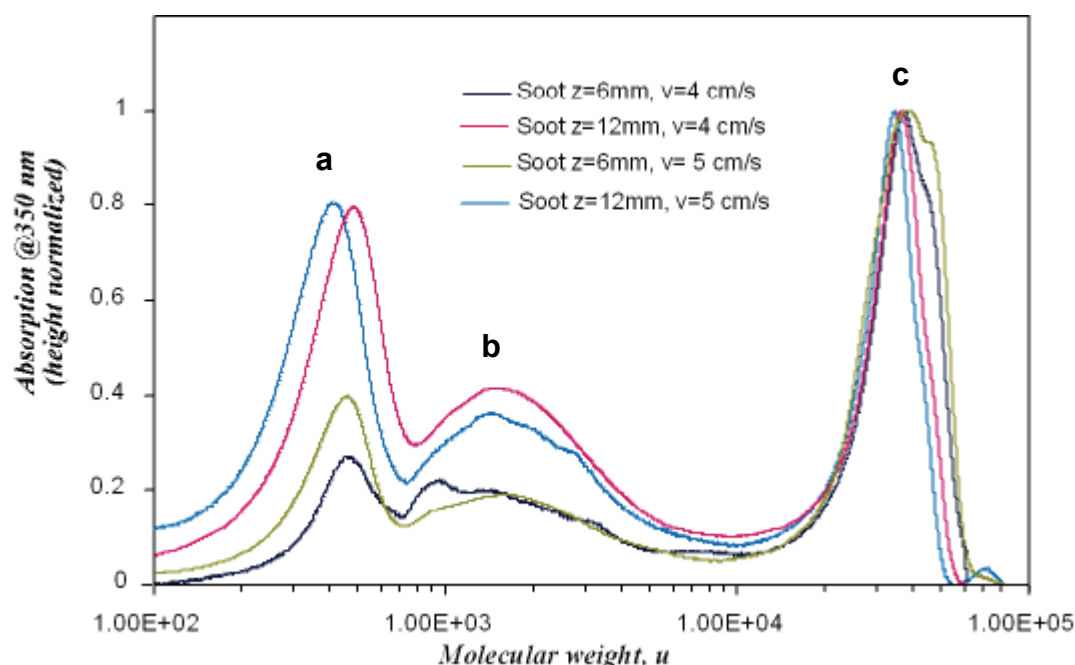


Fig. 3.19 Molecular weight distributions (MW) inferred by SEC of soot in methane flames for $z=6\text{mm}$ and $z=12\text{mm}$ at $v=4\text{ cm/s}$ and at $v=5\text{ cm/s}$.

The peak (**c**: 1.00E4-1.00E5 u) is generally predominant and associated to soot aggregate

structures (Alfè M., et al, 2008).

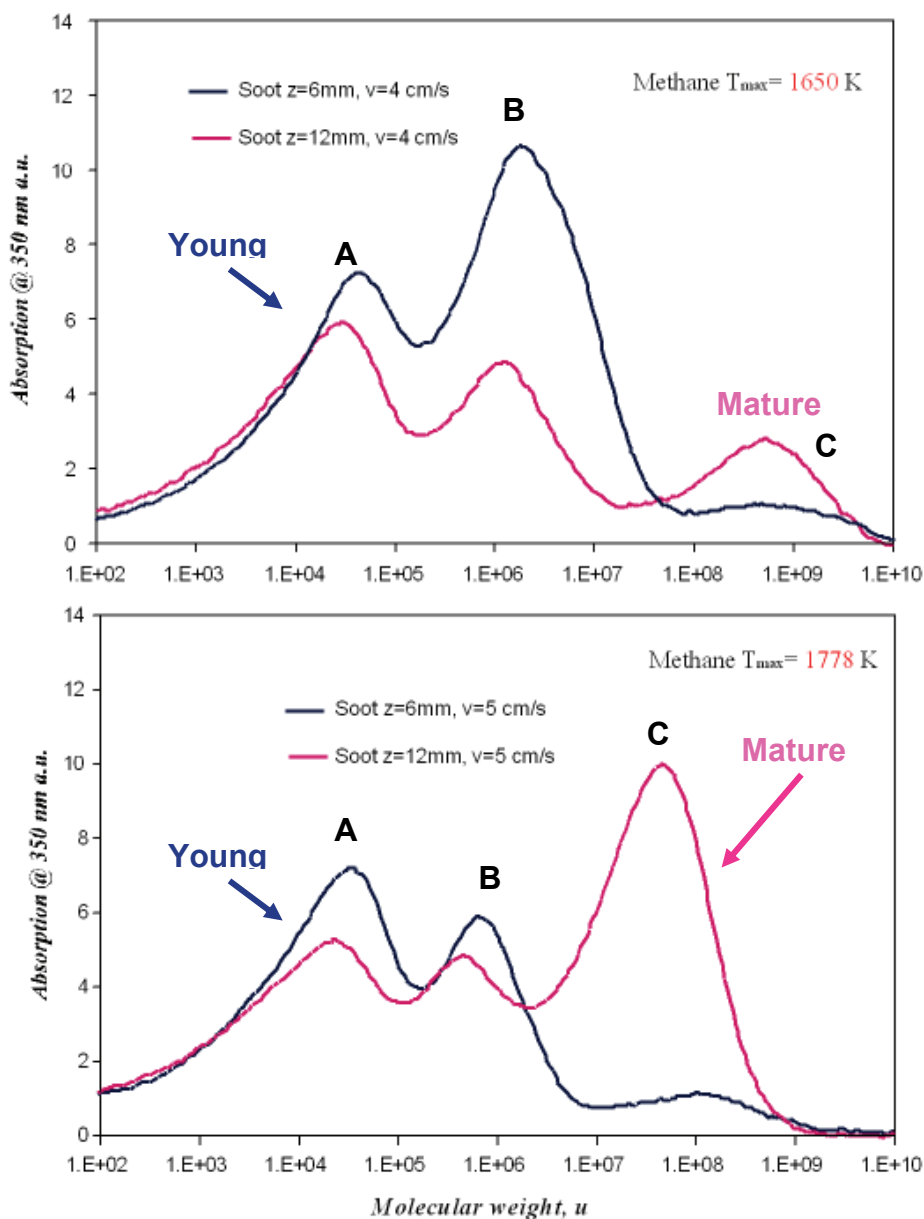


Fig. 3.20 Molecular weight distributions (MW) inferred by SEC of soot in methane flames for $z=6\text{mm}$ and $z=12\text{mm}$ at $v=4\text{ cm/s}$ and at $v=5\text{ cm/s}$.

To obtain more information on the MW distribution in the in the particle-size region (10^5 - 10^{10}u) the size exclusion chromatography (SEC) analysis of soot for the molecular weight evaluation, was carried out on a Jordi Gel divinylbenzene (DVB) Solid Bead (non-porous) column. The solvent used as eluent was NMP. Filtration of soot in NMP suspension was carried out on filter units (Anotop 10, Whatman Int. Ltd.) with porosity of 20 nm. The SEC chromatograms of young and mature soot sampled in the methane flames are reported in Figure 3.20. Soot presents a multimodal MW distribution consisting of three

main peaks (Alfè M., et al., 2008, D'Anna A., et al., 2009): the first one (**A**) is located in the molecule-region (10^2 - 10^5 u) and the last two in the particle-size region (**B**: 10^6 - 10^7 u and **C**: 10^8 - 10^{10} u).

The **A** peak (10^2 - 10^5 u) is below the permeation limit of the column ($<10^5$ u) and has been studied in more detail by using a SEC column with a higher resolution power in this specific MW range and reported in figure 3.15.

The **B** peak (10^6 - 10^7 u) MW distribution in the particle-size region can be attributed to heavier material, consisting of small soot particles with diameter about 10 nm by assuming a spherical shape and a density of 1.8 g/cm³. Moreover, it can be noted that the young soot, otherwise of mature soot, exhibit a relatively small peak in the 10^8 - 10^{10} u MW range (**C**) in both the flames.

The contribution of the lower MW soot components (peak **A**: 10^2 - 10^5 u and peak **B**: 10^6 - 10^7 u) is higher in the case of a young soot ($z=6$ mm) and decreased in a mature soot, independently on the flame temperature. This demonstrates that these species disappear as soot formation goes on, possibly in favour of large size soot particles formation. This trend is indeed typical of intermediates in the processes leading to the mature soot formation.

Overall, it is important to note that the **C** peak (10^8 - 10^{10} u) in methane soot at 1778K is much more predominant than **C** peak in methane flames at 1650K, suggesting that, the growth process of soot in methane flames at 1778K flame is more enhanced than in methane flame at 1650K.

3.2 Benzene flames

In this section the experimental results obtained in fuel-rich benzene/O₂/N₂ flames are resumed. The flames were produced at a constant mixture composition (C/O = 0.8) and different cold-gas flow velocities (3 and 4 cm/s). By changing the cold gas velocity different flame temperatures have been obtained.

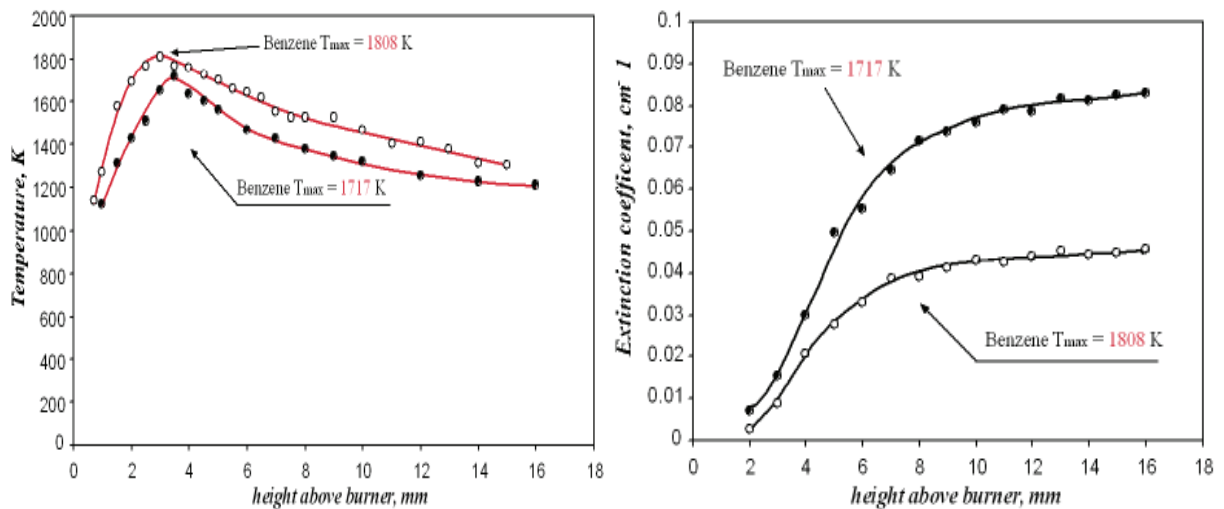


Fig. 3.21 Temperature and extinction coefficient of benzene flames at $v=3$ cm/s (left) and at $v=4$ cm/s (right).

In Fig. 3.21 the temperature profiles and the extinction coefficients for both the flames are reported. It can be observed that the maximum temperature is located at different positions and in the higher temperature flame the main oxidation zone moves upstream.

In the flame with cold-gas flow velocity=3 cm/s the maximum flame temperature is 1717 K and is located at about 3 mm height above burner, while in the flame with cold-gas velocity= 4 cm/s the maximum flame temperature is 1808K and is located at about 4 mm height above burner.

3.2.1 Concentration profiles of Gas species

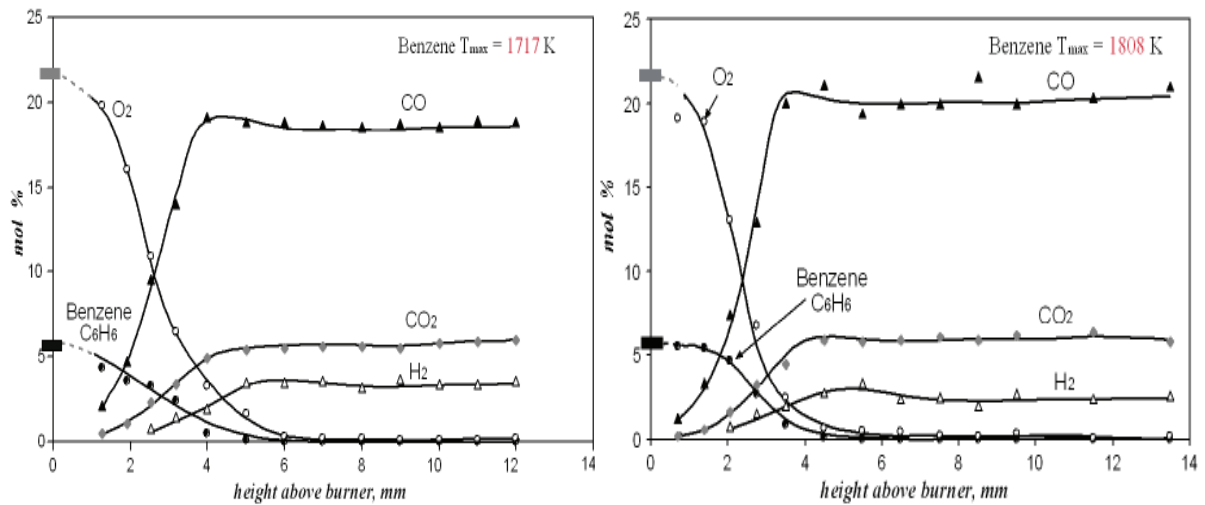


Fig. 3.22. Concentration profiles of reactants and main combustion products of benzene flames at $v=3$ cm/s (left) and at $v=4$ cm/s (right).

The limit of the main oxidation zone is at about 5 mm for the benzene flame with a cold-gas flow velocity of 3 cm /s and at about 4.5mm for the benzene flame with a cold-gas flow velocity of 4 cm/s.

In the main oxidation zone fuel and oxygen are completely consumed and the maximum formation of combustion products (CO , CO_2 , H_2) occurs (figure 3.22).

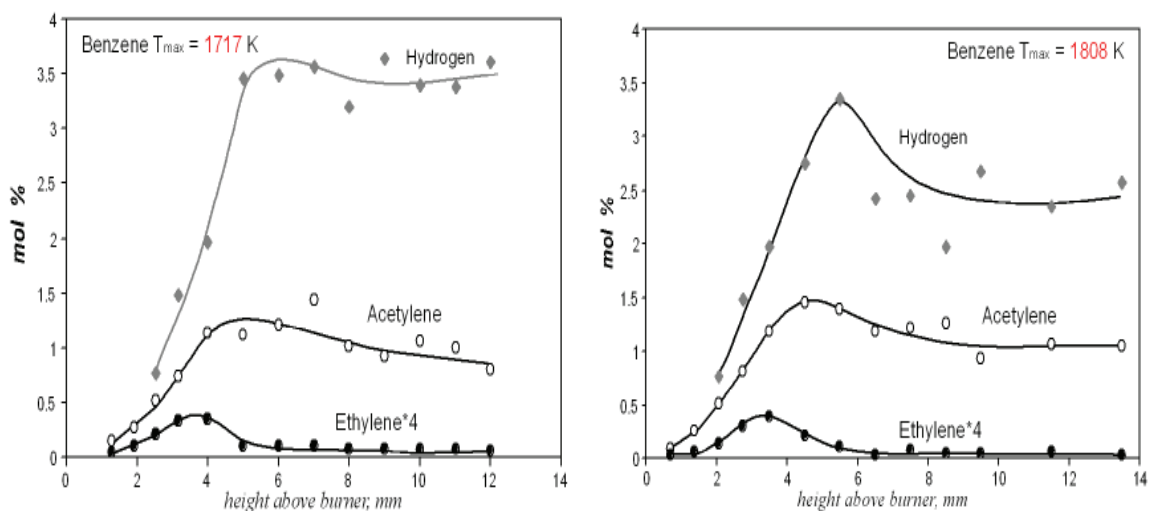


Fig. 3.23 Concentration profiles of hydrogen, ethylene and acetylene in benzene flames at $v=3$ cm/s (left) and at $v=4$ cm/s (right).

In Fig. 3.23 the concentration profiles of hydrogen, acetylene and ethylene are reported.

Hydrogen concentration rises in the main oxidation zone reaching a quite constant value. The most abundant hydrocarbon species produced in the rich combustion of benzene is acetylene.

Acetylene is already present at the beginning of the flame and reaches the peak concentration value at the end of the main oxidation zone, where the fuel concentration approaches to the minimum value.

Downstream of the main oxidation zone, acetylene slightly decreases, levelling off to a quite constant value independent on the flame temperature. Ethylene profile, in the main oxidation region, has the typical rises-decay trend of reaction intermediates in both the flames.

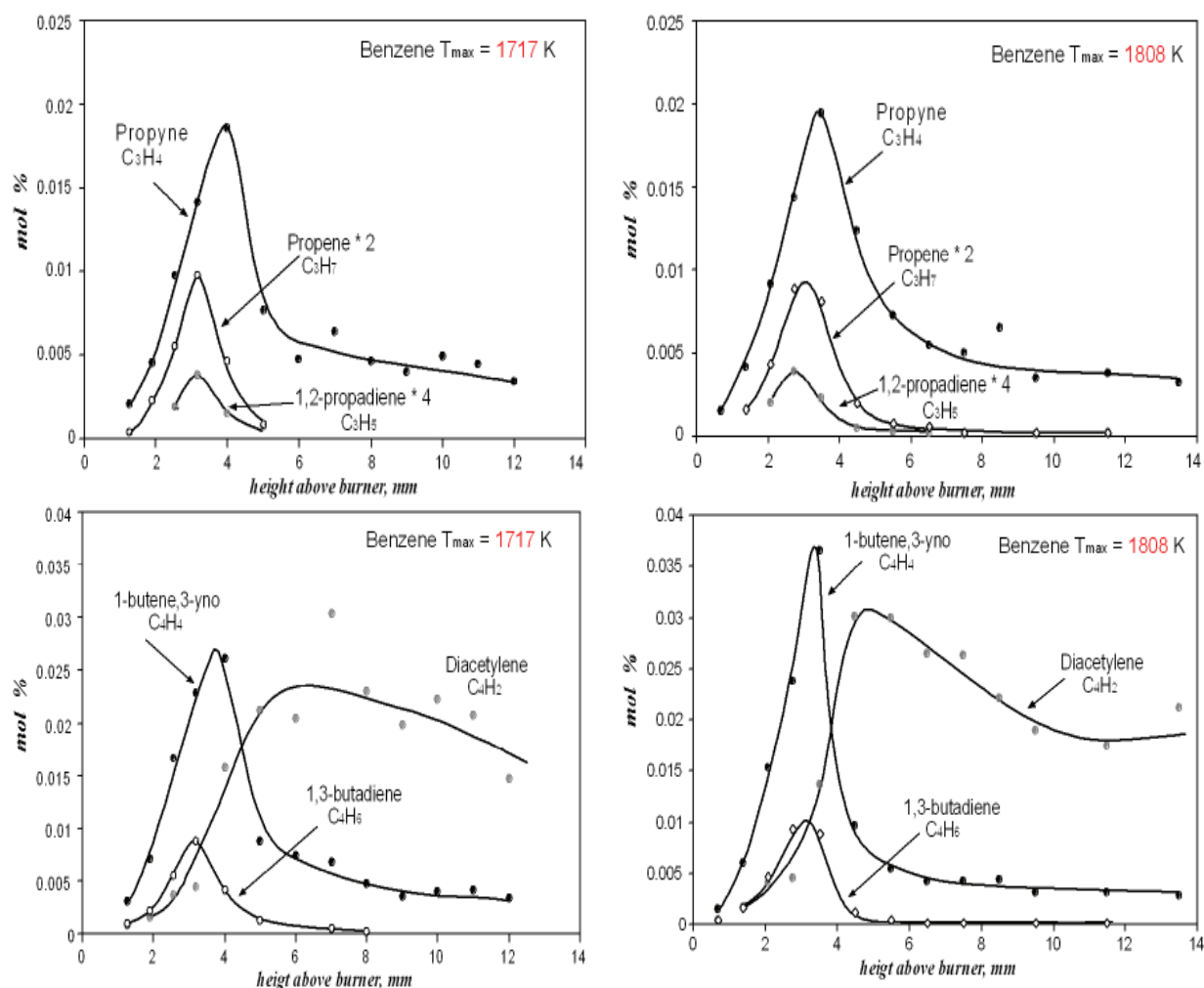


Fig. 3.24 Concentration profiles of the most abundant C_3 (upper) and C_4 hydrocarbons (lower) in benzene flames at $v=3$ cm/s (left) and at $v=4$ cm/s (right).

Propyne, propene, 1,2-propadiene, 1-buten,3-yne, diacetylene and butadiene, reported in Fig. 3.24, are reaction intermediates. Their concentrations decrease in the pyrolytic region

of the flames. Diacetylene concentration remains quite constant in the pyrolysis region of the flame.

The C3-C4 concentration profiles do not show significant differences in both the flames except for a larger formation of diacetylene consistent with the higher formation of acetylene in higher temperature conditions.

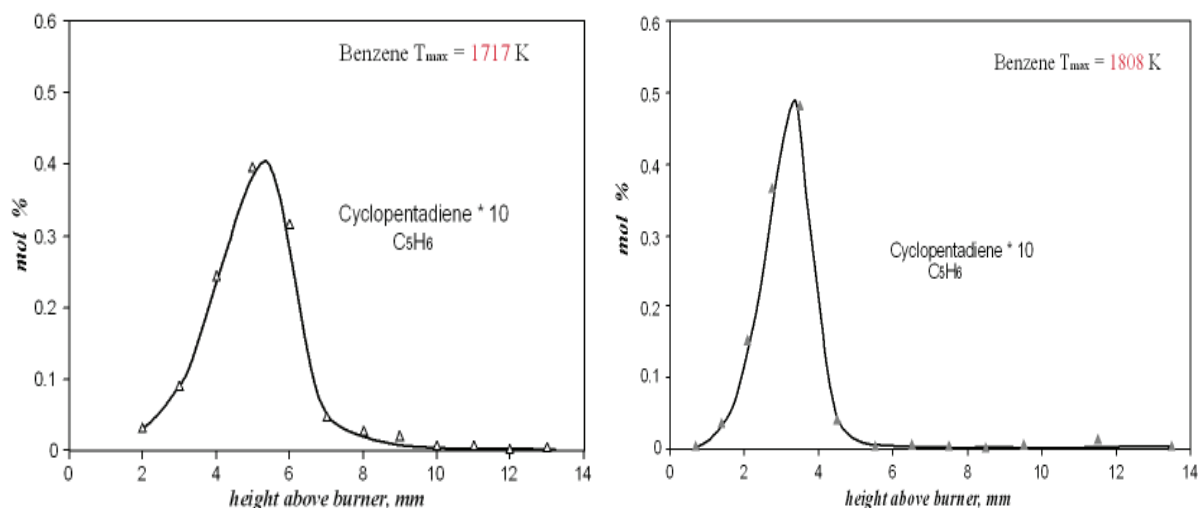


Fig. 3.25 Concentration profiles of cyclopentadiene in benzene flames at $v=3$ cm/s (left) and at $v=4$ cm/s (right).

Cyclopentadiene (Fig. 3.25) presents a rise-decay profile peaked in the main oxidation region, consistently with its role of intermediate in benzene oxidation and naphthalene formation.

3.2.2 Concentration profiles of condensed phases

Fig. 3.26 reports the concentration profiles of soot, condensed species and PAH up to 300u.

In the lower temperature flame the concentrations of both condensed species and PAHs present a similar profile.

They exhibit a rise-decay profile just before the maximum soot formation rate, indicating their role in soot formation process, while the soot concentration rises in the main oxidation zone reaching a quite constant value in a pos-oxidation zone.

It can be observed that the condensed species concentration is higher in the high temperature flame, while soot concentration is lower.

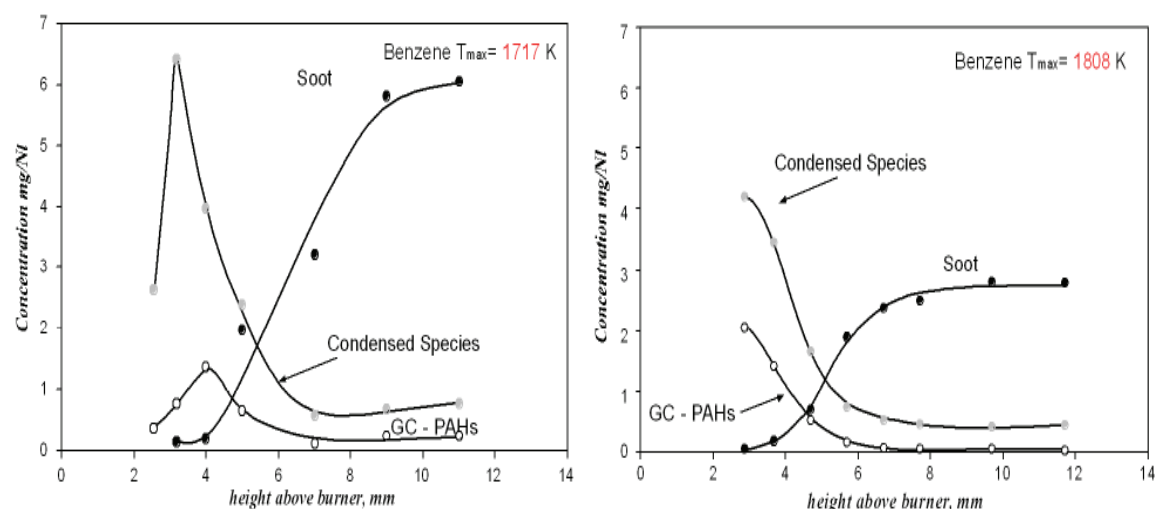


Fig. 3.26 Concentration profiles of GC-PAH, DCM soot extract and soot in benzene flames at $v=3$ cm/s (left) and at $v=4$ cm/s (right)

3.2.3 Analysis of condensed species (Gaschromatography-Mass spectrometry)

The profiles of single PAH measured, reported in Fig. 3.27-3.30, exhibit the usual distribution with a larger abundance of small PAH (naphthalene and acenaphthylene) and a lower amount of larger PAH up to coronene.

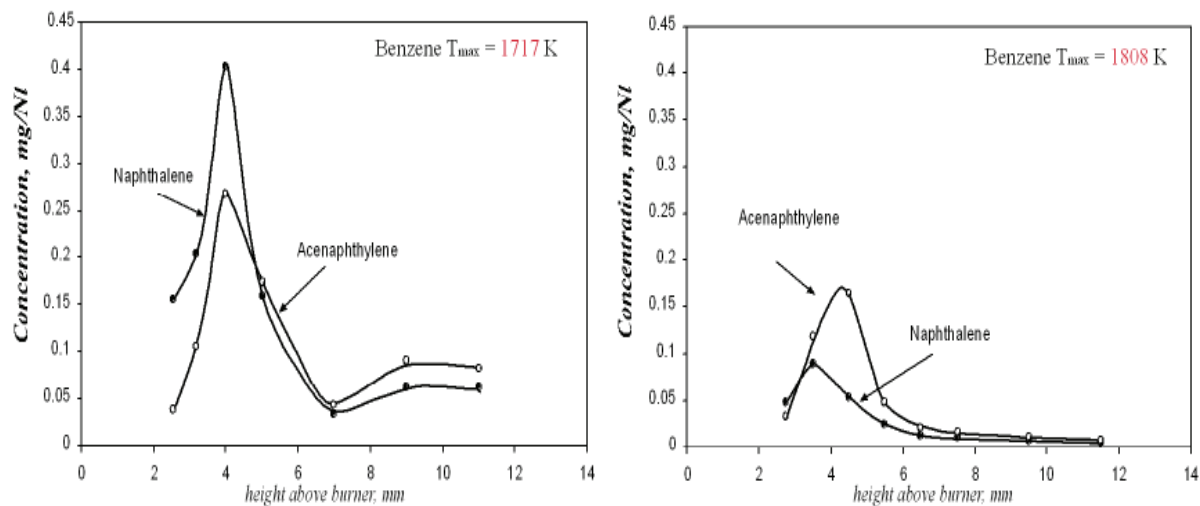


Fig.3.27 Concentration profiles of acenaphthylene and naphthalene in benzene flames at $v=3$ cm/s (left) and at $v=4$ cm/s (right).

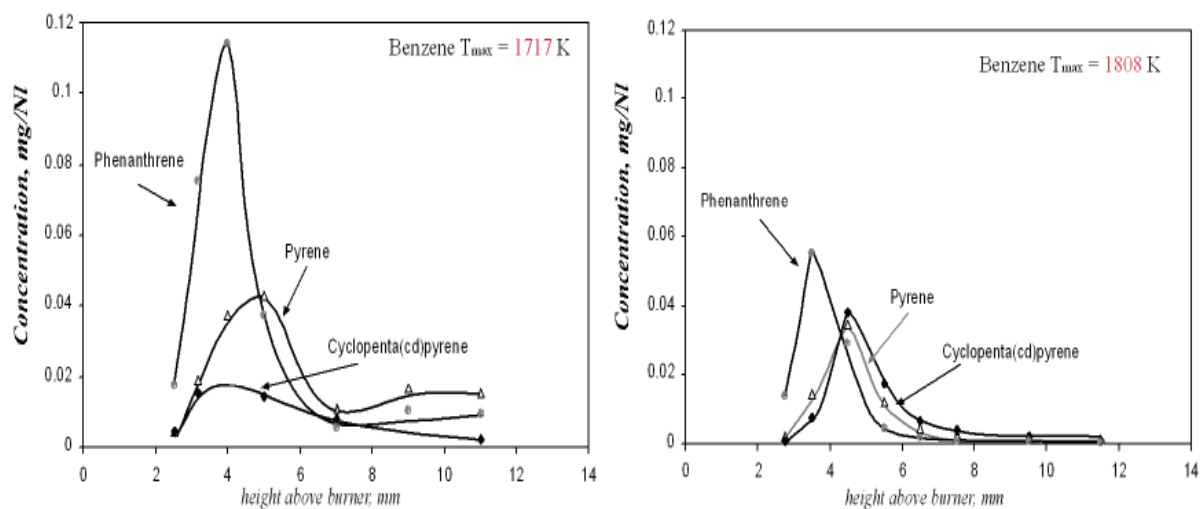


Fig.3.28 Concentration profiles of cyclopenta(cd)pyrene, pyrene and phenanthrene in benzene flames at $v=3$ cm/s (left) and at $v=4$ cm/s (right).

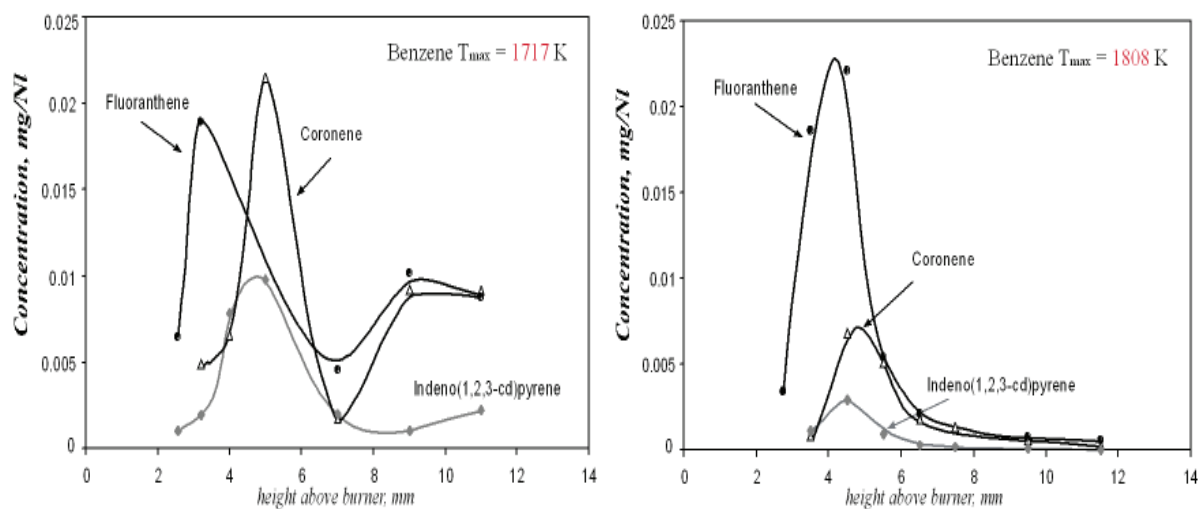


Fig.3.29 Concentration profiles of fluoranthene, coronene and indeno(1,2,3-cde)pyrene in benzene flames at $v=3$ cm/s (left) and at $v=4$ cm/s (right).

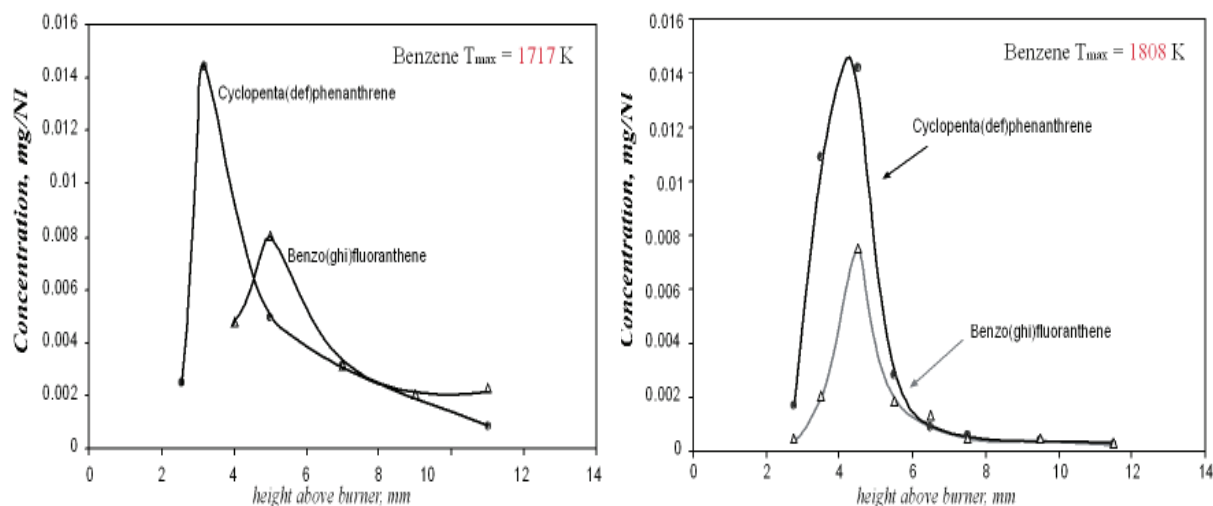


Fig.3.30 Concentration profiles of benzo(ghi)fluoranthene and cyclopenta(def)phenanthrene in benzene flames at $v=3$ cm/s (left) and at $v=4$ cm/s (right).

3.2.4 Soot characterization

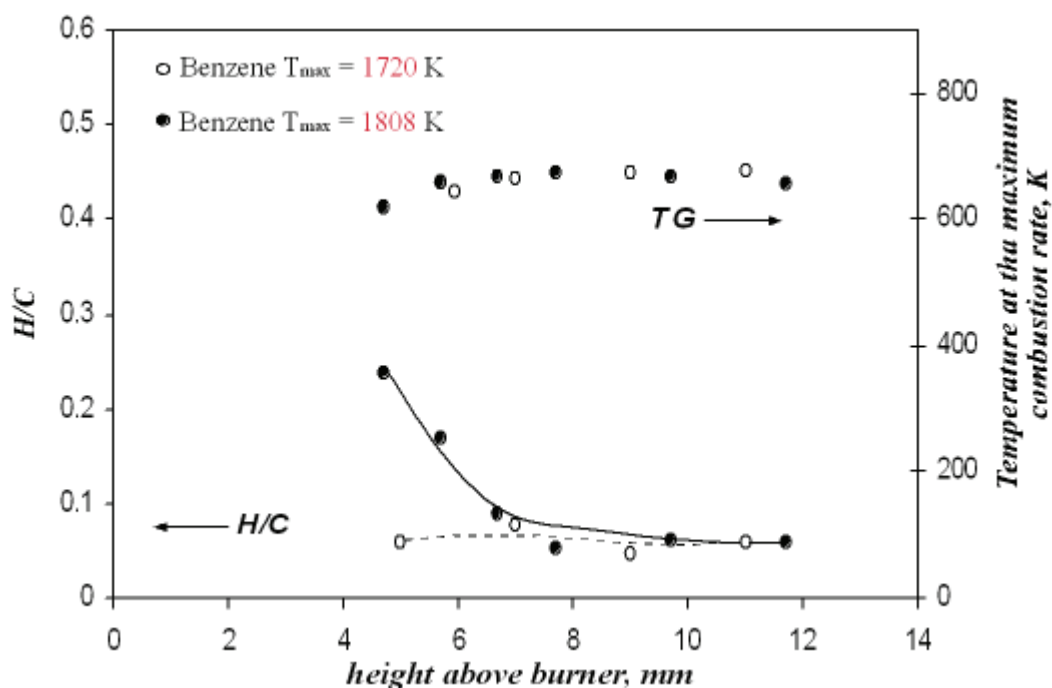


Fig. 3.31 Temperatures of the maximum combustion rate under air (30 ml min^{-1}) and H/C atomic ratio of low-temperature benzene soot at $v=4$ cm/s (●) and high-temperature benzene soot at $v=5$ cm/s (○) as a function of height above burner.

The temperature of the maximum combustion rate of soot (i.e. the temperature to which the maximum weight loss occurs) along the flame axis is reported in Fig. 3.29. As higher is the maximum combustion temperature lower is the oxidation reactivity.

Soot exhibits an increase of the maximum combustion temperature, from 600 to 650°C, along the flame testifying the decrease of soot oxidation reactivity during the soot formation/maturation process. It can be noted that the oxidation reactivity of high-temperature flame soot is similar to the low-temperature flame soot.

The H/C atomic ratios also are reported in Fig. 3.29. Is important to note that, similarity to the TG analysis, the H/C ratio in benzene flames do not presents significant differences from the flames in the post-oxidation zone and the different flame temperatures do not show particular differences on the soot structure.

3.2.5 UV-Visible spectroscopy

Fig. 3.32 reports the normalized absorbance of condensed species in benzene flames at different cold gas velocity.

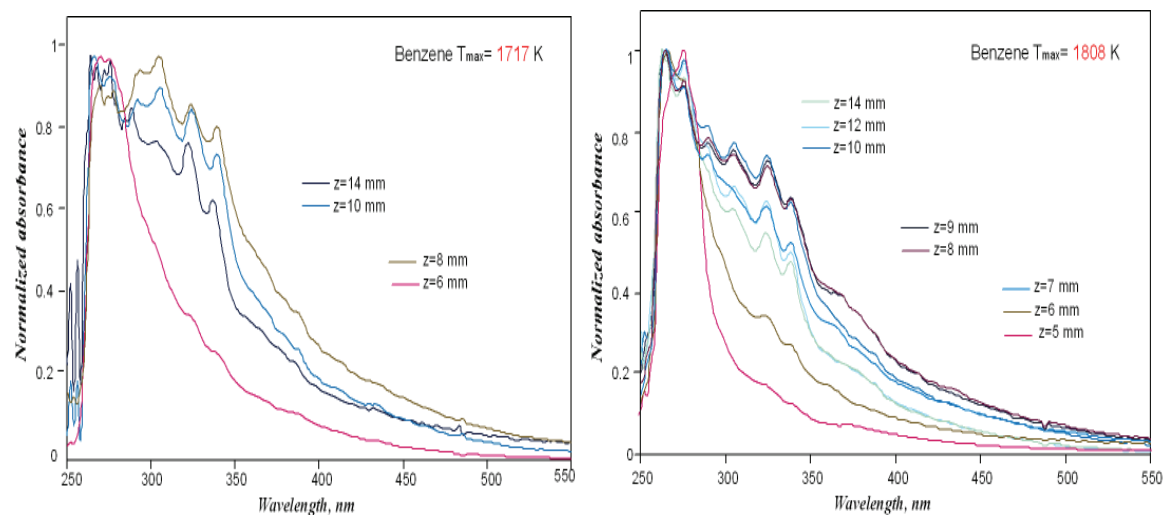


Fig. 3.32 Normalized absorbance of condensed species in benzene flames at $v=3$ cm/s (left) and at $v=4$ cm/s (right).

The normalized absorbance profiles show an aromaticity increase of condensed species along the flames.

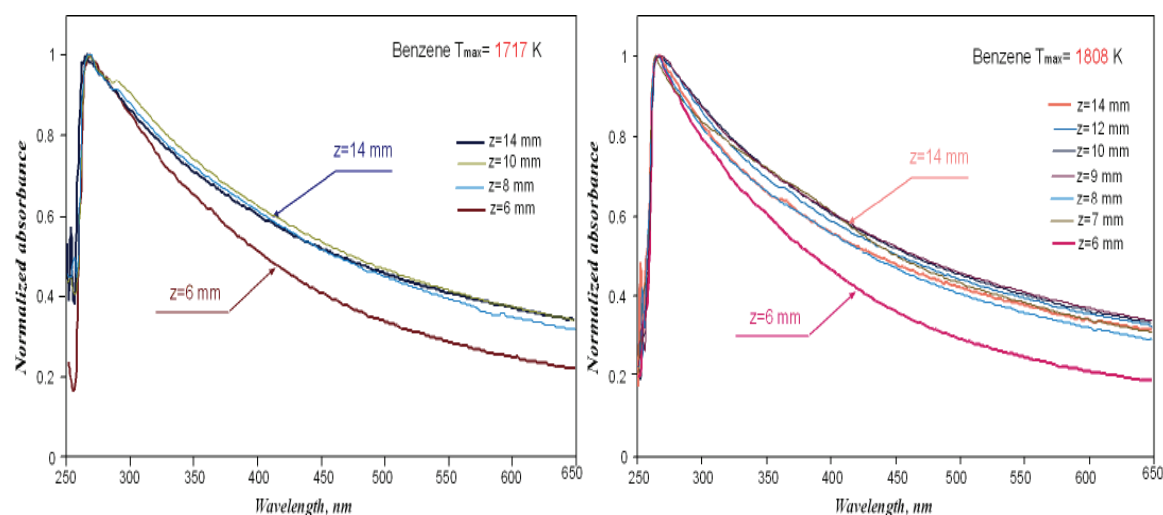


Fig. 3.33 Normalized absorbance of soot in benzene flames at $v=3$ cm/s (left) and at $v=4$ cm/s (right).

In Fig. 3.33 the normalized absorbance of soot at different height above burner are reported. Soot absorbance shows that the soot aromaticity increases along the flames and

does not appear to be significant differences in both the flames.

It is important to note that, the normalized absorbance of soot and condensed species don't exhibit significant differences between the flames.

The soot absorption coefficients in the UV (300 nm) and in the visible (500 nm) are reported as a function of height above burner in figure 3.34.

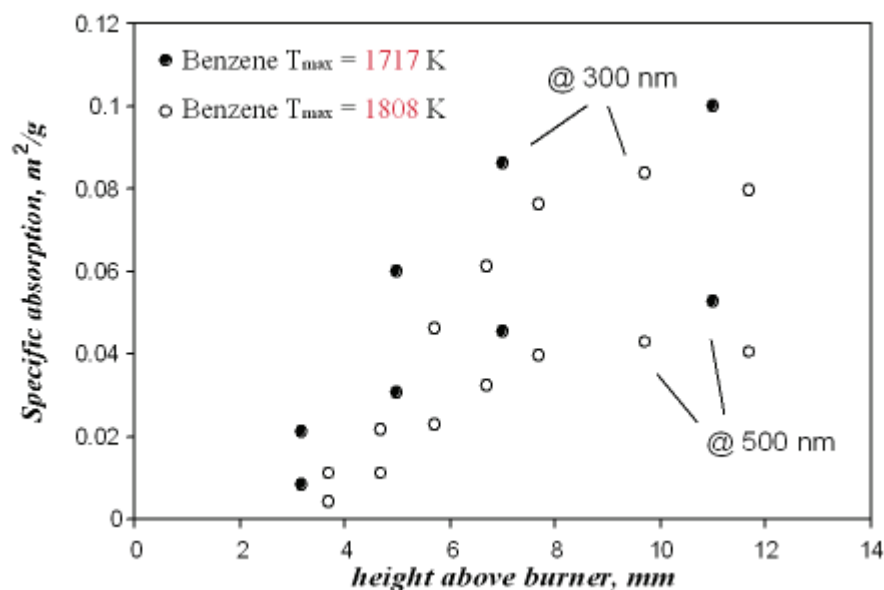


Fig. 3.34 Specific absorption (m²/g) of benzene soot at $v=3$ cm/s measured at 300 nm (●) and 500 nm (●) and at $v=4$ cm/s measured at 300 nm (○) and 500 nm (○).

The soot absorption coefficients, do not exhibit significant differences both in the UV and in the visible regions and it is noteworthy that the soot absorptivity in the two flames dramatically changes along the height flame.

Moreover, it can be noticed that the mass absorption coefficient of mature soot in this benzene flame results to be quite similar to that measured at higher temperatures, this suggest that the aromaticity of benzene soot is not influenced by flame temperature and generally, much higher than that measured for soot produced from aliphatic fuels as methane (figure 3.14).

3.2.6 Size Exclusion Chromatography of condensed species and soot

A typical molecular weight distributions of condensed species (DCM-extract) sampled in benzene flames is reported in Fig 3.35.

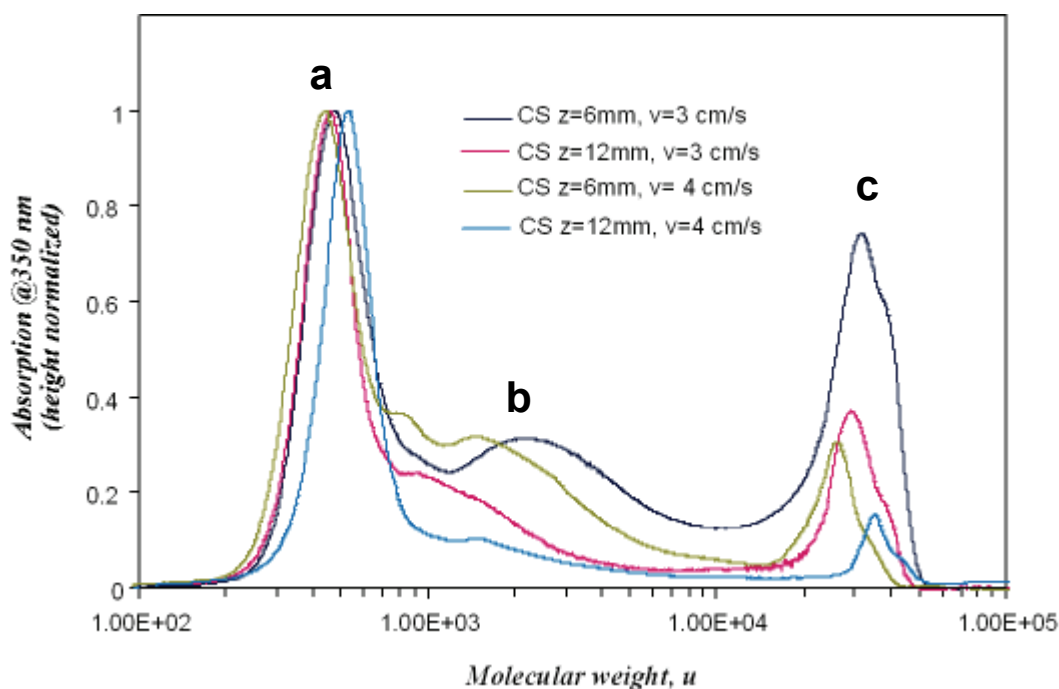


Fig. 3.35 Molecular weight distributions (MW) inferred by SEC of condensed species in benzene flames for $z=6\text{mm}$ and $z=12\text{mm}$ at $v=3\text{ cm/s}$ and at $v=4\text{ cm/s}$.

The molecular weight distributions of condensed species exhibit significant differences moving from the soot inception to the zone of mature soot. DCM-extract is characterized by the predominance of a sharp peak in the 200-400 u range mostly composed by large-PAH (**a**) (Alfè M., et al., 2008) and a smaller peak in the range from 600 to 2000 u (**b**) composed of polymeric-like aromatic species. A minor peak is also detected at $MW > 1E5$ u (**c**).

PAHs peak is predominant in both flames particularly at larger flame heights (Alfè M., et al., 2008).

In Fig. 3.36, the normalized SEC chromatograms of soot sampled at $z=6\text{mm}$ of height above burner are reported. The MW/size distribution of soot in the benzene flame appears to be different from the aliphatic flames.

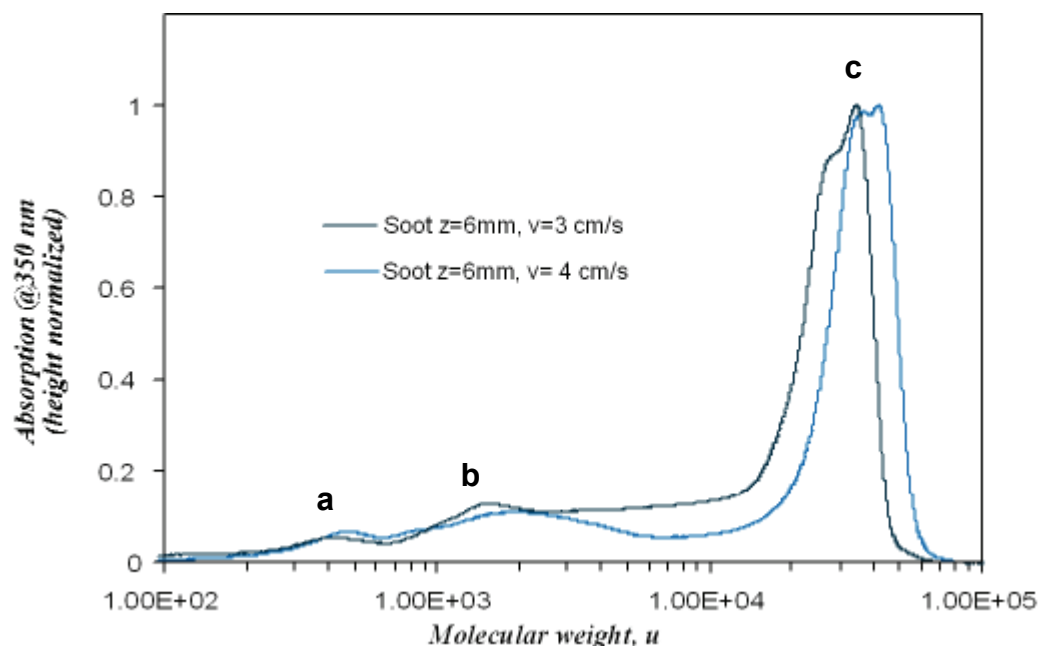


Fig. 3.36 Molecular weight distributions (MW) inferred by SEC of soot in benzene flames for $z=6\text{mm}$ and $z=12\text{mm}$ at $v=3\text{ cm/s}$ and at $v=4\text{ cm/s}$.

The PAH peak (**a**: 200-400u) is present in both flames but lower than PAH peak present in methane flames, there is a lower presence of polymer-like aromatic species (**b**: 300–2000 u), while the PAH peak (**c**: $1.00\text{E}4\text{-}1.00\text{E}5\text{ u}$) is predominant for both flames and are identify the aggregate structures (Alfè M., et al, 2008).

The MW/size distribution of benzene soot appears simply as large soot particles/aggregates already in the soot inception region. This is different than the aliphatic flames where the MW/size distribution is initially wider and richer in small soot particles which slowly evolve toward large size (Alfè M., et al, 2007).

The differences in the axial evolution of the soot size distribution along aliphatic and benzene flames can be interpreted by considering that soot formation occurs much earlier in the benzene flame where the overlapping of the oxidation and pyrolytic regions is known to occur. The soot profiles exhibit no significant differences in both flames.

The SEC chromatograms of young and mature soot sampled in the benzene flames are reported in Figure 3.37. The MW in the in the particle-size region ($10^5\text{-}10^{10}\text{ u}$) were obtained by SEC analysis carried out on a Jordi Gel divinylbenzene (DVB) Solid Bead (non-porous) column.

Soot presents a multimodal MW distribution consisting of two main: the first one (**A**) is located in the molecule-region 10^2 - 10^5 u and the second (**B**) in the molecular region of 10^6 - 10^7 u.

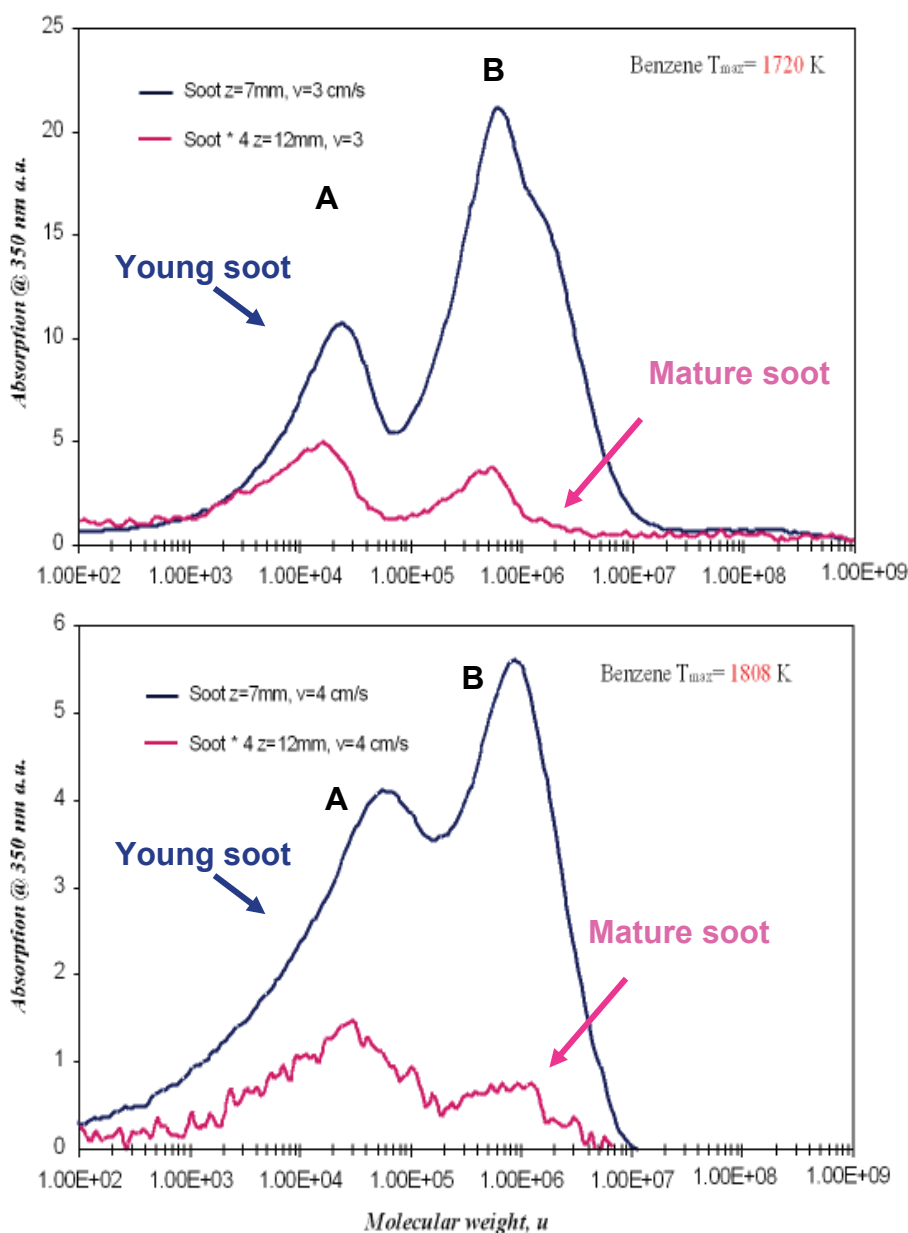


Fig. 3.37 Molecular weight distributions (MW) inferred by SEC of soot in benzene flames for $z=7\text{mm}$ and $z=12\text{mm}$ at $v=3\text{ cm/s}$ and at $v=4\text{ cm/s}$.

It can be noted that the contribution of the lower MW soot components (peak **A**: 10^2 - 10^5 u and peak **B**: 10^6 - 10^7 u) is higher in the case of a young soot ($z=6\text{ mm}$) and decreased in a mature soot, independently of the temperature flames. This demonstrates that these species disappear as soot formation goes on, possibly in favour of large size soot particles formation. This trend is indeed typical of intermediates in the processes leading to the mature soot formation.

3.3 Ethylene flames

In this section the experimental results obtained in fuel-rich ethylene/O₂ flames are resumed. The experimental condition are reported in tab. 2.3.

The flame was produced at a constant mixture composition (C/O = 0.8) and cold-gas flow velocity at 3 cm/s.

The overall structure of fuel-rich ethylene/oxygen flame at atmospheric pressure is given by the profiles of temperature and of the concentrations of the reactants and major products. The temperature profile was reported in fig 3.38.

It can be observed that the maximum flame temperature is 1620 K and is located about 2.5 mm height above burner.

The temperature rises linearly up to the peak values, where ethylene and O₂ (Fig. 3.40) are disappearing and both CO and CO₂ (Fig. 3.40) are produced with maximum rates.

While in figure 3.39 the extinction coefficient profile is reported. It rises linearly along the flame, but differently by methane/ethylene flames, for ethylene/oxygen flame the extinction coefficients are higher than methane and benzene flames, this trend is typical of ethylene flames, where the soot formation is higher than methane/benzene flames.

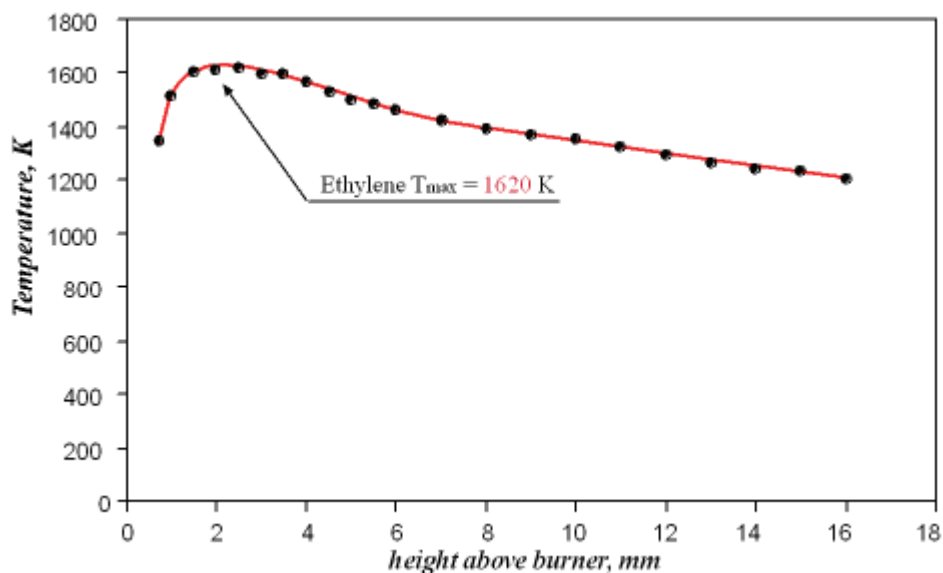


Fig. 3.38 Temperature of ethylene flame at $v=3$ cm/s.

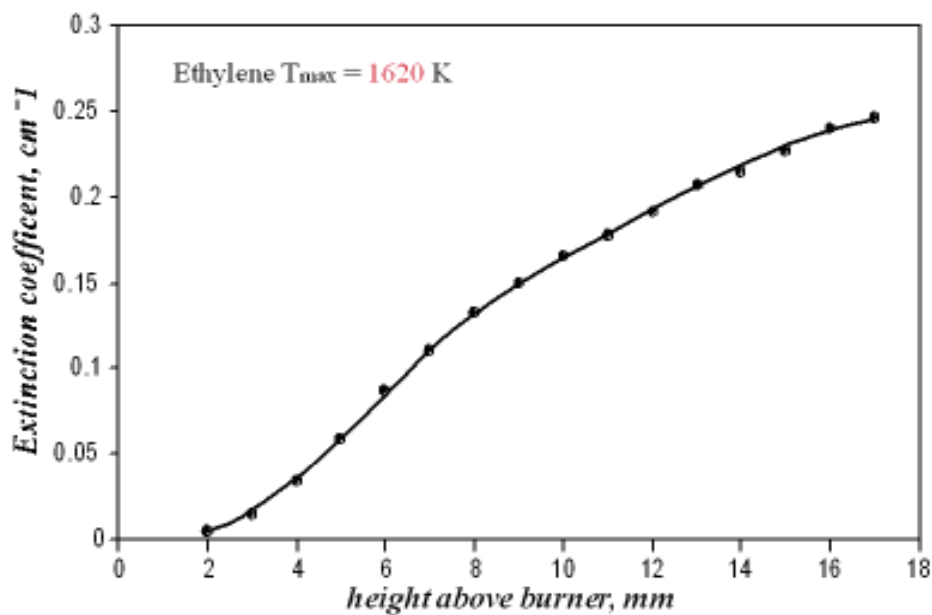


Fig. 3.39 Extinction coefficient of ethylene flame at $v=3$ cm/s.

3.3.1 Concentration profiles of Gas species

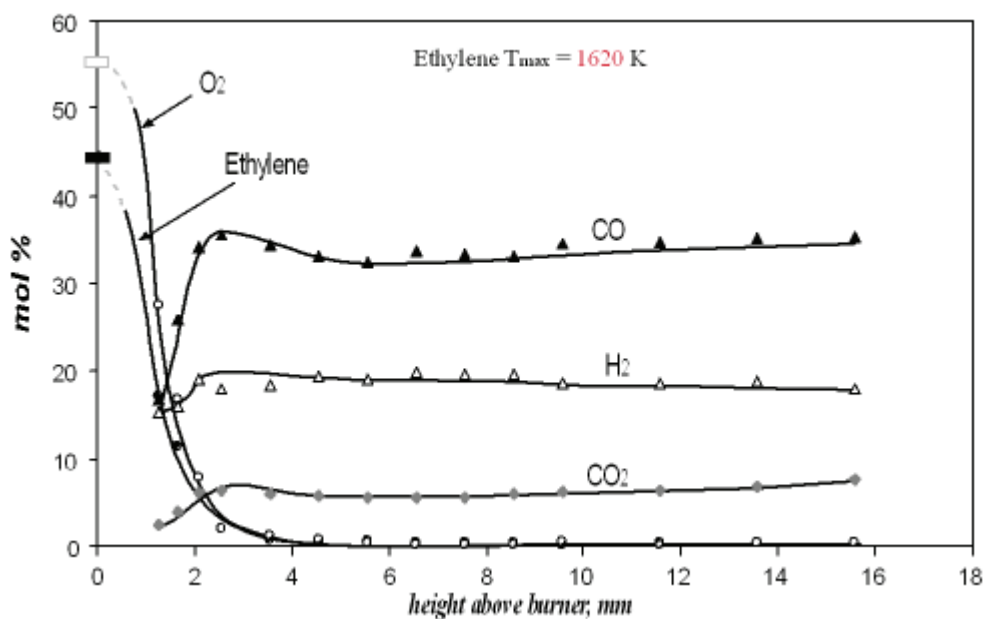


Fig. 3.40 Concentration profiles of reactants and main combustion products of ethylene flame at $v=3$ cm/s.

In figure 3.40 are reported the reagents profiles and the main combustion products of ethylene flame. It can be noted that the limit of the main oxidation zone is about 3.5 mm for the ethylene flame. In this zone, the fuel and oxygen are completely consumed and the maximum formation of combustion products (CO , CO_2 , H_2) occurs (figure 3.40).

Downstream of the main oxidation zone, CO and CO₂ approach constant concentrations and the temperature falls, due to heat losses.

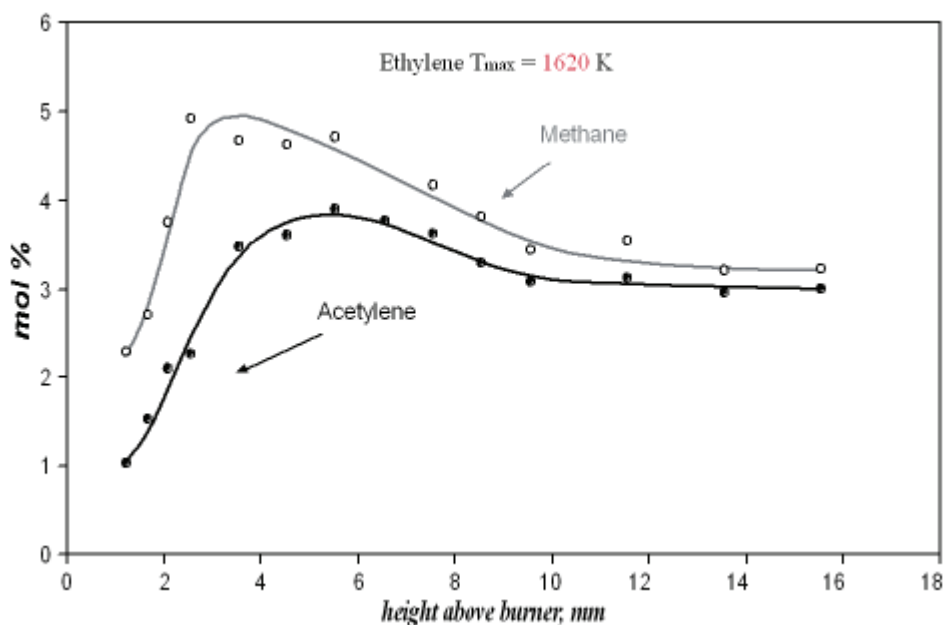


Fig. 3.41 Concentration profiles of methane and acetylene in ethylene flame at $v=3\text{cm/s}$.

In Fig. 3.41 the concentration profiles of methane and acetylene are reported. Methane and acetylene profile in the main oxidation region, have the typical rises-decay trend of reaction intermediates.

Methane concentration profiles rises-decreases in the main oxidation zone and reaches a quite constant value in a post-oxidation region.

Otherwise methane and benzene flames, in this case, the most abundant hydrocarbon species produced in the rich combustion of ethylene flame is methane.

Acetylene profile is already present at the beginning of the flame and reaches the peak concentration value at the end of the main oxidation zone, where the fuel concentration approaches to the minimum value. Downstream of the main oxidation zone, acetylene slightly decreases, levelling off to a quite constant value.

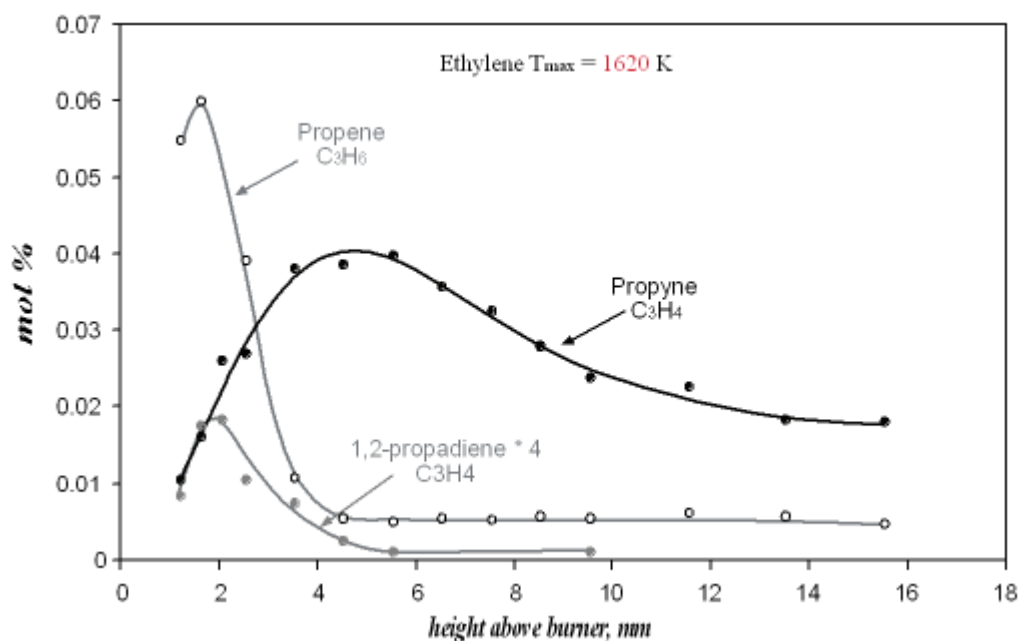


Fig. 3.42 Concentration profiles of the most abundant C_3 hydrocarbons in ethylene flame at $v=3$ cm/s.

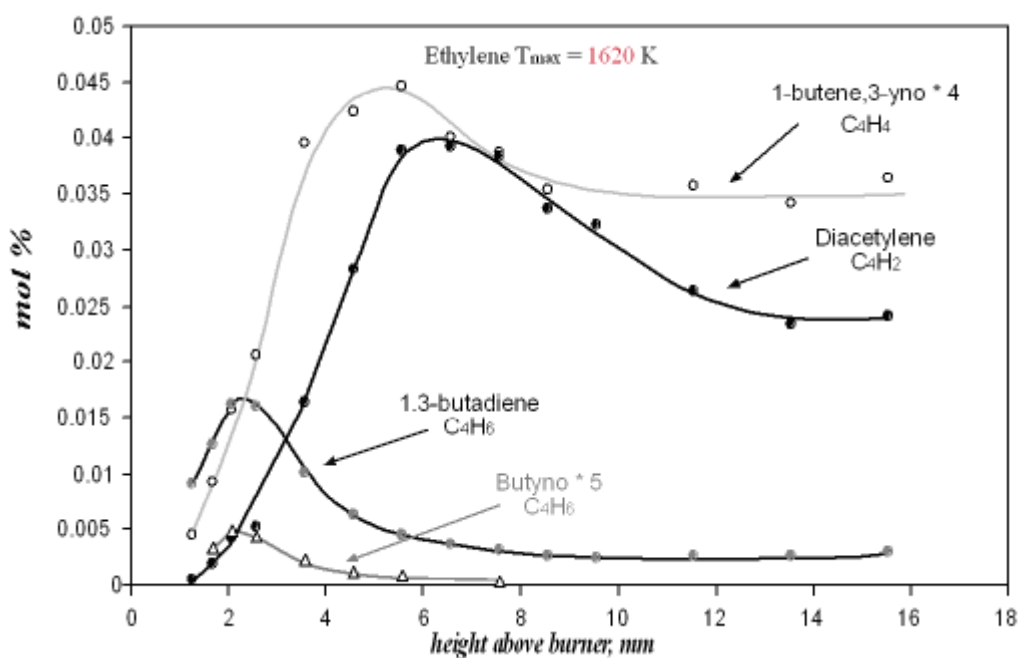


Fig. 3.43 Concentration profiles of the most abundant C_4 hydrocarbons ethylene flame at $v=3$ cm/s.

Propyne, propene, 1,2-propadiene, 1-buten,3-yno, diacetylene, butadiene and butyno, reported in Fig. 3.42-3.43, are reaction intermediates. Their concentrations decrease in the pyrolytic region of the flame. Diacetylene and 1-buten,3-yno concentrations remain quite constant in the pyrolysis region of the flame.

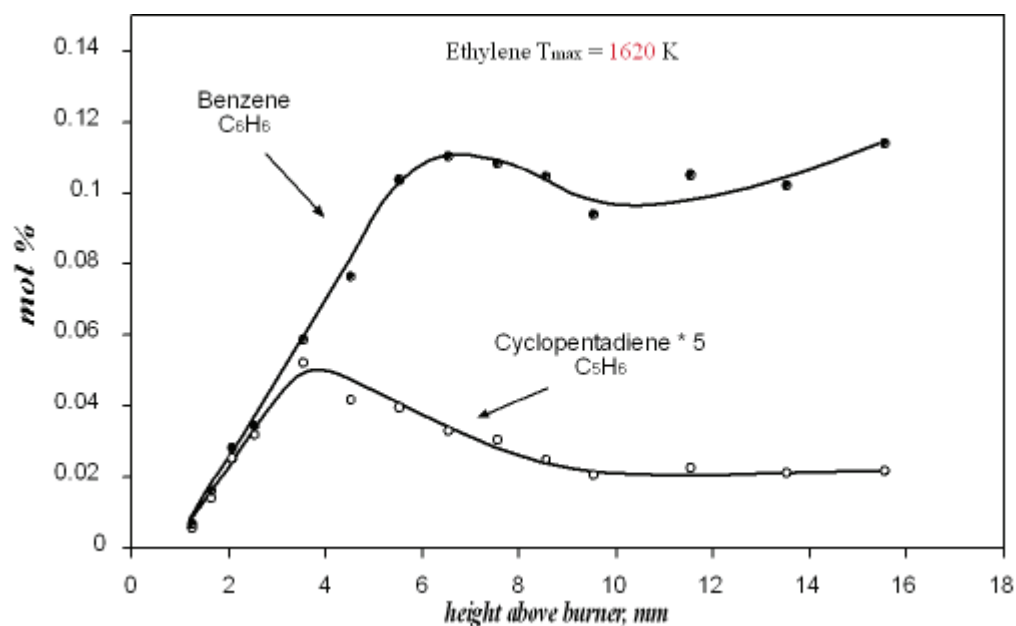


Fig. 3.44 Concentration profiles of cyclopentadiene and benzene in ethylene flames at $v=3$ cm/s .

Cyclopentadiene (Fig. 3.44) presents a rise-decay profile peaked in the main oxidation region before the maximum formation rate of benzene, consistently with its role both in benzene oxidation and in naphthalene formation, while benzene concentration rise-decays in the main oxidation zone, after the main oxidation zone, benzene profile presents a rise profile in according to extinction and soot profile (figure 3.39-3.45).

33.2 Concentration profiles of condensed phases

Fig. 3.45 reports the concentration profiles of soot, condensed species and PAH up to 300u.

Condensed species and PAHs present a similar profile and exhibit a rise-decay profile just before the maximum soot formation rate, indicating their role in soot formation process and after the maximum soot formation rate they assume a rise profile, while the soot concentration presents a rise profile and the main oxidation zone reaches a quite constant value in a pos-oxidation zone.

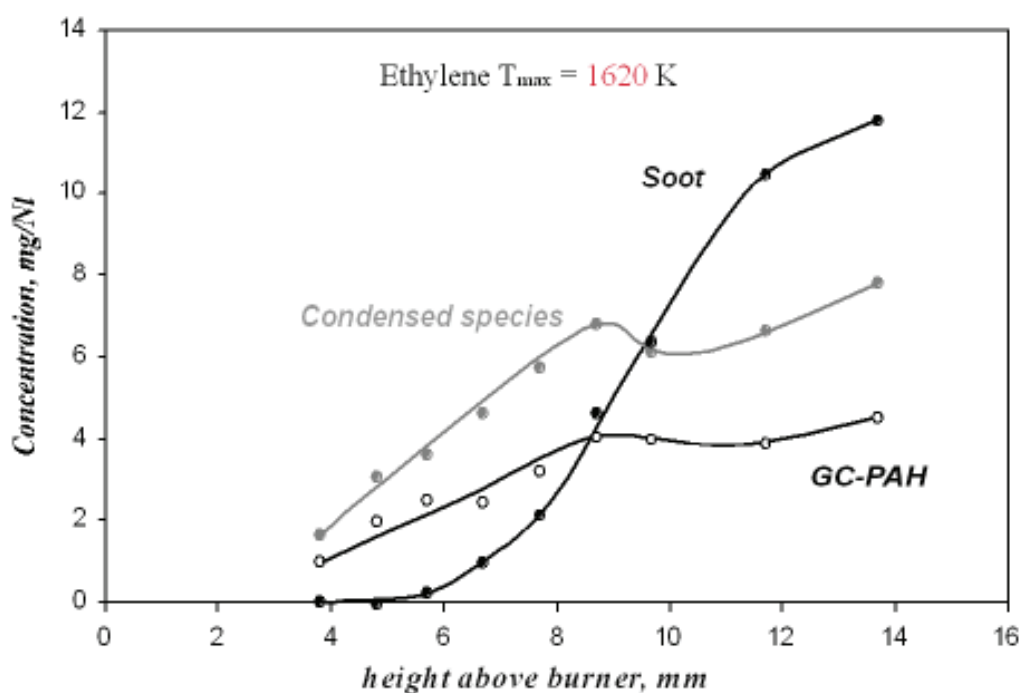


Fig. 3.45 Concentration profiles of GC-PAH, DCM soot extract and soot in ethylene flame at $v=3$ cm/s.

3.3.2 Analysis of condensed species (Gaschromatography-Mass spectrometry)

The profiles of single PAH measured, reported in Fig. 3.46-3.49, exhibit the usual distribution with a larger abundance of small PAH (naphthalene and acenaphthylene) and a lower amount of larger PAH up to coronene.

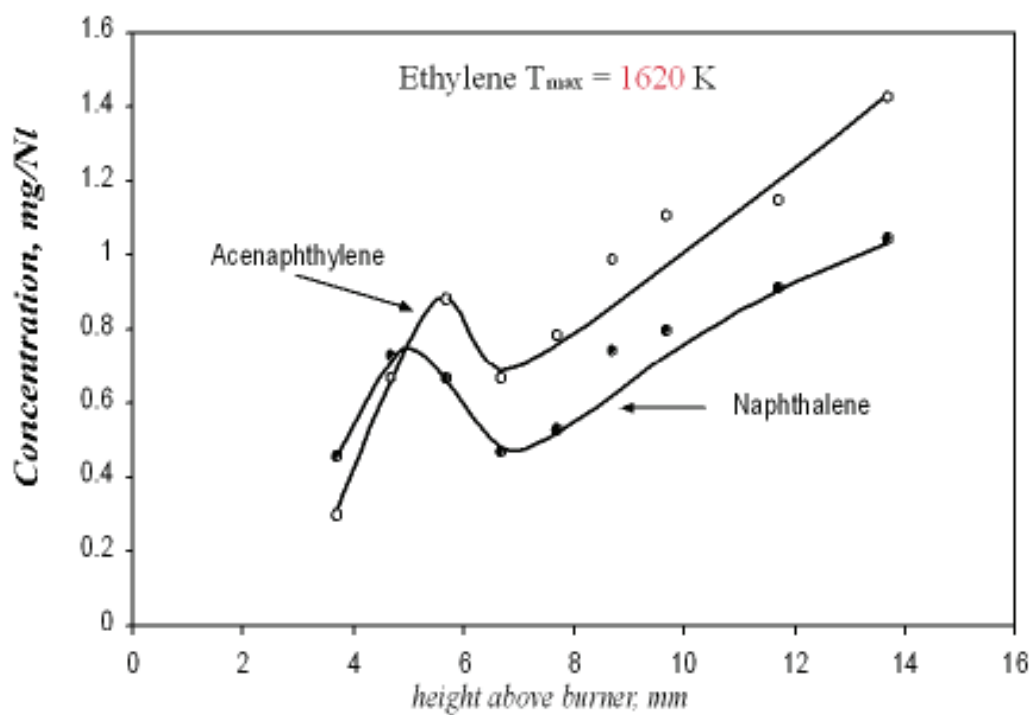


Fig.3.46 Concentration profiles of acenaphthylene and naphthalene in ethylene flame at $v=3$ cm/s.

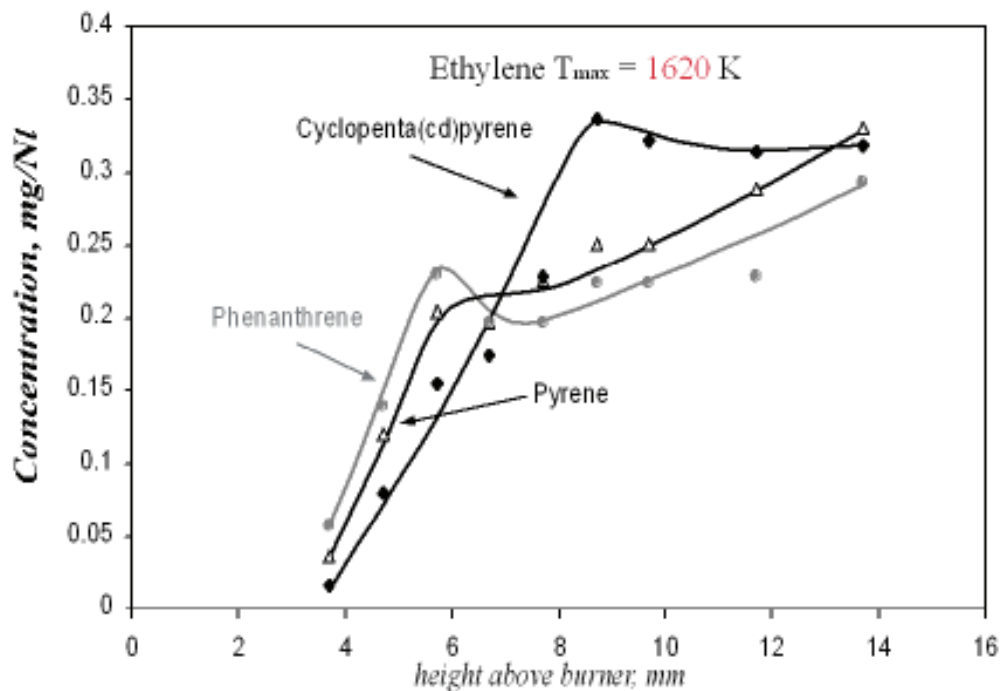


Fig.3.47 Concentration profiles of cyclopenta(cd)pyrene, pyrene and phenanthrene in ethylene flame at $v=3$ cm/s.

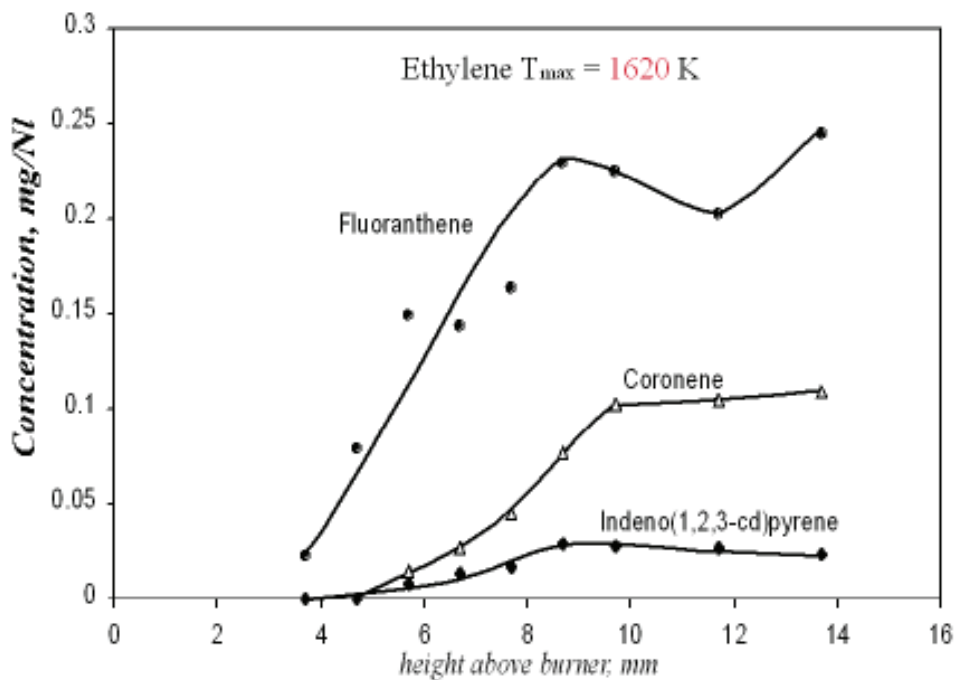


Fig.3.48 Concentration profiles of fluoranthene, coronene and indeno(1,2,3-cde)pyrene in ethylene flame at $v=3$ cm/s.

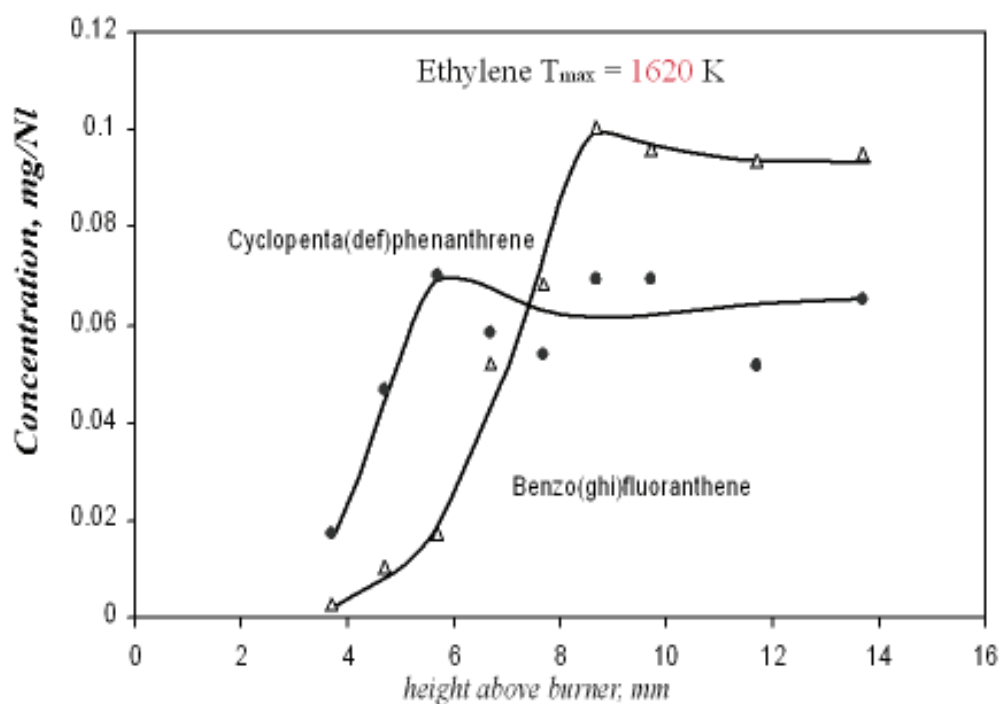


Fig.3.49 Concentration profiles of benzo(ghi)fluorantene and cyclopenta(def)phenantrene in ethylene flame at $v=3$ cm/s.

3.3.4 Soot characterization

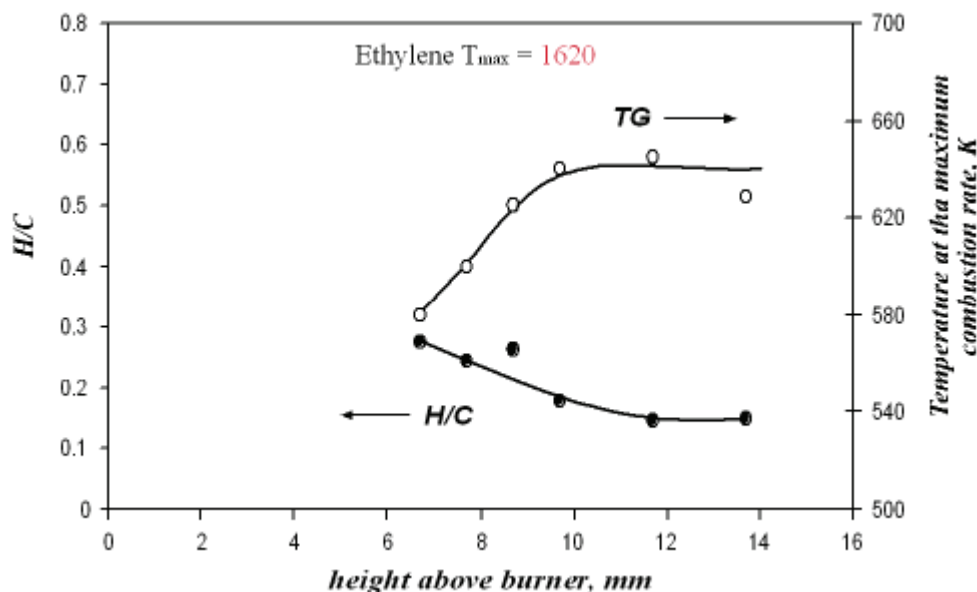


Fig. 3.50 Temperatures of the maximum combustion rate under air (30 ml min^{-1}) and H/C atomic ratio of ethylene soot at $v=3 \text{ cm/s}$ as a function of height above burner.

The temperature of the maximum combustion rate of soot (i.e. the temperature to which the maximum weight loss occurs) along the flame axis is reported in Fig. 3.50. As higher is the maximum combustion temperature lower is the oxidation reactivity.

Soot exhibits an increase of the maximum combustion temperature, from 580 to 640°C, along the flame testifying the decrease of soot oxidation reactivity during the soot formation/maturation process and in the post-oxidation zone the oxidation reactivity of the soot assumes a quite constant value.

It interesting to note that, the oxidation reactivity of ethylene soot is lower than methane/benzene flames soot, this shows the lower reactivity of ethylene soot respect the methane /benzene soot.

The H/C atomic ratios also are reported in Fig. 3.50, shows that the H/C decrease along the flame this implies a change of the internal electronic structure in terms of the increase of sp^2/sp^3 hybridization ratio corresponding to the increase of graphitic planar structures in according to e UV-Visible spectroscopy reported in figure 3.52 that shows an aromatic increase of soot along the flame.

3.3.5 UV-Visible spectroscopy

In figure 3.51 are reported the normalized absorbance of condensed species in ethylene flame at different height above burner.

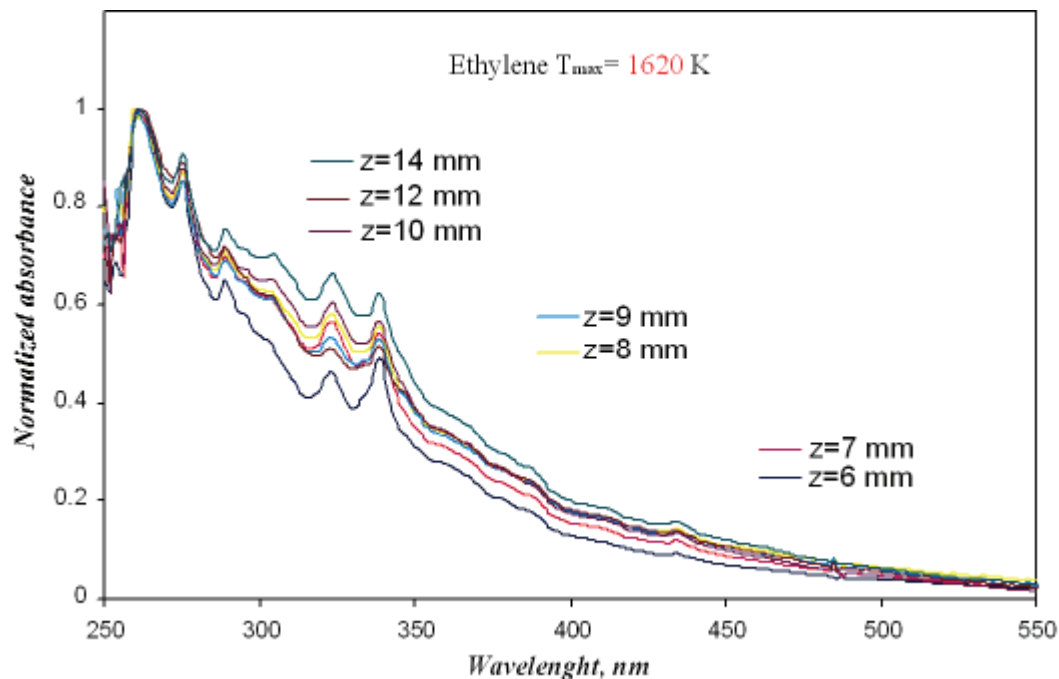


Fig. 3.51 Normalized absorbance of condensed species in ethylene flame ($v=3$ cm/s) at different height above burner.

The normalized absorbance profiles show an aromaticity increase of condensed species along the flames.

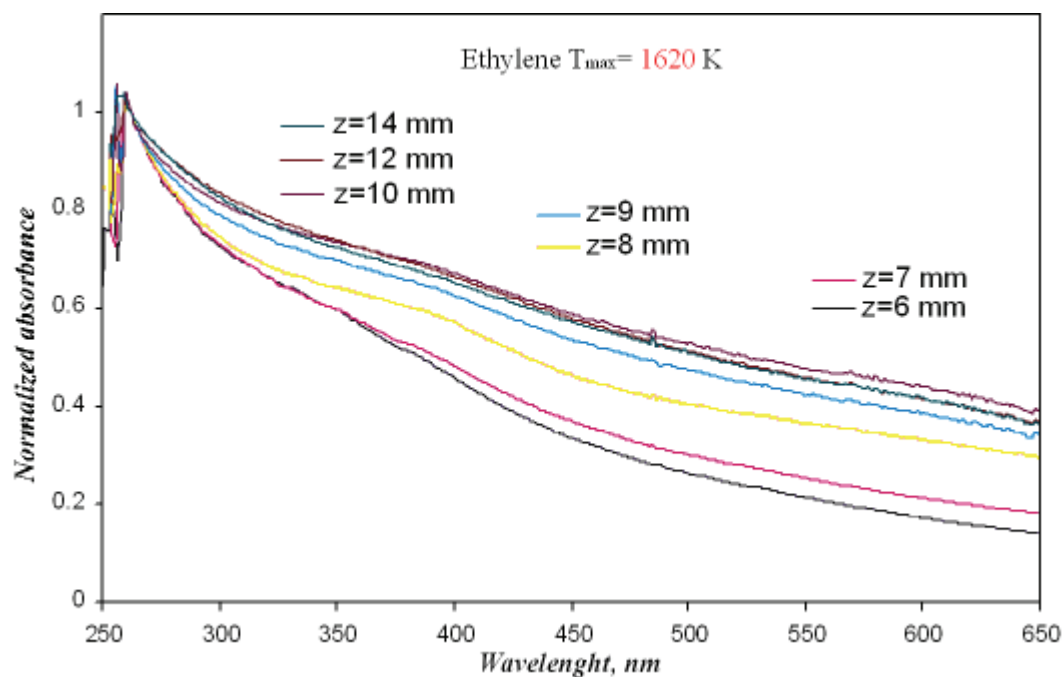


Fig. 3.52 Normalized absorbance of soot in ethylene flame ($v=3$ cm/s) at different height above burner.

In figure 3.59 are reported the normalized absorbance of soot at different height above burner. It can be noted that the soot aromaticity increases along the flame.

The soot absorption coefficients in the UV (300 nm) and in the visible (500 nm) are reported as a function of height above burner in figure 3.53.

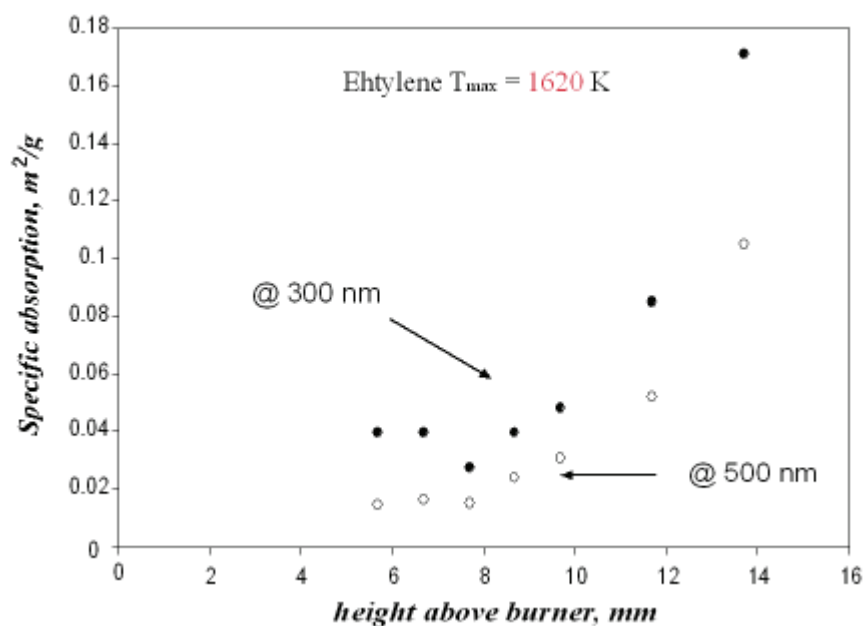


Fig. 3.53 Specific absorption (m^2/g) of benzene soot at $v=3$ cm/s measured at 300 nm (●) and 500 nm (●) and at $v=4$ cm/s measured at 300 nm (○) and 500 nm (○).

The soot absorption coefficients, do not exhibit significant differences both in the UV and in the visible regions and it is noteworthy that the soot absorptivity dramatically changes along the height flame.

3.3.6 FTIR analysis of condensed species and soot

In this section the FTIR was used for to analyze the composition of condensed species and soot sampled by ethylene flame at two different height above burner in particular 8mm and 14mm by FT-IR analyses in the $3800-650\text{ cm}^{-1}$ wavenumber region.

In figure 3.54 are reported the FTIR analysis of condensed species product in ethylene flame at different height above burner.

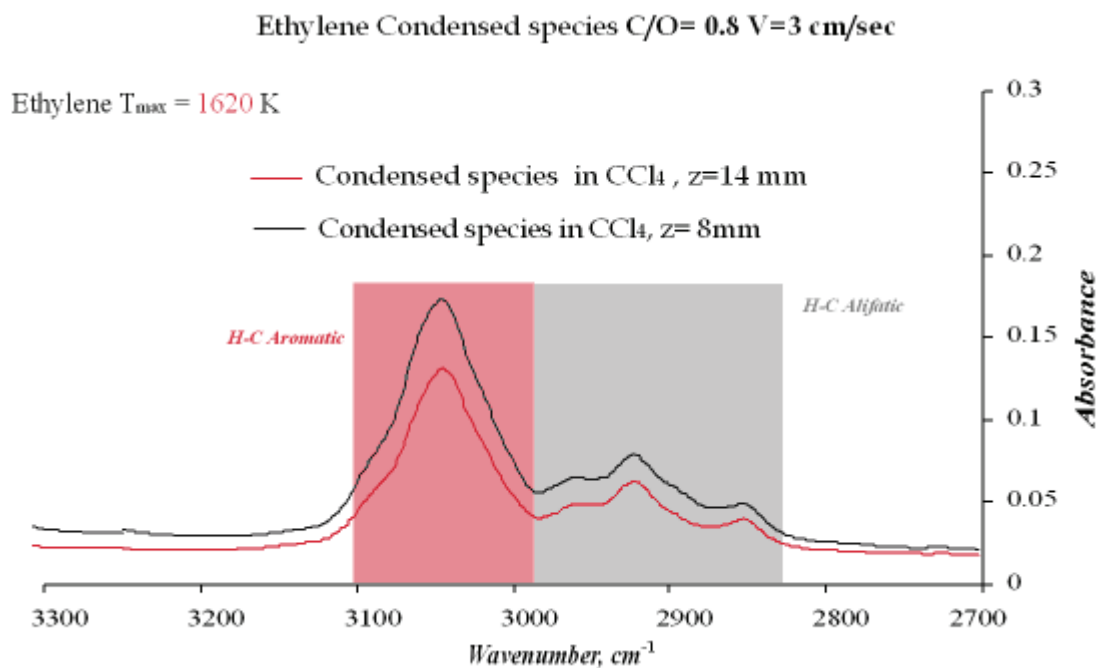


Fig. 3.54 FTIR analysis of condensed species in ethylene flame at $z=8$ mm and $z=14$ mm.

Higher contents of aromatic C–H (stretch at $\lambda=3050$ cm^{-1}) and lower concentration of aliphatic H–C (Alkane CH_3 with asymmetric stretch at $\lambda=2960$ cm^{-1} ; Alkane CH_2 with asymmetric stretch at $\lambda=2920$ cm^{-1} ; Alkane CH_3 with symmetric stretch at $\lambda=2860$ cm^{-1}), it can be noted.

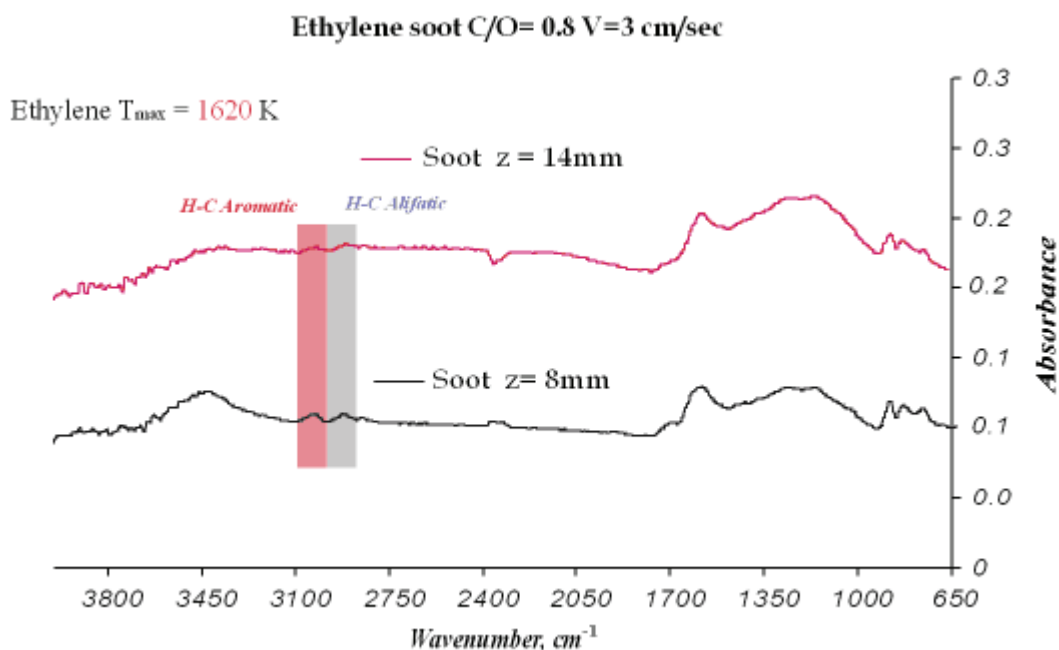


Fig. 3.55 FTIR analysis of soot in in ethylene flame at $z=8$ mm and $z=14$ mm.

In figure 3.55, the FTIR analysis of soot product by ethylene flame at $z=8$ mm and $z=14$ mm, are reported.

It can be noted that the contents of aromatic H-C and aliphatic H-C decreases along the flame, in according to the H/C ratio.

The presence of a carbonyl group is detected and attributed to its peak ($\lambda=1720\text{ cm}^{-1}$), and from an aromatic C=C vibration that is enhanced by the carbonyl (C=O) group bonded ($\lambda=1600\text{ cm}^{-1}$) to the PAH structures (D. M. Smith et al., 1995).

Oxygen-carbon stretches imputed to the ether (1260 cm^{-1}), esters (1100 cm^{-1}) and hydroxyl (1050 cm^{-1}) groups are not observed very well, otherwise for the three peaks in the range of $\lambda=900\text{-}700\text{ cm}^{-1}$ that are observed in both the height above burner and imputed to C-H out-of-plane bending of highly substituted aromatic compounds (A. Santamaria et al., 2006, J. A. Jassim et al., 1986), that decrease along the flame.

3.3.7 Size Exclusion Chromatography of condensed species and soot

A typical molecular weight distributions of condensed species (DCM-extract) inferred by SEC in ethylene flame are reported in Fig 3.56.

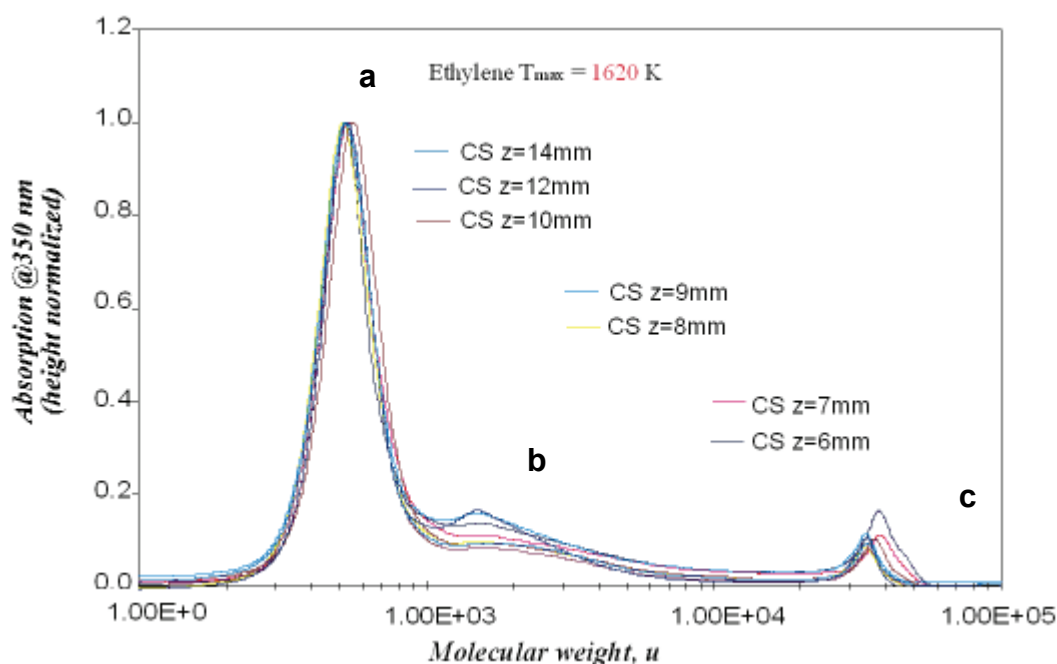


Fig. 3.56 Molecular weight distributions (MW) inferred by SEC of condensed species in ethylene flame ($v=3\text{ cm/s}$) at different height above burner.

The molecular weight distributions of condensed species do not show significant differences moving from the soot inception to the zone of mature soot. DCM-extract is characterized by the predominance of a sharp peak in the 200-400 u range mostly composed by large-PAH (**a**) (Alfè M., et al., 2008) and a much smaller peak in the range from 600 to 2000 u (**b**). A minor peak is also detected at $MW > 1E5\text{ u}$ (**c**).

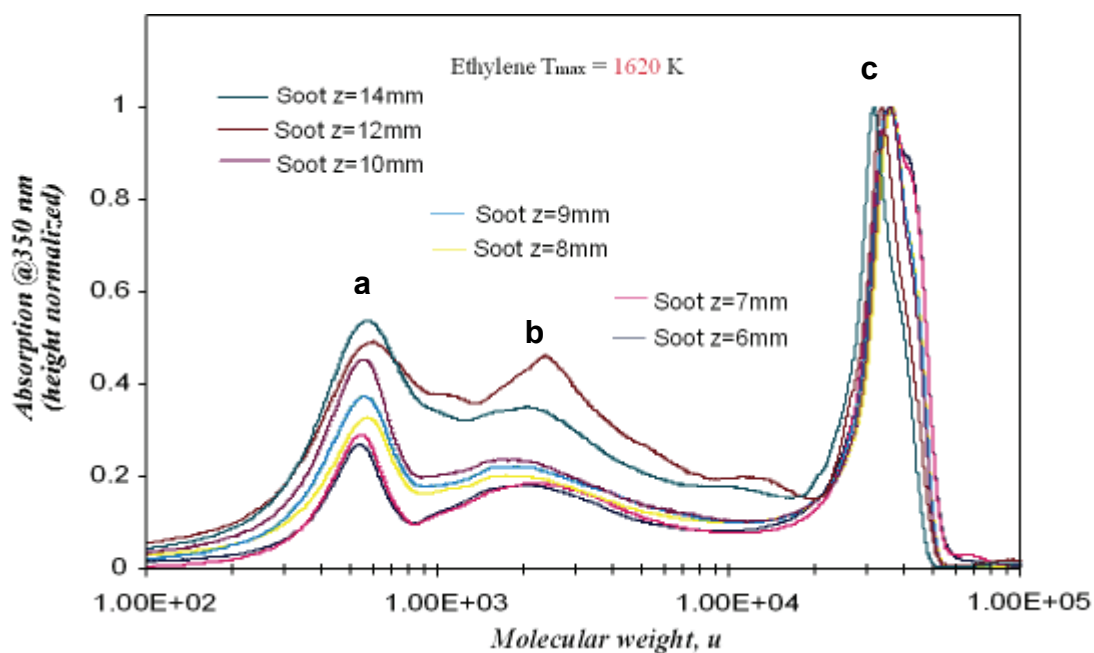


Fig. 3.57 Molecular weight distributions (MW) inferred by SEC of soot in ethylene flame ($v=3$ cm/s) at different height above burner.

In Fig. 3.57 the molecular weight distributions inferred by SEC of soot samples are reported. It can be noted that the contribution of PAH peak (a: 200-400u) is comparable to that of larger MW species (peaks b and c). The peak (c: $1.00E4-1.00E5$ u) is associated to soot aggregate structures (Alfè M., et al, 2008).

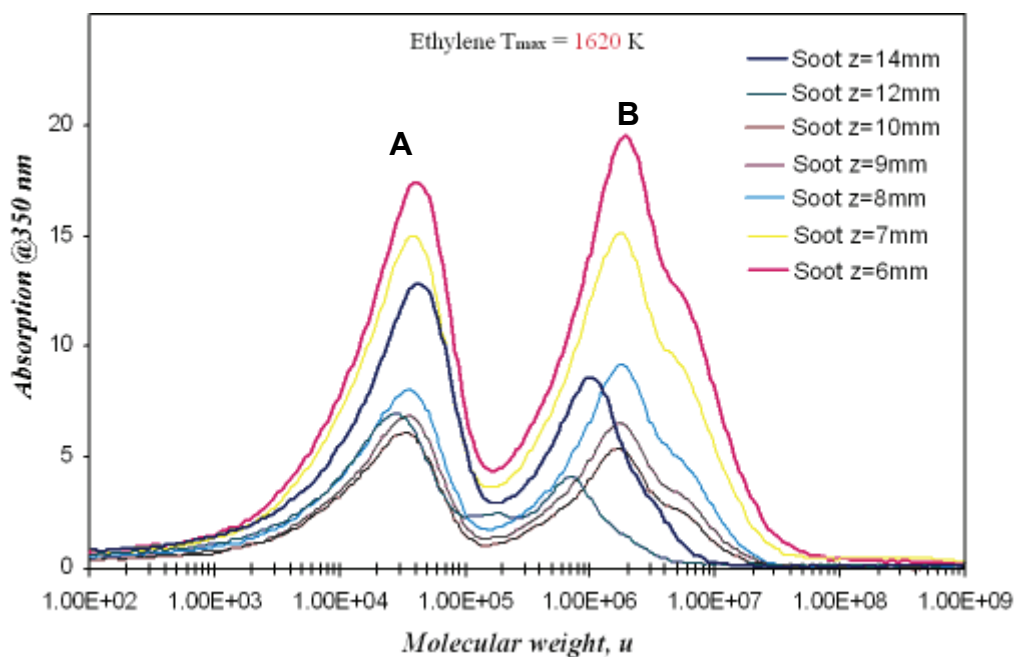


Fig. 3.58 Molecular weight distributions (MW) inferred by SEC of soot in ethylene flame ($v=3$ cm/s) at different height above burner.

The SEC chromatograms of young and mature soot sampled in the ethylene flame are reported in Figure 3.58. The MW in the in the particle-size region (10^5 - 10^{10} u) were obtained by SEC analysis carried out on a Jordi Gel divinylbenzene (DVB) Solid Bead (non-porous) column.

Soot presents a multimodal MW distribution consisting of two main: the first one (**A**) is located in the molecule-region 10^2 - 10^5 u and the second (**B**) in the molecular region of 10^6 - 10^7 u.

The **A** peak (10^2 - 10^5 u) is below the permeation limit of the column ($<10^5$ u) and has been studied in more detail by using a SEC column with a higher resolution power in this specific MW range and reported in figure 3.56.

The **B** peak (10^6 - 10^7 u) MW distribution in the particle-size region can be attributed to heavier material. Moreover, it can be noted that C peak is not present.

It can be noted that the contribution of the lower MW soot components (peak **A**: 10^2 - 10^5 u and peak **B**: 10^6 - 10^7 u) is higher in the case of a young soot ($z=6$ mm) and decreased in a mature soot. This demonstrates that these species disappear as soot formation goes on, possibly in favour of large size soot particles formation. This trend is indeed typical of intermediates in the processes leading to the mature soot formation.

3.4 Bubbling Fluidized Bed BFB Gasification system

The results reported in this section have been obtained as part of the on-going research performed at Second University of Naples, department of Environmental Sciences, on the evaluation of the effect that different reactant gases, i.e. steam, carbon dioxide and air enriched in oxygen content, as well as different bed materials, have on the composition of syngas and on the main performance parameters of co-gasification process.

Some peculiar aspects of the process as the large production of tar or carbon fines can create concerns about the operation of the plant and the economic sustainability of the process.

By consequence the analysis of tar and particulates produced during the gasification process and object of this study is important.

In this section the gas and condensed phases analyses are reported for different bed materials as Quartz sand, Olivine, and a mixture of bed materials (70% Olivine -30% Dolomite).

The experimental condition were obtained using a mixture of fuel composed by plastics (30%), coal (50%) and wood (20%) with fuel flow rate of 20 g/min; oxidant used was air with flow rate of 3000 Nl/h; cold gas velocity of $v=0.4-0.05$ m/s, and oxygen/stoichiometric oxygen ratio E.R. = 0.25. Finally the bed temperature was stabilized on 850 °C.

The composition of syngas has been obtained by on-line gas-chromatography analysis downstream the cleaning syngas. The main component of syngas were H₂, CO, CO₂ and CH₄. Condensed species were analyzed by means of gas chromatography/mass spectrometry (GC-MS) for the quantification of PAH up to 300 u. GC-MS was performed by gas chromatograph equipped with a mass spectrometer with an electron impact/chemical ionization ion source.

3.4.1. Gas and condensed-phases analysis

In Fig. 3.59 the concentration of the main components of syngas CO, CO₂, H₂, and CH₄ are reported for three different bed materials.

In Figs.3.60-3.62, the concentration of light hydrocarbons (C_nH_m with n<7) are reported. Methane and ethylene (Fig. 3.60) are more abundant than acetylene (Fig. 3.61). The lower concentration of acetylene is attributed to the relatively lower bed temperature which limits the dehydrogenation of ethylene. This BFB temperature, indeed, is much lower than the temperature of methane flames (about 1700 K) which favours the acetylene formation (Fig. 3.3).

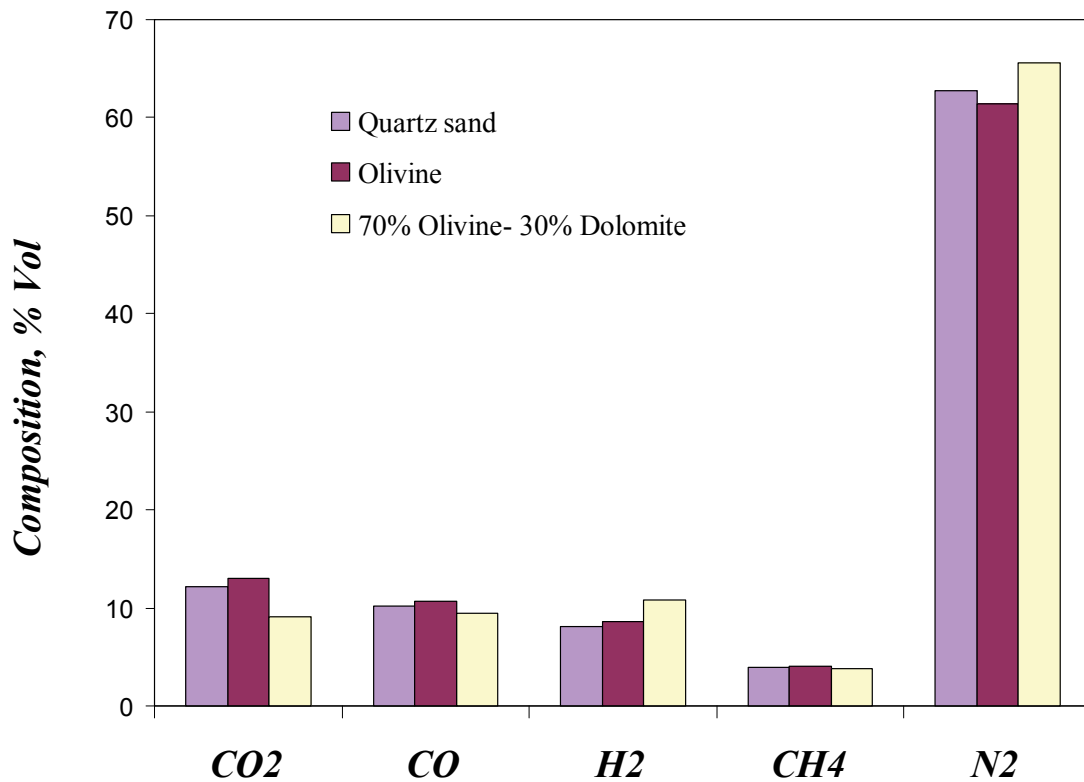


Fig.3.59 Concentration of CO, CO₂, H₂ and N₂ in BFB for different material bed (Quartz sand, Olivine and 70% Olivine-30% Dolomite).

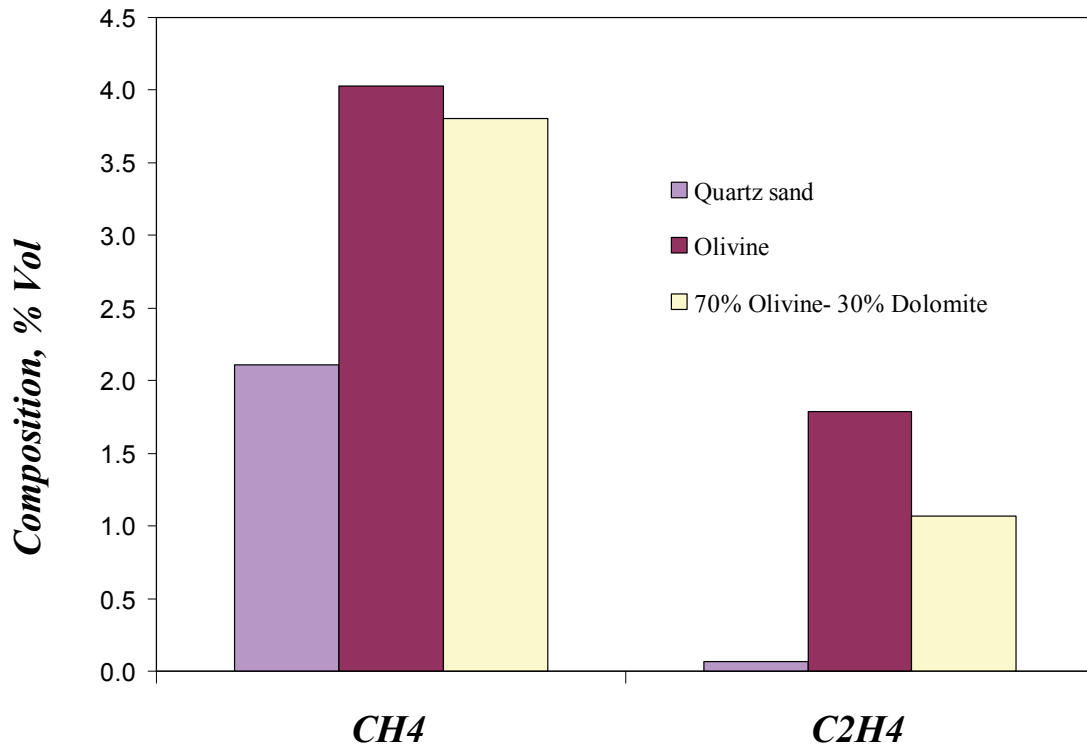


Fig.3.60 Concentration of CH₄ and C₂H₄ in BFB for different bed materials (Quartz sand, Olivine and 70% Olivine-30% Dolomite).

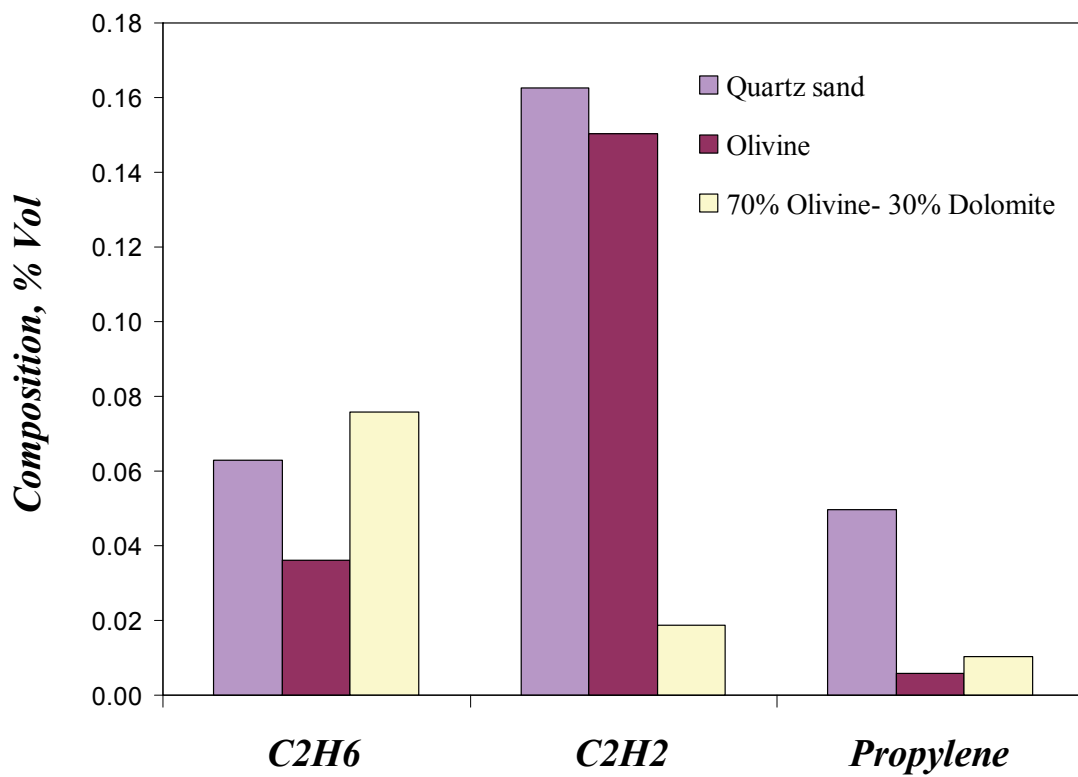


Fig.3.61 Concentration of C₂H₆, C₂H₂ and Propylene in BFB for different bed materials (Quartz sand, Olivine and 70% Olivine-30% Dolomite).

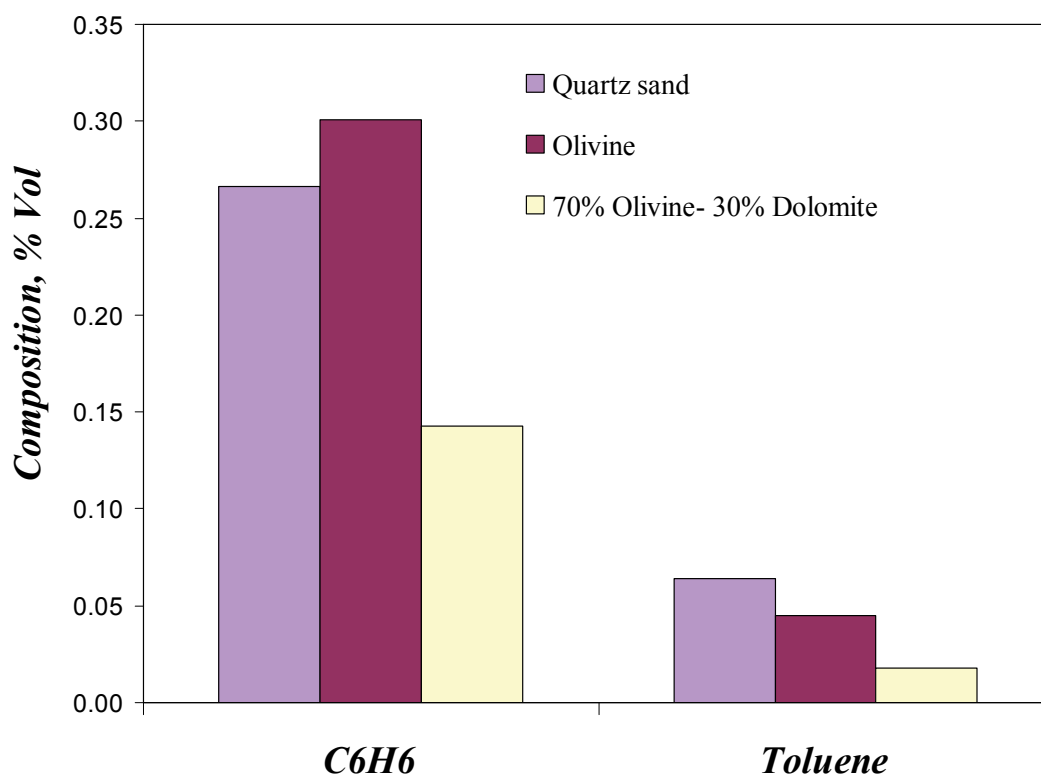


Fig.3.62 Concentration of C_6H_6 and Toluene in BFB for different material bed (Quartz sand, Olivine and 70% Olivine-30% Dolomite).

3.4.2 PAH formation in BFB reactor

In this section the PAH analysis at the exhaust of the BFB with the bed temperature of about 1120 K are reported for the three different bed materials.

The analysis of condensed species were carried out by means of gas chromatography/mass spectrometry (GC-MS) for the identification and quantification of PAH up to 300 u.

The PAHs concentrations, reported in Figs. 3.63-3.66, show the usual distribution with a larger abundance of small PAH (naphthalene and acenaphthylene) and a lower presence of larger PAH up to coronene.

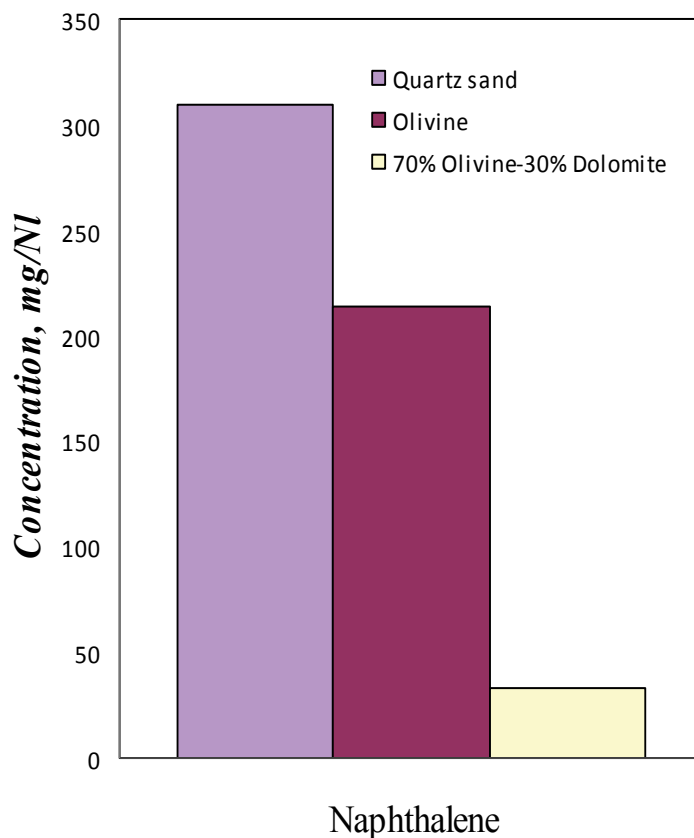


Fig.3.63 Concentration of Naphthalene in syngas for different bed materials.

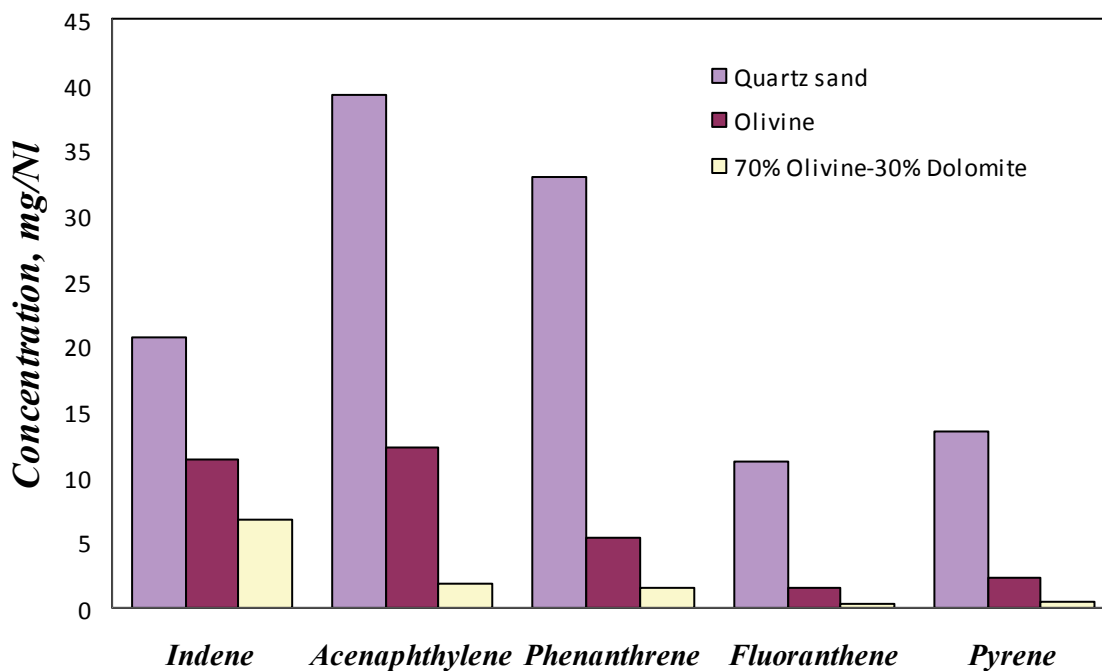


Fig.3.64 Concentration of Indene, Acenaphthylene, Phenanthrene, Fluoranthene, Pyrene in syngas analyzed for different bed materials .

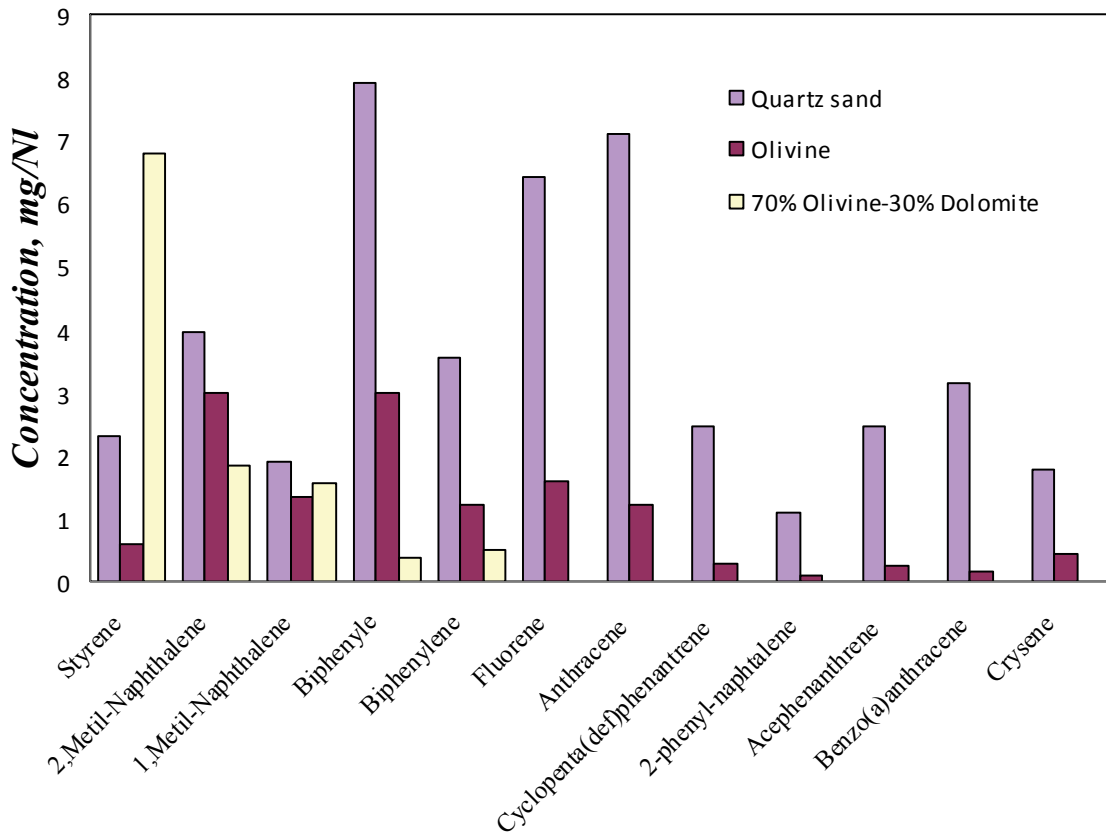


Fig.3.65 Concentration of different PAHs in syngas analyzed for different bed materials.

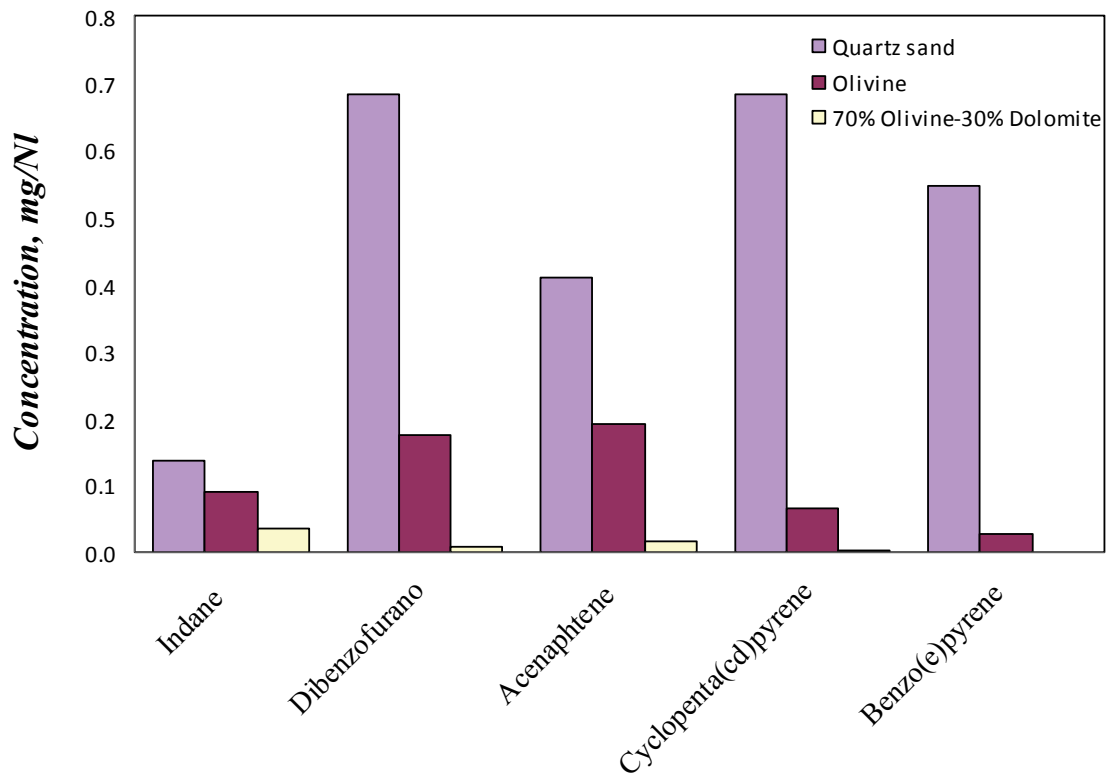


Fig.3.66 Concentration of different PAHs in syngas analyzed for different bed materials.

3.4.3 Comparison between gas and condensed-phases species formed in methane flames and in the bubbling fluidized bed.

In this section the comparison between the higher temperature systems such as the atmospheric-pressure laminar premixed flames and a lower temperature system as a Bubbling Fluidized Bed (BFB) system is reported.

Table 1 shows the results of the gas phase concentration of the exhaust from the two methane flames and bubbling fluidized beds respectively. The data obtained for the bubbling beds were corrected for the dilution in order to make comparable the concentration with those measured in the methane flames. In the higher temperature conditions of methane laminar premixed flames, there is a greater hydrogen formation with a lower CO₂ production with respect to the BFB reactor.

	Methane fame v= 4 cm/s	Methane fame v= 5 cm/s	Quartz sand	Olivine	70% Olivine 30% Dolomite
CO	33,23	32,36	27,59	27,62	27,57
CO₂	8,66	7,62	32,84	33,77	26,43
H₂	42,86	48,90	21,89	22,35	31,32
Methane	9,69	5,59	10,71	10,45	11,06
Ethylene	0,5555	0,30	5,70	4,62	3,11
Acetylene	4,81	5,14	0,44	0,39	0,055
Propylene	0,0333	0,022	0,134	0,015	0,03
1,3-Butadiene	0,003	0,0015	0	0	0
Benzene	0,149	0,0665	0,716	0,785	0,415

Tab.3.1 % Gas Analysis of the exhaust from methane flames and bubbling fluidized bed

The lower concentration of acetylene in the BFB testifies that the dehydrogenation degree and thus the pyrolytic routes are inhibited in the lower temperature conditions of the BFB. In spite of the lower concentration of acetylene a higher formation of benzene can be observed that has to be related to the characteristics of P8 fuel rich in very aromatic components as PET and coal. Generally to the higher benzene formation is associated a higher PAH formation with a distribution shifted toward higher molecular weight species

as shown by the condensed species PAH composition for methane flames at two different heights above burner, respectively 6 mm (left) and 12 mm (right), reported in Figs. 3.67-3.68. Indeed the larger abundance of acenaphthylene and larger PAH is generally noticeable.

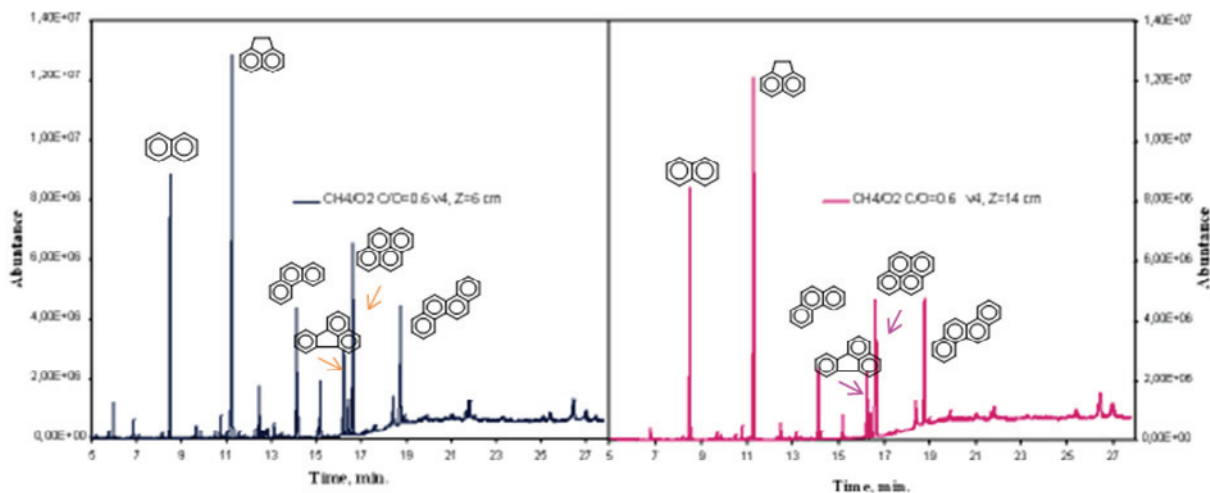


Fig.3.67 Chromatograms of condensed species obtained by GC-Ms in the methane flame at $v=4$ cm/s.

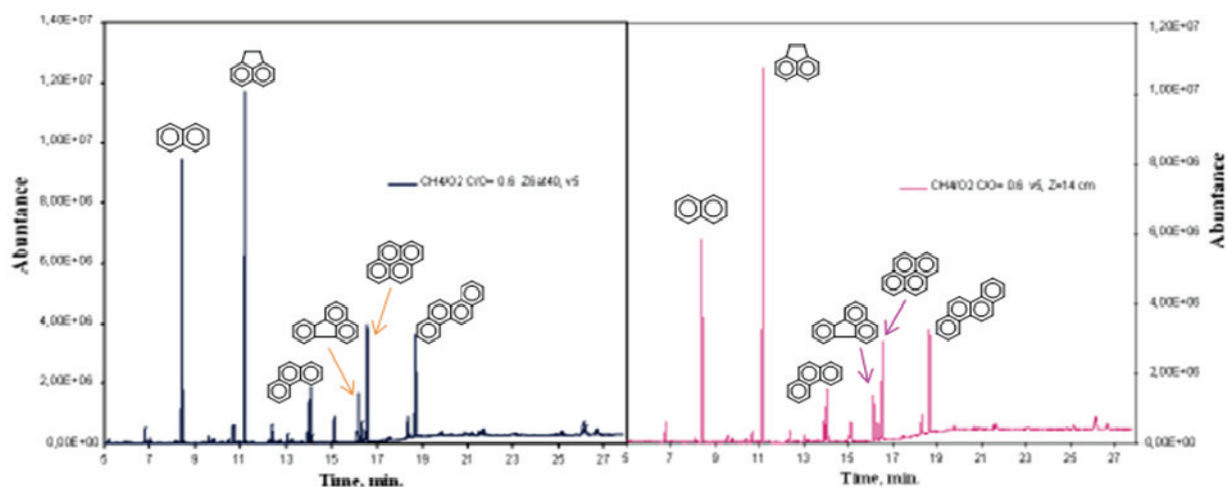


Fig.3.68 Chromatograms of condensed species obtained by GC-Ms in the methane flame at $v=5$ cm/s.

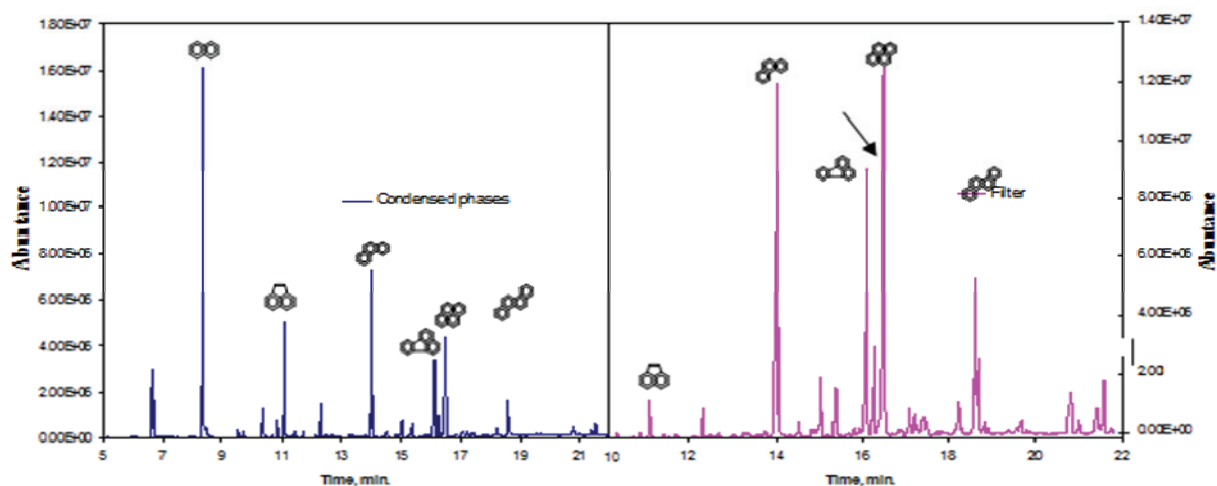


Fig.3.69 Chromatograms obtained by GC-MS of condensed species and species trapped in the filter in the BFB reactor.

The analysis of PAH in the total condensed species and trapped on the filter in BFB are reported in Fig. 3.69. It can be noted that in spite of the larger benzene formation the PAH are predominantly constituted of two-ring components as naphthalene whereas acenaphthylene, typical products of high temperature combustion, is quite lower. This testifies that the molecular growth up to larger PAH is inhibited in the lower temperature conditions of BFB.

It is worth to note that a different distribution of PAHs in condensed species and on the filter is shown. In the condensed phases there is a higher amount of small PAHs as naphthalene can be observed whereas the larger PAH as pyrene are predominant on the filter. This is justified by the fact that the filter is located downstream the bubblers where naphthalene is trapped.

The effect of the bed nature is very evident when dolomite is used because a syngas richer in hydrogen, CO, methane and a lower formation of PAHs has been found. This is probably due to its catalytic property leading to the tar cracking.

The molecular weight distributions (MW) inferred by SEC of condensed species in BFB are reported in Fig. 3.70.

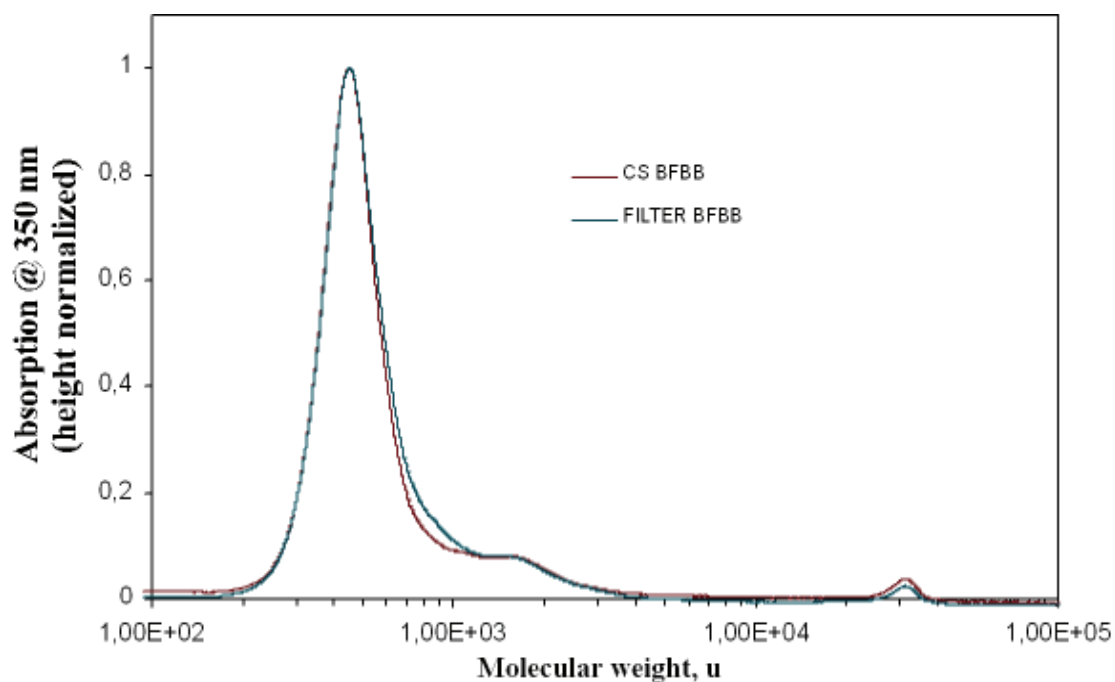


Fig.70 Molecular weight distributions (MW) inferred by SEC of condensed species in BFB.

The MW distribution is similar to those found in the methane flames condensed species: the PAH peak (200-400u) is predominant in both the sampled materials (condensed species and filter).

It is worth to note that the concentration of the higher MW class (3E4u) is lower with respect to the methane flames (Fig. 3.18).

More experimental work will be necessary to understand if there is a temperature effect on the formation of the higher MW classes.

CONCLUSIONS

CONCLUSIONS

Advancements in the chemical and spectroscopic techniques for the analysis of particulate matter produced in combustion processes were obtained in the course of this thesis work.

Particular emphasis was given to the characterization of fine and ultrafine fractions and to the study of the effect of combustion parameters as flame temperature and fuel chemical properties.

The effect of temperature was studied in premixed atmospheric pressure fuel-rich flames burning at two different cold-gas flow velocities corresponding to different flame temperatures.

In particular, methane/O₂ flames (C/O= 0.6 at two different cold gas velocity: 4 and 5 cm/s) and benzene/O₂/N₂ (C/O= 0.8 at two different cold gas velocity: 3 and 4 cm/s) were studied and a preliminary characterization of the flame structures was performed determining the temperature and concentration profiles of reactants and combustion products including gas phase and condensed-phase species.

In the methane/O₂ flame burning at lower temperature a lower formation of acetylene and higher formation of cyclopentadiene, benzene and condensed species has been found in correspondence of a higher soot yield. This is indicative of a participation of benzene and condensed species rather than acetylene, in soot inception and maturation processes.

It was found that the H/C ratio of soot decreases along both the flames, but it is slightly lower in the higher temperature flame consistently with the inherent higher degree of dehydrogenation (larger presence of hydrogen and acetylene). The soot oxidation reactivity increases along the flame as H/C decreases, but it does not appear to be affected by the flame temperature. Also the PAHs distribution in methane flames and the soot aromaticity appeared to be not affected by the flame temperature (1650-1770K), and soot aromaticity is lower than the aromaticity of soot measured in flames of other less hydrogenated hydrocarbons. This suggests that the methane soot almost retains the spectroscopic characteristics of young soot without undergoing along the flame a high degree of graphitization associated to growth processes.

Benzene/O₂/N₂ flames were produced at a constant mixture composition (C/O = 0.8) and different cold-gas flow velocities (3 and 4 cm/s) corresponding at different flame temperatures.

Acetylene is the main hydrocarbon species produced in the rich combustion of benzene not significantly influenced by the flame temperature whereas soot formation was found to be lower in the high temperature flame.

The soot absorption coefficients, do not exhibit significant differences both in the UV and in the visible regions while the soot absorptivity in the two flames dramatically changes along the height flame. Moreover, it can be noticed that the aromaticity of benzene soot is not influenced by flame temperature and generally, much higher than that measured for soot produced from aliphatic fuels as methane.

Finally, the study of premixed laminar flames were applied to the ethylene flame in particular to ethylene/O₂ at a constant mixture composition (C/O = 0.8) and fixed coal gas velocity of $v=4$ cm/s, that corresponds a maximum temperature of 1620K.

In this case, differently by methane and benzene flames, methane and acetylene are the main hydrocarbon species produced in the rich combustion of ethylene. The condensed species and soot show that ethylene flame produces a higher formation of soot and condensed species than methane and benzene flame.

In ethylene flame, the soot absorption coefficients do not exhibit significant differences in the UV and in the visible regions while the soot absorptivity presents a significant changes along the height flame, generally higher respect to methane and benzene flames.

The sampling and analytical techniques set up on the basic combustion flame experiment have been transferred to real systems as pre-pilot and pilot fluidized bed gasification reactors.

The gasification tests have been carried out in a Bubbling Fluidized Bed (BFB), 102mmID and 2.5m high, at a fixed equivalence ratio (ER=0.25), a gas velocity in the range 0.4-0.5m/s and a reactor temperature of 850 °C. A fuel mixture having 50% of German brown coal, 30% of plastic waste (PE, PP and PET) and 20% of wood was chosen as reference fuel named P8 and was used with different bed materials as Quartz sand, Olivine, and a mixture of bed materials (70% Olivine -30% Dolomite).

Gas analysis has shown that the main components of syngas are CO, CO₂, and H₂. Methane and ethylene are more abundant than acetylene. The lower concentration of hydrogen and acetylene with respect to methane combustion is attributed to the different fuel characteristics as well as to the relatively lower bed temperature which limits the dehydrogenation reactions.

The larger formation of benzene in the BFB is mostly related to the larger aromaticity of P8 fuel.

In spite of the larger benzene concentration it has been observed that the lower temperature of the fluidized bed with respect to the methane/oxygen flames causes a production of lighter PAH with larger contributions of naphthalene whereas acenaphthylene, typical products of high temperature combustion, is quite negligible.

The analysis of PAH performed separately on the sample collected in the ice trap and on the filter allows the enhancement of higher molecular weight PAH detection by gaschromatography.

FIGURES

Figures:

- Fig. 1.1** *Microscope image of the carbonaceous particulate produced in a flame*
- Fig.1.2** *Schematic diagram of the size distribution (expressed as mass per increment in log particle diameter) and formation mechanisms for atmospheric aerosols (from Whitby and Cantrell, 1976)*
- Fig.1.3** *Scheme of soot formation process (from H. Bockhorn 'Soot Formation in Combustion' Springer-Verlag Berlin Heidelberg 1994)*
- Fig. 1.4** *Temperature dependence of f_{voc} for C_2H_4 -air flames at $\text{C/O}=0.72$ (*), C_2H_2 - air at $\text{C/O}=0.70$ (o) and C_6H_6 -air flames at $\text{C/O}=0.74$ (●) (from Bohm et al, 1988)*
- Fig. 2.1** *Scale-laboratory combustion system*
- Fig. 2.2** *Sampling line for gas analysis on the pre-pilot Bubbling Fluidized Bed (BFB) plant*
- Fig. 2.3** *Bubbling Fluidized Bed (BFB)*
- Fig 2.4** *Analytical characterization scheme of particulate matter.*
- Fig 2.5** *Scheme of fluorescence emission energy.*
- Fig 2.6** *SEC polystyrene calibration curve (O). Other standard compounds are reported on the curve as follows: () polyacenaphthylene, dicoronylene, paracyclophane, fullerite, pyrene, and toluene.*
- Fig. 3.1** *Temperature and extinction coefficient profiles measured along the axis of methane flames burning at $v=4$ cm/s ($T_{\text{max}} 1650\text{K}$) and at $v=5$ cm/s ($T_{\text{max}} 1780\text{K}$).*

- Fig. 3.2** Concentration profiles of reactants and main combustion products in the high temperature ($v=4$ cm/s (left) and low temperature ($v=5$ cm/s) (right) methane flames.
- Fig. 3.3** Concentration profiles of hydrogen, ethylene and acetylene in the low temperature ($v=4$ cm/s) (left) and high temperature ($v=5$ cm/s) (right) methane flames.
- Fig. 3.4** Concentration profiles of the most abundant C_3 (upper) and C_4 hydrocarbons (lower) in the low temperature ($v=4$ cm/s) (left) and high temperature ($v=5$ cm/s) (right) methane flames .
- Fig. 3.5** Concentration profiles of cyclopentadiene and benzene in methane flames in the low temperature at $v=4$ cm/s (left) and high temperature ($v=5$ cm/s) methane flames at (right).
- Fig. 3.6** Concentration profiles of GC-PAH, DCM soot extract and soot in methane flames at $v=4$ cm/s (left) and at $v=5$ cm/s (right)
- Fig.3.7** Concentration profiles of acenaphthylene and naphthalene in the low temperature at $v=4$ cm/s (left) and high temperature ($v=5$ cm/s) (right) methane flames.
- Fig.3.8** Concentration profiles of cyclopenta(cd)pyrene, pyrene and phenanthrene in the low temperature ($v=4$ cm/s) (left) and high temperature ($v=5$ cm/s) (right) methane flames.
- Fig.3.9** Concentration profiles of fluoranthene, coronene and indeno(1,2,3-cde) in the low temperature ($v=4$ cm/s) (left) and high temperature ($v=5$ cm/s) (right) methane flames.
- Fig.3.10** Concentration profiles of benzo(ghi)fluorantene and cyclopenta(def)phenantrene in methane flames at $v=4$ cm/s (left) and at $v=5$ cm/s (right).
- Fig. 3.11** Temperatures of the maximum combustion rate under air (30 ml min^{-1}) and H/C atomic ratio of low-temperature methane soot at $v=4$ cm/s (\bullet) and high-temperature methane soot at $v=5$ cm/s (\circ) as a function of height above burner.
- Fig. 3.12** Normalized UV-visible spectra of condensed species in methane flames at $v=4$ cm/s (left) and at $v=5$ cm/s (right).
- Fig. 3.13** Normalized absorbance of soot in methane flames at $v=4$ cm/s (left) and at $v=5$ cm/s (right).
- Fig. 3.14** Specific absorption (m^2/g) of methane soot at $v=4$ cm/s measured at 300 nm (\bullet) and 500 nm (\bullet) and at $v=5$ cm/s measured at 300 nm (\circ) and 500 nm (\circ).

- Fig. 3.15** FTIR analysis of condensed species in methane flames for $z=8$ mm at $v=4$ cm/s and at $v=5$ cm/s.
- Fig. 3.16** FTIR analysis of soot in methane flames for $z=8$ mm at $v=4$ cm/s and at $v=5$ cm/s.
- Fig3.17** ...From the SEC chromatogram to a MW distribution.
- Fig. 3.18** Molecular weight distributions (MW) inferred by SEC of condensed species in methane flames for $z=6$ mm and $z=12$ mm at $v=4$ cm/s and at $v=5$ cm/s.
- Fig. 3.19** Molecular weight distributions (MW) inferred by SEC of soot in methane flames for $z=6$ mm and $z=12$ mm at $v=4$ cm/s and at $v=5$ cm/s.
- Fig. 3.20** Molecular weight distributions (MW) inferred by SEC of soot in methane flames for $z=6$ mm and $z=12$ mm at $v=4$ cm/s and at $v=5$ cm/s.
- Fig. 3.21** Temperature and extinction coefficient of benzene flames at $v=3$ cm/s (left) and at $v=4$ cm/s (right).
- Fig. 3.22** Concentration profiles of reactants and main combustion products of benzene flames at $v=3$ cm/s (left) and at $v=4$ cm/s (right).
- Fig. 3.23** Concentration profiles of hydrogen, ethylene and acetylene in benzene flames at $v=3$ cm/s (left) and at $v=4$ cm/s (right).
- Fig. 3.24** Concentration profiles of the most abundant C_3 (upper) and C_4 hydrocarbons (lower) in benzene flames at $v=3$ cm/s (left) and at $v=4$ cm/s (right).
- Fig. 3.25** Concentration profiles of cyclopentadiene in benzene flames at $v=3$ cm/s (left) and at $v=4$ cm/s (right).
- Fig. 3.26** Concentration profiles of GC-PAH, DCM soot extract and soot in benzene flames at $v=3$ cm/s (left) and at $v=4$ cm/s (right)
- Fig.3.27** Concentration profiles of acenaphthylene and naphthalene in benzene flames at $v=3$ cm/s (left) and at $v=4$ cm/s (right).

- Fig.3.28** Concentration profiles of cyclopenta(cd)pyrene, pyrene and phenanthrene in benzene flames at $v=3$ cm/s (left) and at $v=4$ cm/s (right).
- Fig.3.29** Concentration profiles of fluoranthene, coronene and indeno(1,2,3-cde)pyrene in benzene flames at $v=3$ cm/s (left) and at $v=4$ cm/s (right).
- Fig.3.30** Concentration profiles of benzo(ghi)fluorantene and cyclopenta(def)phenantrene in benzene flames at $v=3$ cm/s (left) and at $v=4$ cm/s (right).
- Fig. 3.31** Temperatures of the maximum combustion rate under air (30 ml min^{-1}) and H/C atomic ratio of low-temperature benzene soot at $v=4$ cm/s (●) and high-temperature benzene soot at $v=5$ cm/s (○) as a function of height above burner.
- Fig. 3.32** Normalized absorbance of condensed species in benzene flames at $v=3$ cm/s (left) and at $v=4$ cm/s (right).
- Fig. 3.33** Normalized absorbance of soot in benzene flames at $v=3$ cm/s (left) and at $v=4$ cm/s (right).
- Fig. 3.4** Specific absorption (m^2/g) of benzene soot at $v=3$ cm/s measured at 300 nm (●) and 500 nm (●) and at $v=4$ cm/s measured at 300 nm (○) and 500 nm (○).
- Fig. 3.35** Molecular weight distributions (MW) inferred by SEC of condensed species in benzene flames for $z=6\text{mm}$ and $z=12\text{mm}$ at $v=3$ cm/s and at $v=4$ cm/s.
- Fig. 3.36** Molecular weight distributions (MW) inferred by SEC of soot in benzene flames for $z=6\text{mm}$ and $z=12\text{mm}$ at $v=3$ cm/s and at $v=4$ cm/s.
- Fig. 3.37** Molecular weight distributions (MW) inferred by SEC of soot in benzene flames for $z=7\text{mm}$ and $z=12\text{mm}$ at $v=3$ cm/s and at $v=4$ cm/s.
- Fig. 3.38** Temperature of ethylene flame at $v=3$ cm/s.
- Fig. 3.39** Extinction coefficient of ethylene flame at $v=3$ cm/s.
- Fig. 3.40** Concentration profiles of reactants and main combustion products of ethylene flame at $v=3$ cm/s.

- Fig. 3.41** Concentration profiles of methane and acetylene in ethylene flame at $v=3\text{cm/s}$.
- Fig. 3.42** Concentration profiles of the most abundant C_3 hydrocarbons in ethylene flame at $v=3\text{ cm/s}$.
- Fig. 3.43** Concentration profiles of the most abundant C_4 hydrocarbons ethylene flame at $v=3\text{ cm/s}$.
- Fig. 3.44** Concentration profiles of cyclopentadiene and benzene in ethylene flames at $v=3\text{ cm/s}$.
- Fig. 3.45** Concentration profiles of GC-PAH, DCM soot extract and soot in ethylene flame at $v=3\text{ cm/s}$.
- Fig.3.46** Concentration profiles of acenaphthylene and naphthalene in ethylene flame at $v=3\text{ cm/s}$.
- Fig.3.47** Concentration profiles of cyclopenta(cd)pyrene, pyrene and phenanthrene in ethylene flame at $v=3\text{ cm/s}$.
- Fig.3.48** Concentration profiles of fluoranthene, coronene and indeno(1,2,3-cde)pyrene in ethylene flame at $v=3\text{ cm/s}$.
- Fig.3.49** Concentration profiles of benzo(ghi)fluorantene and cyclopenta(def)phenantrene in ethylene flame at $v=3\text{ cm/s}$.
- Fig. 3.50** Temperatures of the maximum combustion rate under air (30 ml min^{-1}) and H/C atomic ratio of ethylene soot at $v=3\text{ cm/s}$ as a function of height above burner.
- Fig. 3.51** Normalized absorbance of condensed species in ethylene flame ($v=3\text{ cm/s}$) at different height above burner.
- Fig. 3.52** Normalized absorbance of soot in ethylene flame ($v=3\text{ cm/s}$) at different height above burner.
- Fig. 3.53** Specific absorption (m^2/g) of benzene soot at $v=3\text{ cm/s}$ measured at 300 nm (●) and 500 nm (●) and at $v=4\text{ cm/s}$ measured at 300 nm (○) and 500 nm (○).
- Fig. 3.54** FTIR analysis of condensed species in ethylene flame at $z=8\text{mm}$ and $z=14\text{mm}$.

Fig. 3.55 FTIR analysis of soot in ethylene flame at $z=8\text{mm}$ and $z=14\text{mm}$.

Fig. 3.56 Molecular weight distributions (MW) inferred by SEC of condensed species in ethylene flame ($v=3\text{ cm/s}$) at different height above burner.

Fig. 3.57 Molecular weight distributions (MW) inferred by SEC of soot in ethylene flame ($v=3\text{ cm/s}$) at different height above burner.

Fig. 3.58 Molecular weight distributions (MW) inferred by SEC of soot in ethylene flame ($v=3\text{ cm/s}$) at different height above burner.

Fig.3.59 Concentration of CO , CO_2 , H_2 and N_2 in BFB for different material bed (Quartz sand, Olivine and 70% Olivine-30% Dolomite).

Fig.3.60 Concentration of CH_4 and C_2H_4 in BFB for different bed materials (Quartz sand, Olivine and 70% Olivine-30% Dolomite).

Fig.3.61 Concentration of C_2H_6 , C_2H_2 and Propylene in BFB for different bed materials (Quartz sand, Olivine and 70% Olivine-30% Dolomite).

Fig.3.62 Concentration of C_6H_6 and Toluene in BFB for different material bed (Quartz sand, Olivine and 70% Olivine-30% Dolomite).

Fig.3.63 Concentration of Naphthalene in syngas for different bed materials.

Fig.3.64 Concentration of Indene, Acenaphthylene, Phenanthrene, Fluoranthene, Pyrene in syngas analyzed for different bed materials .

Fig.3.65 Concentration of different PAHs in syngas analyzed for different bed materials.

Fig.3.66 Concentration of different PAHs in syngas analyzed for different bed materials.

Fig.3.67 Chromatograms of condensed species obtained by GC-MS in the methane flame at $v=4\text{ cm/s}$.

Fig.3.68 *Chromatograms of condensed species obtained by GC-MS in the methane flame at $v=5$ cm/s.*

Fig.369 *Chromatograms obtained by GC-MS of condensed species and species trapped in the filter in the BFB reactor.*

Fig.70 *Molecular weight distributions (MW) inferred by SEC of condensed species in BFB.*

Tab 1.1 *Composition of the dry air at ground level.*

Tab.1.2 *Typical structure and carcinogenicity classification for principal PAHs - 1: human carcinogen, 2A: probably human carcinogen, 2B: possible human carcinogen, 3: non-carcinogen.*

Tab. 2.1 *Methane/O₂ operating conditions.*

Tab. 2.2 *Benzene/O₂/N₂ operating conditions.*

Tab. 2.3 *Ethylene/O₂ operating conditions.*

Tab.2.4 *Experimental condition for the bubbling fluidized bed.*

Tab.3.1 *% Gas analysis of the exhaust from methane flames and bubbling fluidized bed.*

REFERENCES

References

- ✓ **Alfè, M., Apicella, B., Barbella, R., Tregrossi, A., Ciajolo, A.**, Fourth European Combustion Meeting (ECM), (2009).

- ✓ **Alfè, M., Apicella, B., Barbella, R., Rouzaud, J-N., Tregrossi, A., Ciajolo, A.**, Proc. Combust. Inst. 32, 697–704 (2009).

- ✓ **Alfè M., Barbella R., Mallardo M., Tregrossi A, Ciajolo A.**: *"The formation of pollutants in fuel-rich methane combustion"* Chemical Engineering Transaction, 16, 2008. 291-298. Proceedings of 2nd Advanced Atmospheric Aerosol Symposium (AAAS), November 9-12th, Napoli, Italy (2008)

- ✓ **Alfè M., Barbella R., Mallardo M., Tregrossi A, Ciajolo A.**: "The effect of temperature on the chemical structure of premixed methane flames" Proceedings of the 31th Meeting on Combustion - Torino, June 17-20, paper VII-10 (2008).

- ✓ **Alfè M., Apicella B., Tregrossi A., Ciajolo A.**, Carbon, 46, 2059-2066 (2008).

- ✓ **Alfè, M., Apicella, B., Barbella, R., Tregrossi A., Rouzaud, J-N., Ciajolo A.**, Third European Combustion Meeting (ECM) (2007).

- ✓ **Alfè, M., Apicella, B., Barbella, R., Ciajolo, A., Tregrossi, A.**, *Aromaticity of Carbonaceous Particulates by Means of Spectroscopic Analysis*, Joint Meeting of Scandinavian-Nordic and Italian Sections of The Combustion Institute, Ischia, 6.1.1, (2003).

- ✓ **Apicella B, Carpentieri A., Alfè M., Barbella R., Tregrossi A., Pucci P., Ciajolo A.**, Proc. Combust. Inst. 31, 1, 547-553 (2007).

- ✓ **Apicella, B., Alfè, M., Barbella, R., Tregrossi, A., Ciajolo, A.**, *Aromatic Structures of Carbonaceous Materials and Soot Inferred by Spectroscopic Analysis*, Carbon, 42, 1583-1589, (2004)

-
- ✓ **Apicella, B., Ciajolo, A., Barbella, R., Tregrossi, A.,** *Comparative Analysis of Structure of Carbon Materials Relevant in Combustion*, *Chemosphere*, 51, 1063-1069, (2003)

 - ✓ **Apicella, B., Ciajolo, A., Suelves, I., Morgan, T. J., Herod, A. A., Kandiyoti, R.,** *Structural Characterization of Products from Fuel-Rich Combustion: an Approach Based on Size Exclusion Chromatography*, *Combust. Sci. Technol.*, 174: 345-359, (2002)

 - ✓ **Arena U., Romeo E., Mastellone M.L.** Recursive Operability Analysis of a Pilot Plant Gasifier, *J. Loss Prevention in the Process Industries*, 21/1:50-65 (2008a).

 - ✓ **Arena U., Zaccariello L., Mastellone M.L.,** Tar removal during the fluidized bed gasification of a plastic waste, *Waste Management*, 29:783-791 (2009) .

 - ✓ **Arena U, Zaccariello L, Mastellone M.L.,** Gasification of a plastic waste in a fluidized bed of olivine. Proc. of CFB9 - 9thInt. Conf. on Circulating Fluidized Beds. Edited by J. Werther, W. Nowak, K.-E. Wirth and E.-U. Hartge, ISBN 978-3-930400-57-7, p. 691-696 (2008b).

 - ✓ **Arena U. and Mastellone M.L.,** Fluidized Bed Pyrolysis of Plastic Wastes, chapter 16 in Scheirs, J. & Kaminsky, W. (Eds.), *Feedstock Recycling and Pyrolysis of Waste Plastics*, J. Wiley&Sons Ltd, pp. 435-474 (2006)

 - ✓ **Benignus, V.A. Et Al.,** *Effect of Low Level Carbon Monoxide on Compensatory Tracking and Event Monitoring*. *Neurotoxicology and teratology*, 9: 227–234 (1987)

 - ✓ **Bohm, H., Hesse, D., Jander, H., Luers, B., Pietscher, J., Wagner, H.G., Weiss, M.:** *Proceedings of The Combustion Institute*, 22:403 (1988).

 - ✓ **Bockhorn, H., Fetting, F., Wenz, H.W.,** *Ber. Bunsenges. Phys. Chem.*, 87, 1067, (1983)

 - ✓ **Bond T.C., Bergstrom R. W.,** *Aerosol Sci. Technol.* 40 27–67 (2006)

-
- ✓ **Castaldi M.J., Marinov N. M., Melius C. F., Huang J., Senkan S. M., Pitz W. J., Westbrook C. K.:** *Proceedings of The Combustion Institute*, 26 :693 (1996).

 - ✓ **Ciajolo, in: Bockhorn H., D'Anna A., Sarofim A.F., Wang H. (Eds.),** *Combustion generated fine carbonaceous particles*, Karlsruhe University Press, Karlsruhe, pp. 333-344 (2009)

 - ✓ **Ciajolo, A., Ragucci, R., Apicella, B., Barbella, R., de Joannon, M., Tregrossi, A.,** *Chemosphere*, 42 (5-7), 835-841 (2001)

 - ✓ **Ciajolo, A., Apicella, B., Barbella, R., Tregrossi, A.,** *Correlation of the Spectroscopic Properties with the Chemical Combustion of Flame-Formed Aromatic Mixtures*, *Combust. Sci. Technol.*, 153, 19-22, (2000)

 - ✓ **Ciajolo, A., Barbella, R., Tregrossi, A., Bonfanti, L.,** *Spectroscopic and Compositional Signatures of PAH-Loaded Mixtures in the Soot Inception Region of Premixed Ethylene Flames*, *Proc. Combust. Inst.*, 27, 1481-1487, (1998)

 - ✓ **Ciajolo, A., D'Anna, A., Barbella, R., Tregrossi, A., Violi, A.,** *The Effect of Temperature on Soot Inception in Premixed Ethylene Flames*, *Proc. Combust. Inst.*, 26, 2327-2333, (1996)

 - ✓ **Ciajolo, A., D'Anna, A., Barbella, R.,** *PAH and High Molecular Weight Species Formed in a Premixed Methane Flame*, *Combust. Sci. Technol.*, 100, 271-281, (1994)

 - ✓ **Ciajolo, A., Barbella, R., Mattiello, M., D'Alessio, A.,** *Axial and Radial Measurements of Soot and PAH in a Light Oil Flame*, *Proc. Combust. Inst.*, 19, 1369-1377, (1982)

 - ✓ **Clar , E.,** *Polycyclic Aromatic Hydrocarbons*, Academic Press London and New York, (1974).

-
- ✓ **Crump, K. & Allen, B.,** *Quantitative Estimates of Risk of Leukemia from Occupational Exposure to Benzene.* Washington, DC, US Department of Labor, OSHA Docket H-059b, Exhibit 152, Annex B (1984)

 - ✓ **D'Alessio, A., D'Anna, A., D'Orsi, A., Minutolo, P., Barbella, R., Ciajolo, A.,** *Precursor Formation and Inception in Premixed Ethylene Flames,* Proc. Combust. Inst., 24, 973-980, (1992)

 - ✓ **D'Alessio, A., Gambi, G., Minutolo, P., Russo, S.,** *Optical Characterization of Premixed CH₄/O₂ Flames Across the Soot Formation Threshold,* Proc. Combust. Inst, 25, 645-651, (1994)

 - ✓ **D'Anna, A. and Violi, A.,** *A Kinetic Model for the Formation of Aromatic Hydrocarbons in Premixed Laminar Flame,* Proc. Combust. Inst, 27, 425-433, (1998)

 - ✓ **Derwent, R.G. & Kay, P.J.A.,** *Factors Influencing the ground Level Distribution of Ozone in Europe,* Environmental Pollution, 55: 191–219 (1988)

 - ✓ **Emdee J.L, Brenzinsky K., Glassman I.,** *Phys.Chem J.,* 96, 2151-2161 (1992)

 - ✓ **Frenklach, M., Wang, H.,** *A Detailed Kinetic Modeling Study of Aromatics Formation in Laminar Premixed Acetylene and Ethylene Flames,* Combust. Flame, 110,(1-2) 173, (1997)

 - ✓ **Friedel, R.S.,** *Spectrometry of Fuel,* Plenum, press New York (1970)

 - ✓ **Freudenthal, R.I. and Jones, P. W., eds.,** *Polynuclear Aromatic Hydrocarbons: Chemistry Metabolism and Carcinogenesis, I,* Raven, New York, (1976)

 - ✓ **Fuhrer, J. & Achermann, B., ED.,** *Critical Levels for Ozone: a UN-ECE Workshop Report.* Liebefeld-Bern, Swiss Federal Research Station for Agricultural Chemistry and Environmental Hygiene, (FAC Report, No. 16) (1994)

 - ✓ **Galvez, Herlin-Boime M, Reynaud C., Clinard C Rouzaud .J.-N.,** *Carbon* 40, 2775–2789 (2002)

-
- ✓ **Gelboin, H. V., Pope, C. A.,** *Annu. Rev. Public Health*, 15, 107, **(1994)**

 - ✓ **Haynes B.S., Wagner H.Gg.:** *Prog. En. Comb. Sci.*, 7:229 (1981).

 - ✓ **Homann, K. H., and Wagner, H. Gg.,** *Some New Aspects of the Mechanism of Carbon Formation in Premixed Flames*, *Proc. Combust. Inst*, 11, 371-379, **(1968)**

 - ✓ **Jäger, H.J. Et Al., Ed.,** *Effects of Air Pollution on Agricultural Crops in Europe*. Brussels, European Commission, (Air Pollution Research Report, No. 46) **(1993)**

 - ✓ **Lafleur, A. L., Howard, J. B., Taghizadeh, K., Plummer, E. F., Scott, L. T., Necula, A.,** *Identification of C₂₀H₁₀ Dicyclopentapyrenes in Flame: Correlation with Corannulene and Fullerene Formation*, *J. Phys. Chem.*, 100, 17421-17428, **(1996)**

 - ✓ **Lee, M. L., Novotny, M. V., Bartle, K. D.,** *Analytical Chemistry of Polycyclic Aromatic Compound*, Academic Press New York **(1981)**

 - ✓ **McKinnon, J.T., Meyer, E., Howard, J. B.,** *Infrared Analysis of Flame-Generated PAH Samples*, *Combust. Flame*, 105, 161, **(1996)**.

 - ✓ Monographs on the Evaluation of the Carcinogenic Risk of Chemicals to Humans, Vol. 32, **(1983)**

 - ✓ **Pope, C.A. III. Et Al.,** *Particulate Air Pollution as a Predictor of Mortality in a Prospective Study of U.S. Adults*. *American Journal of Respiratory and Critical Care Medicine*, 151: 669–674 **(1995)**

 - ✓ **Russo C., Alfè M., Barbella R., Mallardo M, Stanzone F., Tregrossi A., Ciajolo A.** “Partitioning of the low MW components of total particulate in premixed benzene flames at different temperatures” *Processes and technologies for a sustainable Energy Ischia*, June 27-30-**(2010)**

 - ✓ **Shim H.-S., Hurt R., Yang N.,** *Carbon* 38 29–45 **(2000)**

-
- ✓ **Tompkins, E.E. and Long, R.**, *The Flux of Polycyclic Aromatic Hydrocarbons and of Insoluble Material in Pre-mixed Acetylene-Oxygen Flames*, Proc. Combust. Inst, 12, 625-634, (1970)

 - ✓ **Tregrossi A., Ciajolo A.**, *Combust. Sci. Technol. in press*, (2009).

 - ✓ **Tregrossi A., Barbella R., Ciajolo A., Alfè M.**: *Combust. Sci. Technol.*, 179:1 (2007).

 - ✓ **Tregrossi, A., Alfè, M., Barbella, R., Ciajolo, A.**, *Spectral Properties of Soot in the UV-Visible Range*, Lisbona, October (2005)

 - ✓ **Tregrossi, A., Ciajolo, A., Barbella, R.**, *The Combustion of Benzene in Rich Premixed Flame at Atmospheric Pressure*, 117: 553-561, (1999)

 - ✓ **US-EPA Air Quality Criteria for Particulate Matter Vol. 1**, EPA 600/P-95/001 af-cf. 3v Washington, (1996)

 - ✓ **Vander Wal R.L., Tomasek A.J.**, *Combust. Flame* 134, 1-9 (2003)

 - ✓ **Whitby K.T. and Cantrell B.**, *Fine particles. Proceeding of: International Conference on Environmental Sensing and Assessment*. Las Vegas, NV, Institute of Electronic Engineers, (1976)

 - ✓ **Warnatz, J.**, *Experimental and Computational Study of Ignition and Flame Propagation in Internal Combustion Engines*, Elsevier Science Ltd, 31-36.

 - ✓ **Westbrook**, *Proc. Combust. Inst.* 26, 693-702 (1996)

 - ✓ **Comment to :**
M. Alfè, B. Apicella, R. Barbella, J-N. Rouzaud, A. Tregrossi, A. Ciajolo
Structure-Property Relationship In Nanostructures Of Young And Mature Soot In Premixed Flames. <http://www.combustioninstitute.org/Connections/4F02.pdf>